NMR Studies of Gas and Water Adsorption in Carbon Based Materials

Shenghua Mao

A dissertation submitted to the faculty of the University of North Carolina at Chapel Hill in partial fulfillment of the requirements for the degree of Doctor of Philosophy in the Curriculum of Applied and Material Sciences.

Chapel Hill
2007

Approved by
Advisor: Yue Wu
Reader: Keith Gubbins
Reader: Alfred Kleinhammes
Reader: Lu-Chang Qin
Reader: Sean Washburn
Reader: Otto Zhou

ABSTRACT

SHENGHUA MAO: NMR Studies of Gas and Water Adsorption in Carbon Based Materials (Under the direction of Yue Wu)

In this dissertation, we used ^{1}H NMR to study the gas and water adsorption in carbon based materials. The NMR studies indicated that at room temperature, the interior of cap-opened Single Wall Nanotubes (SWNTs) becomes available for methane and ethane adsorption. The endohedral adsorption is the dominant mechanism when pressure is lower than 1Mpa. The adsorptions follow Langmuir adsorption isotherm with related adsorption energy of 22.7 KJ/mol for methane and 29.2 KJ/mol for ethane. The average exchange time between molecules adsorbed inside SWNTs and free gas molecules outside is on the order of 80ms. It is shown that exposure to oxygen has no effect on methane and ethane endohedral adsorption, which suggests smaller adsorption energy of oxygen compared to that of methane and ethane.

In the study of the water adsorption in SWNTs at room temperature, the adsorption isotherm from ^{1}H NMR spectrum indicated clear hysteresis loop. Quantitative analysis gave the adsorption amount of 3 mmol/g in SWNTs at saturated vapor, which was

considerably lower compared to 14 mmol/g of bulk liquid water. Combined with T_2 analysis, we believed that the state of adsorped water in SWNTs is in between vapor and bulk liquid. The primary adsorption sites are associated with tube ends and defects, which have strong effects on water adsorption.

The study of adsorption of hydrogen in Boron doped graphite and Boron doped SWNTs proved considerable increment of adsorption energy at moderately high pressure and room temperature, which may lead to a new method for improving hydrogen storage at room temperature.

ACKNOWLEDGMENTS

I'd like to thank first and foremost my advisor, Dr. Yue Wu, for his guidance and help throughout my graduate study. His enthusiasm for science and persistence for research gave me tremendous stimulation and encouragement. His deep and broad knowledge, acute thought, insightful intuition made the successful progress of the research. His guidance will benefit me throughout my further work, which I will appreciate deeply and thoroughly forever.

I need to thank my group members for the training and helping: Xiaoping Tang, Jonathan Baugh, Lilong Li, Marcelo Behar, Yuanyuan Jia, Harsha Kulkarni, Xuekui Xi, Charles Chen, Cassi Galt, B. J. Anderson, Gregory Mogilevsky, Sean Gidcumb, Haijing Wang, and particularly Alfred Kleinhammes. I also thank Dr. Horst Keisemmier for discussion and encouragements. I'd like to express my gratitude to everyone, especially my advisor Dr. Yue Wu, for the help on writing dissertation and preparing presentation.

I benefited from the discussions and collaborations with other groups, particularly Dr. Otto Zhou and Dr. Hedio Shimoda for the carbon nanotube sample preparation, Dr. Luchang Qin and Dr. Qi Zhang for TEM spectrum by. I'd also like to thank Dr. Shanbai

Zhang's group in NREL and Dr. Heben's group in Penn State for the Boron-doped samples. I thank Dr. Keith Gubbins for helpful discussions.

I especially thank my committee members for reading and offering helpful suggestion on my dissertation. They are: Dr. Keith Gubbins, Dr. Alfred Klenhammes, Dr. Luchang Qin, Dr. Sean Washburn, Dr. Yue Wu and Dr. Otto Zhou.

The work was supported by the National Science Foundation (Grant contract No. DMR-0139452 and 0513915), the U.S. Army Research Office (Grant No. DAAD19 -03-1-0326, the ONR MURI (Grant No. N00014-98-1-0597), and the ACS-PRF (No. 37310-ACS).

I appreciate very much for the support from my parents and my sisters and my brother. Last but not the least, I'd like to express my love and gratitude to my wife, Yimei Li, for her help, support and care for me on both the study and life.

TABLE OF CONTENTS

LIST OF FIGURES

Figure

LIST OF ABBREVIATIONS

ACF	Activated Carbon Fiber
BET	Brunauer, Emmett, and Teller isotherm
CNT	Carbon Nanotube
DFT	Density Function Theory
FID	Free Induction Decay
FT	Fourier Transformation
IUPAC	International Union of Pure and Applied Chemistry
NMR	Nuclear Magnetic Resonance
PACs	Primary Adsorption Centers
PAS	Primary Adsorption Site
RT	Room Temperature
SWCNT	Single Wall Carbon Nanotube
SWNT	Single Wall Nanotube
TEM	Transmission Electron Microscopy
XRD	X-Ray Diffraction

CHAPTER 1

Introduction

Since discovered in 1991(Iijima, 1991), carbon nanotube has attracted great research attention owing to their unique structure and mechanical and electric properties (Cheng, Yang & Liu, 2001; Fujiwara et al., 2001; Hata, Takakura & Saito, 2001; Stan & Cole, 1998; Zhao et al., 2002; Zuttel et al., 2002). The most popularly studied carbon nanotube is single walled nanotube (SWNT). The high surface to volume ratio makes carbon nanotube possibly good candidate for energy gas storage. With nano-scale cylindrical structure, SWNT can be used as channel for drug delivery and hosts for biological reaction in specific region, which makes the behavior of water in SWNT an important issue, such as adsorption and transportation of water in SWNT. Although more and more research is being done on these two topics, the question of whether water can be filled in SWNTs and how water behaves in SWNT still remains unclear. In this thesis, we mainly use NMR as a tool to study these issues with our specifically designed experimental setup.

1.1 Adsorption of Gases in SWNT

Typical SWNT has diameter of 5 to 20 $\mathring{A}$ and length of hundreds of micrometers. The hollow space within the tubes can be filled with substances, which lead to possible application of SWNT as gas adsorbents. For the research of adsorption, special interested is paid to methane, ethane and hydrogen, which are energy gases and their storage and transportation are under consideration. The study on oxygen and Nitrogen is mainly concentrated on their effect for the adsorption of other gases. It is also reported that oxygen can change the electronic property of SWNT.

The most commonly studied SWNT are those with diameters comparable to (10,10) tube, which has average diameter of 13.6 $\mathring{A}$. The caps of nanotubes can be opened by oxidation or chemical processes. For gas adsorption in SWNTs, the questions widely studied are: Could gases such as methane and ethane go inside SWNTs? What is the amount of adsorption? SWNTs usually form bundles with tens to hundreds of tubes. Therefore three possible locations might be accessible for gases, including outer surface of the bundle, interstitial sites between the tubes and endohedral sites inside the tubes. Which of the three locations is most accessible to gases? Are there any preferences for gases? What are the states of adsorbed molecules in SWNTs? What is the force leading to the adsorption? Is this a physical adsorption or chemical adsorption? Such questions have generated tremendous researches both theoretically and experimentally.

1.2 Water Adsorption in SWNT

The effect of water in SWNT is of great interest and being widely discussed, since carbon nanotube can be considered as candidates for channels for ion delivery and chemical reaction (Banerjee, Murad & Puri, 2007; Biggin, 2001; Brownstein & Tarr, 1979; Dellago, Naor & Hummer, 2003; Di Leo & Maranon, 2004). As a major fluid for biological system, the effect of water nanotube has drawn innumerous research attentions (Alexander et al., 2004; Chang et al., 2002; Dellago et al., 2003; Dujardin et al., 1994; Gordillo & Marti, 2000; Gordillo & Marti, 2001). The interaction of water in SWNT is quite different from that of other gases as methane and ethane or other simple fluids. The existence of hydrogen bonds makes the fluid-fluid interaction among water molecules much stronger than that between water molecules and carbon atoms (Dellago & Naor, 2005; Muller et al., 1996; Wallqvist, Gallicchio & Levy, 2001; Walther et al., 2001). A reasonable concern is that since carbon nanotube is made of graphene sheet, which is hydrophobic, it may be difficult for water to be adsorbed inside nanotube. Interestingly, the cylindrical structure of SWNT could have significant effect on the potential of nanotube. Results from computational simulation predicted that water can flow inside nanotube by pulse or form ice tube at high pressure and low temperature (Demontis, Stara & Suffritti, 2003; Hummer, Rasaiah & Noworyta, 2001; Maniwa et al., 2002; Wang et al., 2004).

Experimental results from XRD (Maniwa et al., 2002), neutron diffraction

(Alexander et al., 2004), and NMR (Matsuda et al., 2006; Sekhaneh et al., 2006) suggested different pictures of water absorption in SWNT. Mainwa reported that a substantial amount of water is absorbed inside SWNTs at room temperature. The desorption- adsorption of water molecules occurred reversibly above room temperature. Also the liquid-like water is transformed into ice nanotubes at 235 K (Maniwa et al., 2002). By neutron diffraction and molecular dynamic simulation, Alexander et al. found square-ice sheet wrapped into a cylinder inside the carbon nanotube and the interior of the ice tube is filled with water chain (Alexander et al., 2004).

But none of these computational simulation studies and experimental researches mentioned how water is adsorbed inside in nanotube. The process of water adsorption or filling in SWNT remains unclear. With a specifically developed water pressure controlling system, we use NMR to study the adsorption and desorption of water at room temperature (Mao, Kleinhammes & Wu, 2006) along with comparison with water adsorption in porous carbonaceous materials such as activated carbon.

1.3 NMR Techniques for Gas Adsorption and Water Adsorption

Since ^{1}H NMR spectrum signal intensity is proportional to the number of hydrogen spin within the NMR coil region, we can study water adsorption in nanotube by observing the NMR spectrum intensity. This method proved to be very efficient: even tiny variation of the amount of water adsorption will change the spectrum intensity. The

NMR spectral linewidth, spin-lattice relaxation time (T_1) and spin-spin relaxation time T_2 can offer helpful information on the molecular dynamics of water molecular. To improve the spectral quality, we use spin-echo pulse sequence for most of the data acquisition.

1.4 Dissertation Outline

In chapter 2, we describe some basic adsorption isotherms in carbon based materials, which will be used in chapter 3 and chapter 4. The Langmuir adsorption and BET adsorption theories will be introduced. Also we will discuss the critical temperature of methane, ethane, and water and the probability of these gases forming condensation in nanotube. The five types of adsorption isotherm defined by IUPAC will also be introduced.

In chapter 3, we will introduce the NMR techniques used for studying gas adsorption and water adsorption, which includes NMR spectrum acquisition techniques such as spin echo pulse sequence, T_1 and T_2 experiments.

Chapter 4 will discuss gas adsorption in SWNT. The contents will cover adsorption of methane and ethane in SWNT at room temperature, the location of gases in SWNT, and the amount of adsorption of different gases. The effect of oxygen to adsorption will also be discussed. Most of the work can be found in the published paper (Kleinhammes et al., 2003).

In Chapter 5, we will discuss the adsorption of water in open-ended SWNT at room

temperature. The adsorption and desorption process of water in SWNT is studied by NMR. We observed strong hysteresis effect during these processes. Our result indicated that water could not form regular liquid state in SWNT at room temperature. Unlike most molecular dynamics simulation, which predict considerable amount of water inside SWNT channel, our experimental result suggested that at saturation vapor pressure, the amount of water is only about 20% of that expected for water filled SWNTs. The effect of primary adsorption sites (PAS) is proved to be significant in our sample. As a comparison, water adsorption in activated carbon is also studied. The detail of the result is published in reference (Mao et al., 2006).

In chapter 6, we will discuss some primary results of high-pressure adsorption of hydrogen in carbon-based materials. The results indicate that at room temperature, substitutional doping with boron can increase the adsorption energy of hydrogen in graphite and single wall nanotubes. Further research on this topic is in progress in our lab.

CHAPTER 2

Adsorption Phenomenon in Carbon Based Materials

The carbon-based adsorbent materials are usually graphitic such as activated carbons, carbon nanotube (CNT), activated carbon fiber (ACF), and ion doped carbon nanotube. The adsorbates of interest include hydrogen, methane, ethane, nitrogen, oxygen, water and so on. The adsorption mechanisms can be classified as physical adsorption and chemical adsorption. In most cases, gas adsorption in carbon-based materials is physical adsorption. Two famous isotherms are used to depict the adsorption, which are Langmuir isotherm and BET isotherm.

2.1 Definitions and Classification of Adsorption Isotherms

The term adsorption is used to explain the condensation of gases on surfaces. It is important to make a clear difference between adsorption and absorption. Adsorption is referred to the concentration of gas molecules on or near the surface of a solid material, while in absorption the gas molecule can penetrate into the bulk phase of solid. The

adsorbed gas is called adsorbate and the solid where adsorption takes place is called the adsorbent.

Adsorption is divided into two sub-categories, which are physical adsorption (physisorption) and Chemical adsorption (chemisorption). Physisorption is also called Van der Waals adsorption because the interaction between gas molecules and solid surface in this process is Van der Waals force. Physisorption and Chemisorption can be discriminated by whether there are chemical bonds formed during the adsorption.

Physisorption occurs at various temperature and pressure conditions, usually lower temperature and higher pressure will make adsorption much easier to happen. The major driving force for adsorption is the intrinsic binding energy, which is due to Van der Waals interaction. When a material is exposed to a gas, an attractive force acts between the exposed surface of the solid and the gas molecules. The surface area of single wall nanotube that we studied includes both the external and internal surfaces.Unlike chemisorption, which is due to strong chemical attractions, physisorption is very weak because Van der Waals interaction is usually less than 15 kJ/mole, and the heat of adsorption is about 20 ~40 kJ/mole.

In physisorption, the adsorption process coexists with desorption process, when they reach a dynamic equilibrium at certain temperature and pressure, the density of gas molecules at the adsorbent surface will be higher than that of free gas, which means that certain amount of gas is “adsorbed”.

Gas physisorption is non-selective, thus the mechanism of filling the surface is either by step-by-step or layer-by-layer, depending on the available solid surface and the relative pressure. Filling the first layer enables the measurement of the surface area of the material, because the amount of gas adsorbed when the monolayer is saturated is proportional to the entire surface area of the sample. The complete adsorption/desorption analysis is called an adsorption isotherm, which is conventionally plotted on the basis of amount adsorbed versus relative pressure P/P_0 at constant temperature. P_0 is the saturated vapor pressure of the subcritical gas at that temperature. The amount of adsorption is usually presented in the unit of mmol/g. Adsorption isotherm provides a significant amount of information for the interaction of adsorbent and adsorbate, including estimates of the surface area and surface chemistry, and pore volume and pore size distribution.

Based on the classification of IUPAC (International Union of Pure and Applied Chemistry), there are six standard types of adsorption isotherms due to different adsorbate/adsorbent and adsorbate-adsorbent interactions. The adsorption isotherms are named from Type I to type VI isotherms.

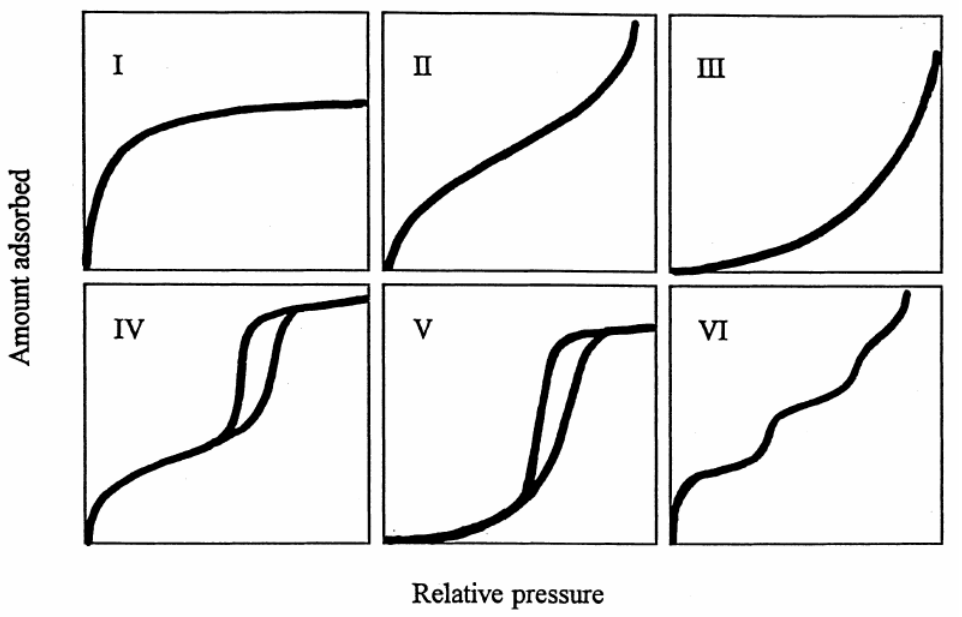

Figure 2.1: IUPAC classification of adsorption isotherms for gas–solid equilibrium.

Of all the adsorption isotherms, type I isotherm (Langmuir adsorption isotherm) and type II isotherm (BET adsorption isotherm) are two mostly encountered types.

The structure of the adsorbent plays an important role on the type of adsorption isotherm. Adsorbents usually have a lot of pores, which are accessible to gas molecules. Porosity is a collective term for these pores and their distribution in the structure of solid adsorbent. The shapes of pores can be either regular as in single wall nanotube or irregular as that in activated carbon, and they can be interconnecting to each other. Pores are also described by volume elements.

Porosity is defined with classification system based on the sizes of pores: Micropores are those with width less than 2 nm, mesopores are pores with widths

between 2 nm and 50 nm, the pores with width greater than 50 nm are called macropores (IUPAC, 1972). The amount of adsorption isotherm is affected significantly by the porosity of the adsorbents.

2.2 Introductions to Adsorption Isotherms

2.2.1 Langmuir Isotherm

Developed by Irving Langmuir in 1916, this adsorption isotherm adsorption isotherm is used to describe the equilibrium established between the molecules in the gas phase and the corresponding adsorbed species (molecules or atoms), which are bound to the surface of the solid. For gas molecules in contact with a solid surface at a fixed temperature, this isotherm describes the partitioning between gas phase and adsorbed species as a function of applied pressure. The free gas and the adsorbed gas are in dynamic equilibrium, and the fractional coverage of the surface depends on the pressure, P, of the overlying gas.

The Langmuir isotherm is based on three assumptions: (1): Adsorption can form only one layer coverage. (2): All surface sites are equivalent and can accommodate at most one adsorbed atom. (3): The ability of a molecule to adsorb at a given site is independent of the occupation of neighboring sites, but the total number of surface sites on the surface is fixed.

When considering adsorption isotherms it is conventional to adopt a definition of

surface coverage θ, which defines the maximum (saturation) surface coverage of a particular adsorbate on a given surface always to be unity, i.e. θ_{max} = 1. Langmuir adsorption can be derived by either kinetic method or thermodynamic method.

2.2.2 Derivation of Langmuir Isotherm: Kinetic Method

Assuming that there are a fixed number of surface sites present on the surface, the adsorption process between gas phase molecules, A, vacant surface sites, S, and occupied surface sites, SA, can be represented by the equation,

$$[S]+[A] \leftrightarrow [SA] \tag{2.1}$$

An equilibrium constant, K, can be written as

$$K=\frac{[SA]}{[S][A]} = \text{Fraction of surface sites occupied } (0 < \theta < 1) \tag{2.2}$$

Here: **[SA]** is proportional to the surface coverage of adsorbed molecules, or proportional to **[S]** is proportional to the number of vacant sites, $(1-\theta)$. **[A]** is proportional to the pressure of gas, P.

The equilibrium that may exist between gas adsorbed on a surface and molecules in the gas phase is a dynamic state, i.e. the equilibrium represents a state in which the rate of adsorption of molecules onto the surface is exactly counterbalanced by the rate of desorption of molecules back into the gas phase. It should therefore be possible to derive

an isotherm for the adsorption process simply by considering and equating the rates for these two processes. Expressions for the rate of adsorption and rate of desorption specifically are:

$$R_{ads} = \frac{f(\theta).P}{\sqrt{2\pi m k_B T}} \exp(-E_{ads} / RT)$$

.

$$R_{des} = v.\frac{f'(\theta).P}{\sqrt{2\pi m k_B T}} \exp(-E_{ads} / RT)$$

(2.3)

Equating these two rates yields an equation of the form:

$$\frac{P.f(\theta)}{f'(\theta)} = C(T) \qquad (2.4)$$

Where the terms *f*(q) and *f* '(q) contain the pre-exponential surface coverage dependence of the rates of adsorption and desorption respectively and all other factors have been taken over to the right hand side to give a temperature-dependent "constant" characteristic of this particular adsorption process, $C(T)$.

Based on the assumptions for Langmuir adsorption isotherm, coverage dependencies for rates of the two processes can be described as:

For adsorption, $f(q) = c\,(1-q)$, which is proportional to the fraction of sites that are unoccupied. For desorption, $f'(q) = c'q$, i.e. proportional to the fraction of sites which are

occupied by adsorbed molecules. Where q is the fraction of sites occupied at equilibrium. Substitution into first equation then yields

$$\frac{P(1-\theta)}{\theta} = B(T) \tag{2.5}$$

Thus it is possible to define the equilibrium constant b as:

$$b = \frac{\theta}{(1-\theta)P} \tag{2.6}$$

where $B(T) = (c'/c).C(T)$.

Rearranging the above formula gives the expression for surface coverage

$$\theta = \frac{bp}{1+bp} \tag{2.7}$$

Further study gives the constant *b* as:

$$b = \frac{\sigma}{\nu_0\sqrt{2\pi m k_B T}} \exp(E_d / k_B T) \tag{2.8}$$

This is the usual form of expressing the Langmuir Isotherm. The equilibrium constant, b, is temperature dependent and related to the Gibbs free energy and hence the enthalpy change for the process. Here b is only a constant (independent of θ) if the enthalpy of adsorption is independent of coverage.

2.2.3 Derivation of Langmuir Isotherm: Thermodynamic method

In Langmuir adsorption, each site can be either occupied by one adsorbate gas molecule or with zero occupancy.

O ---------- ε, site occupied.

□ ---------- 0, site unoccupied.

If we define ε as the energy of an adsorbed gas molecule relative to a free gas molecule at infinite distance, then the Gibbs sum Z is:

$$Z = 1 + \lambda \exp(-\varepsilon / kT) \tag{2.9}$$

Here k is Boltzmann constant, T is the temperature of system, $\lambda = \exp(\mu / kT)$, and μ is the chemical potential of adsorbed molecules.

If energy must be added to remove the gas molecule from the adsorbent site, ε will be negative. The term 1 in the sum arises from occupancy zero, while the term $\lambda \exp(-\varepsilon / kT)$ arises from single occupancy.

The adsorption reaches equilibrium when the chemical potential of free gas molecules equals to the chemical potential of adsorped gas molecules.

$$\mu(\text{free gas}) = \mu(\text{adsorped gas}) \quad \text{and} \quad \lambda(\text{free gas}) = \lambda(\text{adsorped gas}) \tag{2.10}$$

The fraction of adsorped molecules is:

$$\theta = \frac{\lambda \exp(-\varepsilon / kT)}{1 + \lambda \exp(-\varepsilon / kT)} = \frac{1}{\lambda^{-1} \exp(\varepsilon / kT) + 1} \tag{2.11}$$

From thermodynamics theory, the value of λ in terms of the gas pressure is:

$$\lambda = {}^{n}\!/_{n_Q} = {}^{p}\!/_{kTn_Q} \tag{2.12}$$

Here $n=N/V$ is the quantum concentration of particles, $n_Q = (MkT / 2\pi\hbar^2)^{3/2}$ is the quantum concentration associated with one atom in a cube of side equal to the thermal average de Broglie wavelength.

Substitute (2.12) into (2.11), we get

$$\theta = \frac{1}{(n_Q kT / P) \exp(\varepsilon / kT) + 1} = \frac{P}{n_Q kT \exp(\varepsilon / kT) + P} \tag{2.13}$$

with $P_0 = n_Q kT \exp(\varepsilon / kT)$ (2.14)

Hence $\theta = \frac{p}{p_0 + p}$ (2.15)

2.2.4 Dependence of Langmuir adsorption isotherm with b constant

As with all chemical equilibrium, the position of equilibrium will depend upon a number of factors:

(1): The relative stabilities of the adsorbed and gas phase species involved.

(2): The temperature of the system (both the gas and surface, although these are normally the same).

(3): The pressure of the gas above the surface. In general, factors (2) and (3) exert opposite effects on the concentration of adsorbed species - that is to say that the surface coverage may be increased by raising the gas pressure but will be reduced if the surface temperature is raised.

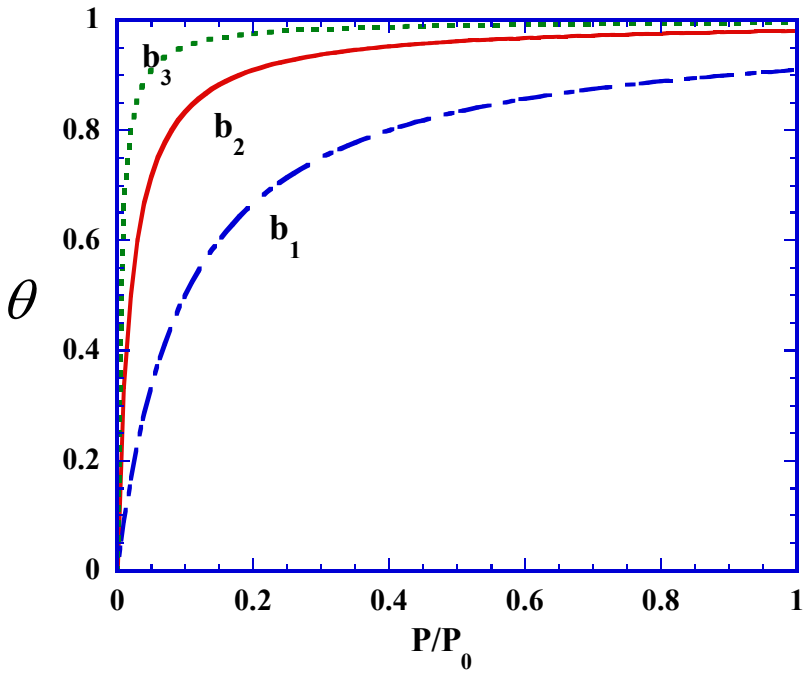

Figure 2.2: Adsorption curve of Langmuir isotherm with different b values, here $b_3 > b_2 > b_1$ and the larger the value of b, the steeper the adsorption increase in the beginning.

The type I isotherm is applicable for the systems with a predominantly micropores structures where majority of micropores are filled at relative pressure below 0.1. The adsorption process usually completes at a relative pressure about 0.5. A typical example for this isotherm is N_2 in activated carbon at 77K will show this type of adsorption. Our experimental result also indicated that at room temperature, methane and ethane in SWNT also follow Langmuir adsorption isotherm.

2.2.5: Type II to type VI isotherms

Brunauer, Emmett, and Teller (BET) originally developed this isotherm theory for multilayer adsorption processes. Unlike Langmuir isotherm, which assumes only one layer adsorption, the BET isotherm considers monolayer coverage is followed by multilayer at high relative pressures. Isotherm rises indefinitely since the layers can grow on top of one another, and it is widely used in industry to determine surface areas.

Type II adsorption occurs in carbons with mixed micro-porosity and meso-porosity. The formula for type II isotherm is defined as:

$$\theta = \frac{N}{S} = \frac{cx}{(1-x)(1+(c-1)x)}$$

where θ is the relative coverage of adsorption.

X =P/P_0 , the relative pressure. , N is the number of adsorbed molecules, S is the number of total available sites at the beginning the adsorption., c is the adsorption

constant. The adsorption isotherms at different values of c are shown as the following plot:

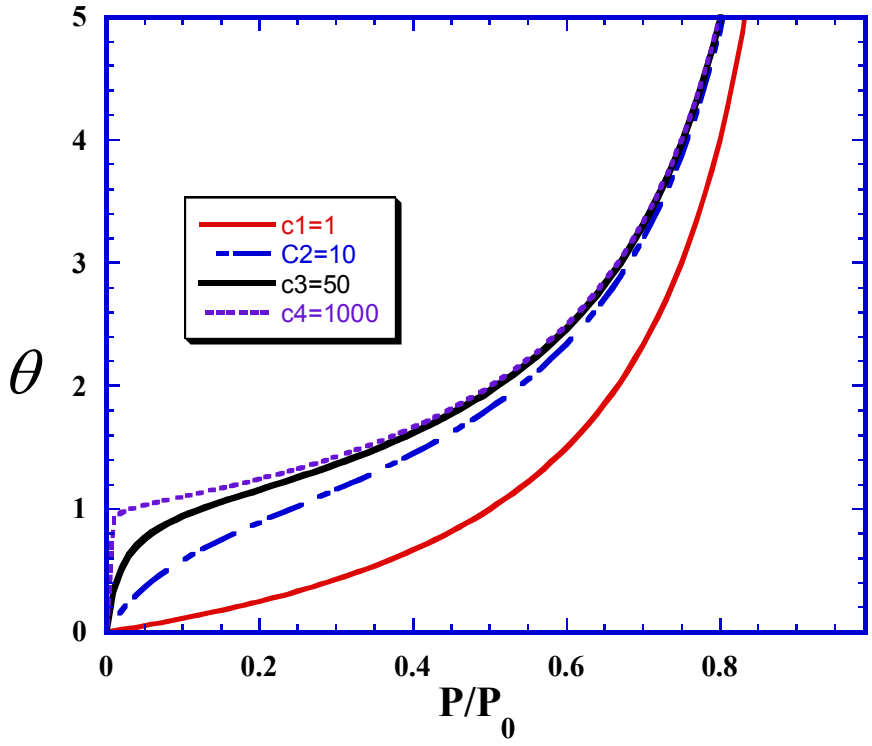

Figure 2.3: BET isotherms for different values of constant c, As c increases, the adsorbate molecules cover the first layer more quickly (θ=1). .

Type III isotherm describes the adsorption when molecules in nonporous or macroporous surfaces with weak interactions(Kiselev, 1968). The adsorbate-adsorbent interactions are usually weak, which lead to low uptakes at low relative pressure. But as a molecule is adsorbed at a primary adsorption site, the stronger adsorbate-adsorbate interaction

becomes the major driving force for the continuing adsorption, further adsorbed molecules tend to be adsorbed at the sites of previous adsorbed molecules, thus lead to an accelerated uptake at higher relative pressures. The classic example is water adsorption on carbons where primary adsorption sites are oxygen based functional groups. Another example is the isotherm of SO_2 on nonporous carbon black that follows a type III isotherm.

Type IV isotherm has hysteresis loop which is associated with the presence of mesoporosity. The shape of hysteresis loop is unique to each adsorption system. Capillary condensation makes rise of uptake to a hysteresis loop at certain relative pressure, at which the uptake is limited.

Type V isotherm is convex to the relative pressure axis and also characteristic of weak adsorbate-adsorbate interactions. Hysteresis loop also exists in this type of isotherm. These isotherms are indicative of micropores or mesoporous solids. The mechanism for shape formation of this type of isotherm is the same as those for type III isotherm.

Type VI isotherm is introduced initially as a hypothetical isotherm. The layer behavior of the shape is due to formation of a complete monolayer before subsequent layer begins. It is assumed that this isotherm arise from adsorption on extremely homogeneous, non-porous surfaces where the monolayer capacity corresponds to the step height (Hasley, 1948). One example is the adsorption of krypton on carbon black at 90 K

(Kratschmer, Rathousky & Zukal, 1999).

In the following chapters, we will discuss the Langmuir isotherms for gas adsorption in SWNT and type V isotherm for water adsorption in SWNT.

2.3 Classification of Gibbs adsorption isotherms

Donohue pointed out that the current IUPAC classification of six adsorption isotherms is not accurate because of two deficiencies(Donohue & Aranovich, 1998a; Donohue & Aranovich, 1998b; Donohue & Aranovich, 1999). First, it is incomplete because experimental results show more types of adsorption shape. Secondly, it gives the incorrect impression that adsorption isotherms are always monotonically increase functions with pressure. However, there are many isotherms that are not monotonic and show maximal. They believe the reason for this deficiency is that the IUPAC classification is based conceptually on ideas about “absolute” adsorption rather than on the Gibbs adsorption. They pointed out that the adsorption isotherm for supercritical gases are fundamentally different from those in IUPAC classification. Experimental data for hydrocarbons, nitrogen, carbon dioxide and other gases on macroporous and macroporous adsorbent for supercritical temperatures showing nonmonotonic isotherms with maximal. Based on their study, they suggested that the Ono-Kondo lattice model is able to predict all types of adsorption behaviors. Hence it is necessary to discuss critical temperature and critical pressure for the adsorption of the gases we studied.

2.4 Critical temperature (T_c) and Critical pressure (P_c)

Critical temperature is the maximum temperature at which a gas can be converted into a liquid by an increase in pressure. Critical pressure is the minimum pressure, which would suffice to liquefy a substance at its critical temperature. Above the critical pressure, increasing the temperature will not cause a fluid to vaporize to give a two-phase system. Critical point is related to a point in the phase diagram that with critical temperature (T_c) and pressure (P_c) above which a gas cannot be liquefied. The related phase diagram is shown below.

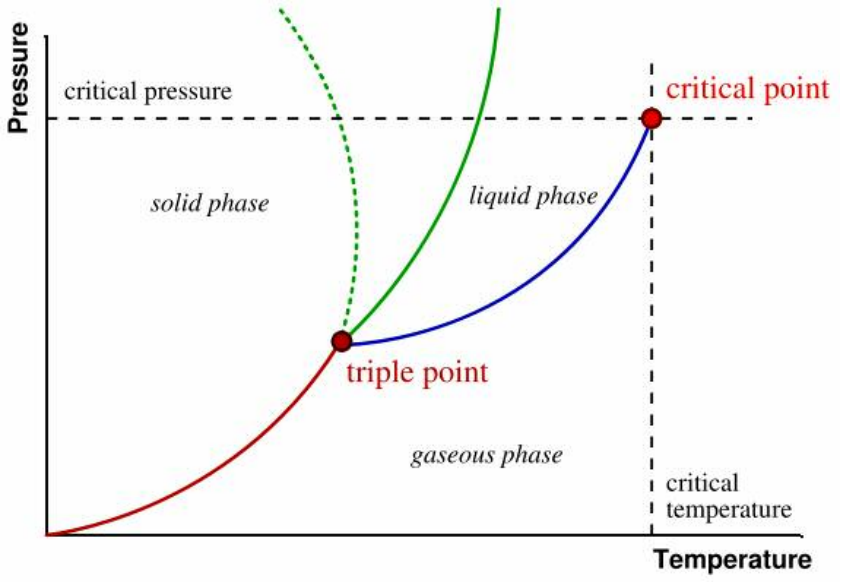

Figure 2.4: Phase diagram of supercritical gases

Supercritical fluid

When the state of a compound or mixture is above its critical pressure (P_c) and

critical temperature (T_c), this compound or mixture is a supercritical fluid. Actually, at such high temperature or pressure, the liquid and gaseous phases become indistinguishable. Hence such system can also be called as supercritical fluid. If the adsorbate to study is a supercritical fluid or supercritical gas, the adsorption isotherm may not follow the IUPAC type isotherm.

The critical temperature and critical pressure of the adsorbates that we are going to study in this thesis is shown below. As we can see that, at room temperature, hydrogen and methane will become supercritical gases when pressure is moderately high, which is possible, similar case happens for ethane when temperature is higher (>305 K). but for water, the standard condition is far way from its supercritical point. Thus, to discuss the adsorption isotherm, we need to discriminate water from methane, ethane and hydrogen.

Critical property of some adsorbates			
Adsorbate	Molecular weight	Critical temperature	Critical pressure
	g/mol	K	Mpa (atm)
Carbon Dioxide (CO_2)	44.01	304.1	7.38 (72.8)
Water (H_2O)	18.02	647.3	22.12 (218.3)
Methane (CH_4)	16.04	190.4	4.60 (45.4)
Ethane (C_2H_6)	30.07	305.3	4.87 (48.1)
Hydrogen *(H_2)*	2.016	32.97	1.293 (12.77)

Table 2.1: Critical properties of some adsorbate gases

Murata reclassified the supercritical gas adsorption isotherms into three types based on increase in fluid-fluid interaction, which are Henry-type isotherms, virial isotherms and

cooperative isotherms. The three types differ in terms of compression factor Z_a and the adsorbed layer density(Murata et al., 2002).

$$Z_a = \frac{P}{<\rho> RT} \qquad \text{..... (2.8)}$$

where P is the pressure of the bulk gas phase, R is the gas constant and T is the temperature. The goodness of this classification is supported by calculations based on density functional theory. This classification can be used to study the hydrogen adsorption on single wall carbon nanotubes.

CHAPTER 3

NMR Techniques for Adsorption Study

Nuclear Magnetic Resonance (NMR) spectroscopy is a powerful tool for structural and dynamic analysis in physical, chemical and biological systems. So far, varieties of NMR techniques have been developed with a very wide range of applications including magnetic resonance imaging.

A simple way of describing NMR is a classical model, which involves Bloch equations, and vector models. A quantum mechanical description is by considering energy levels and transitions. More advanced level of description involves density matrix and observable operators. In this thesis, we mostly use the first and second methods to introduce NMR theory and some techniques used in our research. The detailed description of theory and applications of NMR can be found in classical references (Abragam, 1985; Johnson & Waugh, 1962; Slichter, 1989).

3.1 Splitting of Nuclear Spin Energy Levels in Magnetic Field

NMR spectroscopy is based on the study of nuclear spinning. A nuclear is characterized by a nuclear spin quantum number I. In some nuclei (such as ^{12}C) the spin is zero. However, most nuclei (such as ^{1}H, ^{15}N and ^{13}C) possess an overall spin. The rules for determining the net spin of a nucleus are as follows: If the number of neutrons and the number of protons are both even, then the nucleus has no spin. If the number of neutrons plus the number of protons is odd, then the nucleus has a half-integer spin (i.e. 1/2, 3/2, 5/2) .If the number of neutrons and the number of protons are both odd, then the nucleus has an integer spin (i.e. 1, 2, 3). For nuclei with I=0, there is no nuclear spin, thus no NMR phenomenon.

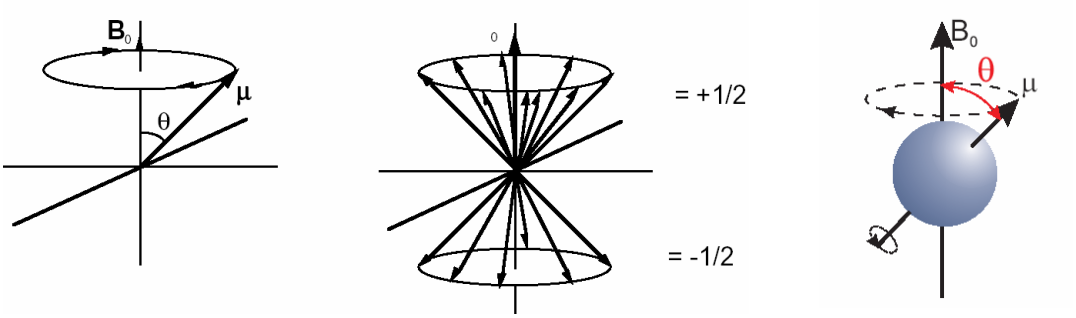

Figure 3.1: Precession of nuclear spin with external field applied

The energy of a nuclear spin with associated nuclear magnetic moment μ in a magnetic field B is given by:

$$E = -\mu B \cos\theta \qquad (3.1)$$

where θ is the angle between the direction of the applied magnetic field and the nuclear spin vector. Nucleuses with total spin number I will have $2I + 1$ possible orientation. In the absence of an external magnetic field, these orientations are of equal in energy. If a magnetic field is applied, the energy levels split. Each level is related to a specific magnetic quantum number m that varies from $-I$ to I. One of the most frequently studied nucleuses is proton. It has spin number 1/2 and 2 energy levels as shown in Figure 3.2.

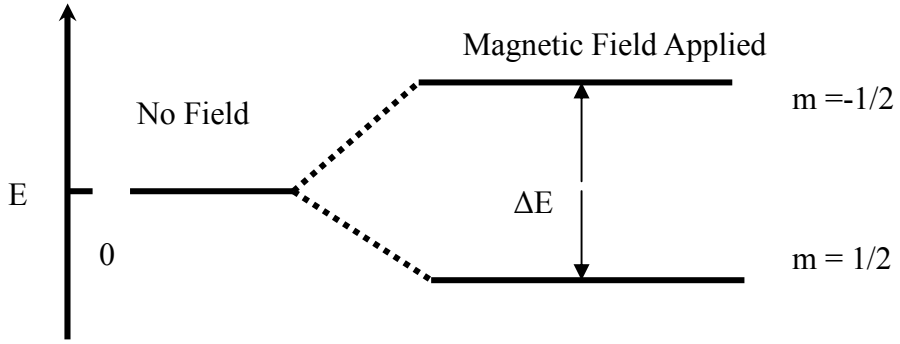

Figure 3.2: Energy levels for a nucleus with spin number 1/2

When the nucleus is in a magnetic field, the initial populations of the energy levels are determined by the Boltzmann distribution. This means that the lower energy level will have slightly higher population than the higher level. When a radiation with certain frequency is applied along the direction perpendicular to the static field, transition between the two levels will happened. The frequency of radiation needed is determined by the difference in energy between the two energy levels.

The nucleus has a positive charge and internal structures and rotation. Therefore, the nucleus possesses a magnetic moment, which is proportional to its spin number I with $\mu = \gamma I \hbar$. The constant γ is called the magnetogyric ratio and is a fundamental nuclear constant, which has a different value for every nucleus. $\hbar$ is the Planck constant divided by 2π.

The energy of a particular energy level is given by:

$$E_m = \gamma \hbar m B_0 \tag{3.2}$$

where B_0 is the strength of the magnetic field at the nucleus. The difference in energy between levels (the transition energy) with $\Delta m = 1$ can be found from:

$$\Delta E = h\nu_0 = \hbar\omega_0 = \gamma \hbar B_0 \tag{3.3}$$

This means that if the magnetic field, B_0, is increased, and so is ΔE. In an external magnetic field B_0, the spin precesses at frequency ω_0. The frequency of precession is termed the Larmor frequency, which is identical to the transition frequency. When the radiation with energy ΔE, the nucleus can absorb this energy and transition between two states will happen, and the energy level populations will be different from that of thermal equilibrium. In the vector picture of NMR, if energy is absorbed by the nucleus, the angle of precession will change. For a nucleus of spin 1/2, absorption of radiation "flips" the magnetic moment so that it opposes the applied field (the higher energy state).

The ratio of the number of spins at lower energy to higher energy is:

$$\frac{N_-}{N_+} = \exp[\frac{\Delta E}{kT}] = \exp[\frac{h\nu_0}{kT}] = \exp[\frac{\hbar\omega_0}{kT}] \tag{3.4}$$

at room temperature,

$$\hbar\omega_0 << kT$$

Thus, (3.5)

$$\frac{N_-}{N_+} \approx 1 + \frac{\hbar\omega_0}{kT}$$

For ^{1}H at field with ν_0 = 200 MHz,

$$\frac{\hbar\omega_0}{kT} \approx 10^{-5} \tag{3.6}$$

This means that the difference of spin populations between the two states is very small. Because this decides absorption of radiation, this means that only a small proportion of target nuclei are in the lower energy state and thus can absorb radiation. So NMR signal is very weak. Methods to increase signal intensity have been developed and are still on going, which include using higher magnetic field, and spin relaxation techniques. By exciting these nuclei, the populations of the higher and lower energy levels will eventually become equal. If this occurs, then there will be no further absorption of radiation. The spin system is saturated. By relaxation processes, these nuclei can return to the lower energy state.

3.2 Detecting of NMR signal

The summation over the total μ_i yields: $\sum_i \mu_i = M_0$, and M_0 is the magnetization at thermal equilibrium.

$$M_0 = \frac{N\gamma^2\hbar^2 I(I+1)B_0}{3kT} \tag{3.7}$$

We often use the term of magnetization to describe the evolution of NMR signals in the vector model.

The simplest detection of NMR signal is by applying a 90-degree pulse to the equilibrium magnetization and flips it to X-Y plane and watching it evolve radiation. The magnetization begins to relax to equilibrium state. The NMR signal is record as the induced voltage in the detection coil, which is proportional to the component of the magnetization in the X-Y plane. In the future, for convenience, we use magnetization to represent NMR signal.

In the external filed B, The magnetization precesses under the torque $M \times B$:

$$\frac{dM}{dt} = \gamma(M \times B) \tag{3.8}$$

Here we do not consider the T_1 and T_2 relaxations:

In the case where the external field is along vertical direction (Z axis),

$$B = B_0\hat{k} = B_Z\hat{k}, \tag{3.9}$$

$$M(t=0) = M_0\hat{i} = M_X\hat{i} \tag{3.10}$$

The equation of M reduces to: $\frac{dM}{dt} = \gamma(M_y B_Z\hat{i} - M_x B_z\hat{j})$ (3.11)

The solution for this equation is:

$$M(t) = M_0 \cos(\omega_0 t)\hat{i} - M_0 \sin(\omega_0 t)\hat{j} \quad \text{where} \quad \omega_0 = \gamma B_0 \tag{3.12}$$

Since the detection coil is wrapped around the sample, an oscillating voltage will be induced in the coil by the oscillating magnetization in the sample. This oscillation only occur when M has X and Y components. The voltage is usually of microvolts, but it can be amplified and recorded, from which NMR signal is obtained.

When considering the effect of relaxation, the evolution of magnetization can be more accurately expressed by the Bloch Equations, which are:

$$\frac{dM_Z}{dt} = \gamma(M \times B)_Z - (M_Z - M_0)/T_1$$

$$\frac{dM_X}{dt} = \gamma(M \times B)_X - M_X/T_2 \tag{3.13}$$

$$\frac{dM_Y}{dt} = \gamma(M \times B)_Y - M_Y/T_2$$

Solving the above equations, we can obtain:

$$M_Z = M_0(1 - e^{-t/T_1})$$

$$M_X = M_0 \cos\omega t * e^{(-t/T_2)} \tag{3.14}$$

$$M_Y = M_0 \sin\omega t * e^{(-t/T_2)}$$

3.3 Relaxation Processes

In the external field B_0, at equilibrium the number of spins at lower energy state will be a little larger than the number of spins at higher energy state. When excited by radio frequency with Larmor frequency, numbers of spins at both states become equal, which means saturation. When the excitation radiation (RF) is terminated, the spin system will return to equilibrium. There are two major relaxation processes, which are spin - lattice (longitudinal) relaxation and spin - spin (transverse) relaxation.

3.3.1 Spin-Lattice Relaxation (T_1 Relaxation)

Nuclei in an NMR experiment are in a sample. The sample in which the nuclei are held is called the lattice. Atoms in the lattice are in vibrational and rotational motion, which create complex local magnetic field fluctuations. T_1 relaxation is the process of energy release from the saturated spin system into the surrounding environment, induced by local magnetic field fluctuations.

These local field fluctuations have many frequency components. Some of these components will be equal in frequency to the Larmor frequency of the nuclei of interest. These components of the fluctuating field can interact with spins in the higher energy state, causing them to lose energy (returning to the lower state).

The relaxation time, T_1 (the average lifetime of nuclei in the higher energy state) is dependent on the magnetogyric ratio of the nucleus and the atomic motion. As mobility increases, the vibrational and rotational frequencies increase, making it more likely for a component of the lattice field to be able to interact with excited nuclei. However, at extremely high motilities, the probability of a component of the lattice field being able to interact with excited nuclei decreases. T_1 is measured as the time required for the magnetization vector M to be restored to 63% of its original magnitude. Inversion recovery and saturation recovery are two major ways to measure the T_1 relaxation time.

(1) Inverse recovery

The pulse sequence for inverse recovery is shown below:

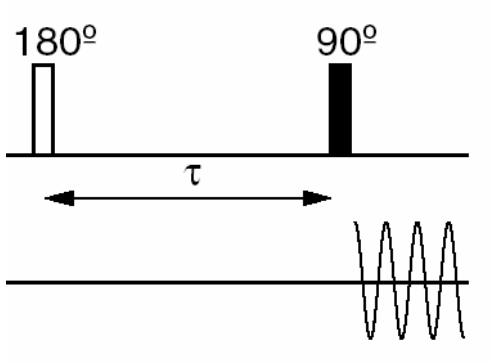

Figure 3.3: Pulse sequence of inverse recovery

The first pulse is 180 degree, which brings the magnetization to negative Z-axis with $M_Z(t=0)=-M_0$. During that period tau, the magnetization begins to relax from $-M_0$, towards equilibrium value M_0 along Z axis, the process is described by:

$$\frac{dM_z}{dt} = -\frac{M_z - M_0}{T_1}. \qquad (3.15)$$

At time of detection, t= τ , the magnetization is $M_z(\tau) = M_0(1-2e^{-\frac{\tau}{T_1}})$: (3.16)

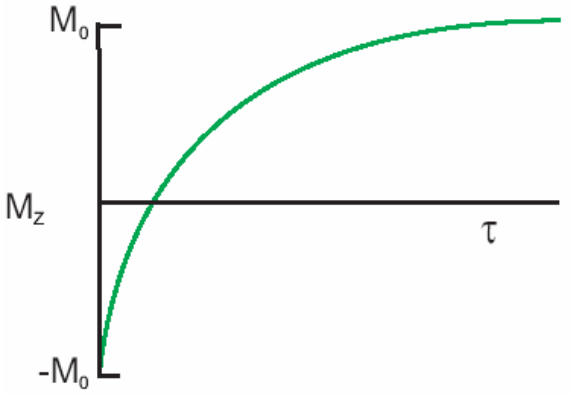

Figure 3.4: Relaxation of magnetization for inversion recovery pulse sequence

The following 90-degree pulse flips the magnetization $M_z(\tau)$ on Z-axis to X-Y plan for detection, so the NMR signal is proportional to the intensity of $M_z(\tau)$. Changing the τ value and plot $M_z(\tau)$ vs. τ, we can get the T_1 value from the curve fitting.

(2) Saturation recovery

In saturation recovery experiment, we first apply a series of pulses with certain duration, which has the total effect of eliminating the original magnetization in the Z axis, after all the RF is turned off, wait for certain time τ for the magnetization to grow along Z-axis, the increase of magnetization at Z axis will follow the rate of T_1 relaxation. Subsequent 90-degree pulse is used for detection. The theory is similar to inversion

recovery, the only difference is that here the initial magnetization is $M_Z(t=0)=0$ and

$$M_z(t) = M_0(1 - e^{-\frac{t}{T_1}}) \tag{3.17}$$

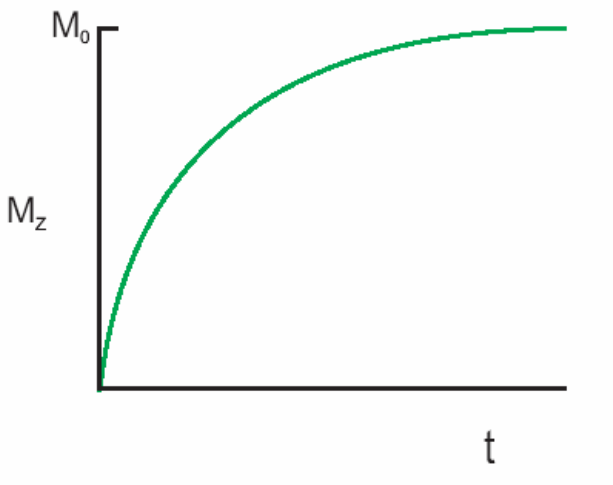

Figure 3.5: Magnetization evolution of saturation recovery sequence

The NMR signal intensity, both in time domain and frequency domain, is proportional to M_t. Usually, we make the plot of $\log\frac{M_0 - M_t}{M_0}$ versus t, and this will give a straight line with slope of $1/T_1$.

3.3.2 Spin-Spin Relaxation (T_2 Relaxation)

Spin-spin relaxation describes the interaction between neighboring spins. In this situation, the nuclei can exchange quantum states; a nucleus in the lower energy level will be excited, while the excited nucleus transits to the lower energy state. There is no net change in the populations of the energy states, but the average lifetime of a nucleus in

the excited state will decrease. This can result dechoherence and decays of M_x, M_Y magnetization, leading to linebroading. The relation of linewidth $\Delta\nu_{1/2}$ of NMR spectrum with T_2 is: $\Delta\nu_{1/2} = \frac{1}{\pi T_2}$. Since T_2 processes follow an exponential decay, the quantity T_2 is defined as the time required for the transverse magnetization vector to drop to 37% of its original magnitude.

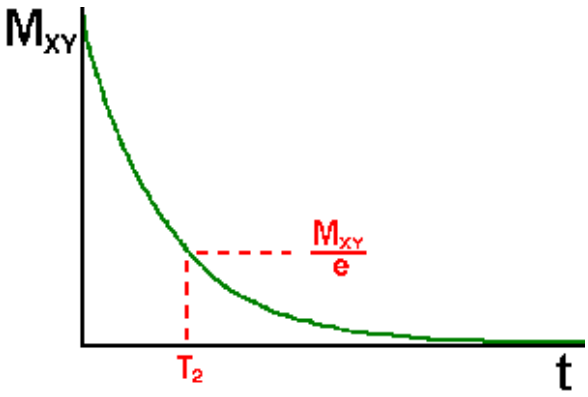

Figure 3.6: Magnetization evolutions during T_2 relaxation. At time τ, magnetization is shown as: $M_y(\tau) = M_0 e^{-\frac{\tau}{T_2}}$

Usually in liquids, $T_1 = T_2$ and the linewidth is narrow. In solids, the T_2 is much shorter than T_1, and the linewidth is much broader than that in liquid. This method can be used to study phase transition of gas or vapor in porous media where the T_1 and T_2 values show dramatic changes during phase transition. The mechanism of T_2 is affected intrinsically by T_1 mechanism, so T_2 is always smaller than T_1.

T_2 is usually measured through a spin echo, which is described as below:

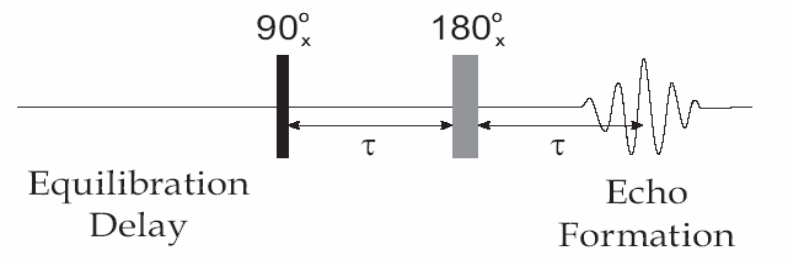

Figure 3.7: Pulse sequence of spin echo

In this pulse sequence, the first 90-degree pulse brings the equilibrium magnetization to X-Y plane, which will decay at the rate of $1/T_2$. With the echo, the magnetic moment in X-Y plane is refocused, and an echo is formed at τ after the 180^o pulse. The intensity of the signals at echo point is: $M_Y = M_0 * e^{2\tau/T2}$. The spin-spin relaxation time T_2 can be obtained by similar procedures as that for T_1.

3.4 FID Intensity and FT Spectrum Area

In this thesis, we will study the intensity of gas adsorped in SWNT. Hence the NMR signal intensity is of most interest. The pulse width, and the amplitude of power supply, and other issues are in progress. The NMR study of gas adsorption is generally based on the spectrum intensity and T_1 and T_2 analysis. The NMR spectrum intensity is proportional to the number of spins (adsorption) in the sample area, under same

experimental parameters and experimental conditions. It is reported that the amplitude of NMR free induction decay (FID) can show the amount of primary sites of water adsorbed in activated carbon, and the results obtained by NMR analysis on water adsorption isotherm agree with those obtained by other methods (Gogelashvili et al., 2002; Gogelashvili et al., 2004).

CHAPTER 4

NMR Study of Gas Adsorption

Adsorption isotherms of methane and ethane in single-walled carbon nanotubes (SWNTs) were measured by ^{1}H nuclear magnetic resonance (NMR) at room temperature. It is shown that the interior of SWNTs becomes available for methane and ethane adsorption after cutting of SWNTs. Such endohedral adsorption dominates methane and ethane adsorption in SWNTs, at least below 1 MPa. The average exchange time between molecules adsorbed inside SWNTs and free gas molecules outside was estimated to be on the order of 80 ms. It is shown that exposure to oxygen has no effect on methane and ethane endohedral adsorption in SWNTs, suggesting that the adsorption energy of oxygen molecules inside SWNTs is small compared to that of methane. ^{13}C NMR study indicates that under atmospheric pressur and room temperature helium atoms could access the interstitial sites of SWNT bundles whereas H_2, CO_2, and N_2 molecules could not.

4.1 Introduction

Single-walled carbon nanotubes possess unique nanoporous structures making interactions between guest molecules and SWNTs fascinating and important. Such interactions could play an important role in the applications of SWNTs in various areas including gas storage(Hirscher et al., 2002a; Nutzenadel et al., 1999),electronic and thermal properties(Collins et al., 2000; Kong et al., 2000; Sumanasekera et al., 2000), field emission(Saito et al., 2002), and biotechnology(Shim et al., 2002). A SWNT is formed by rolling a graphene sheet into a seamless cylinder with diameter on the nanometer scale. These individual SWNTs with similar diameters assemble into bundles in the form of a two-dimensional triangular lattice. Guest molecules could potentially interact with SWNTs via the outer surfaces of bundles, the interstitial channels between the tubes in a bundle, and the inside of the tubes.(Calbi et al., 2001) An important aspect of guest molecule/SWNT interaction is gas adsorption. This is not only important for gas storage but also crucial for understanding many other issues such as changes of electronic and thermal properties of SWNTs upon exposure to gases.(Collins et al., 2000; Kong et al., 2000; Sumanasekera et al., 2000). It also provides important information on the nanopore structures of SWNT bundles. For instance, whether the accessibility of the inside of the tubes for gas adsorption (endohedral adsorption) would depend on the openness of tube ends.

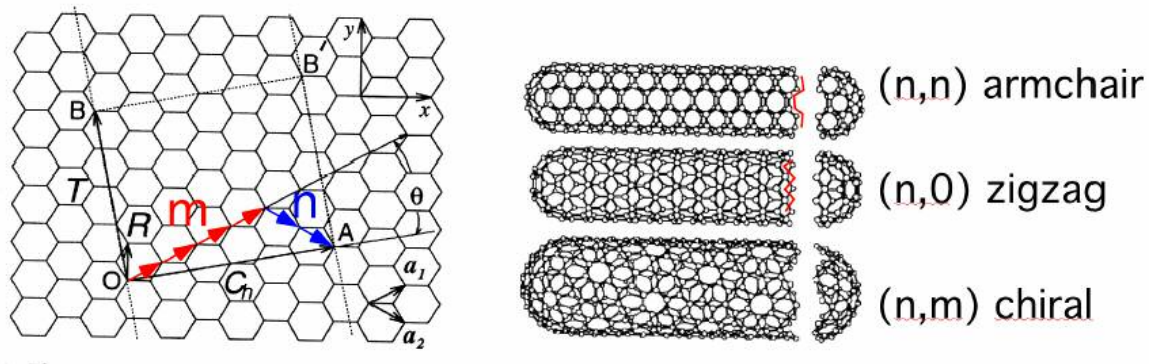

Figure 4.1: Single Wall Carbon Nanotube parameters. Left: Graphene sheet showing section (OBB'A) to be rolled into tube. Here m,n are the classification parameters. Right: examples of tubes, parameters, and names for classes of parameters(Saito, Dresselhaus & Dresselahus, 1999).

Adsorption studies were typically carried out with macroscopic techniques such as volumetric and gravimetric measurements. However, important complementary information, such as molecular dynamics and adsorption sites, could be obtained by microscopic measurements of gas adsorption. Here we describe a study of gas adsorption in SWNTs using NMR. The focus is on the adsorption of methane and ethane in cut SWNTs. It is shown that adsorption inside SWNTs dominates the observed adsorption and the presence of oxygen has no effect on the adsorption of these gases in SWNTs.

4.2 Experimental Setup

SWNTs were synthesized by laser ablation and the raw materials were subsequently purified as described in detail elsewhere.(Tang et al., 2000) Some of the purified SWNTs synthesized using 0.6 at% (each) Ni/Co as catalyst were cut to shorter tubes by sonication

in 3:1 ratio of H_2SO_4 and HNO_3 solution for 24 hours.(H. Shimoda & O. Zhou, 2002) The average length of cut SWNTs is about 0.5 μm. Both the cut and uncut SWNTs are in the form of bundles with average diameters of about 12 nm and obtained by examining pictures of transmission electron microscopy. These samples are over 90% pure SWNTs. A SWNT sample made with 2.4 at% (each) Rh/Pd as catalyst was also used in this study. The average diameter of the nanotubes estimated by Raman measurements is 1.4 nm in samples made with 0.6 at% (each) Ni/Co as catalyst and 0.85 nm in the sample made with 2.4 at% (each) Rh/Pd as catalyst.(Tang et al., 2000) The section of the quartz NMR sample tube within the NMR coil has a volume of 5.3×10^{-2} cm^3 and is filled up with 15 mg of SWNTs. For SWNT diameter of 1.4 nm and an average bundle size of 12 nm (about 37 SWNTs per bundle), the estimated specific density of such a close-packed SWNT bundle is 1.33 g/cm^3. Therefore, SWNTs of 15 mg would occupy an estimated volume of only 1.2×10^{-2} cm^3, 20% of the 5.3×10^{-2} cm^3 NMR sample tube volume within the NMR coil. Thus, although the SWNTs spread out over the entire volume of the sample space, the sample packing was not dense. For gas loading, the NMR sample tube was connected to a stainless steel tubing vacuum system connected to various pressurized gas sources.

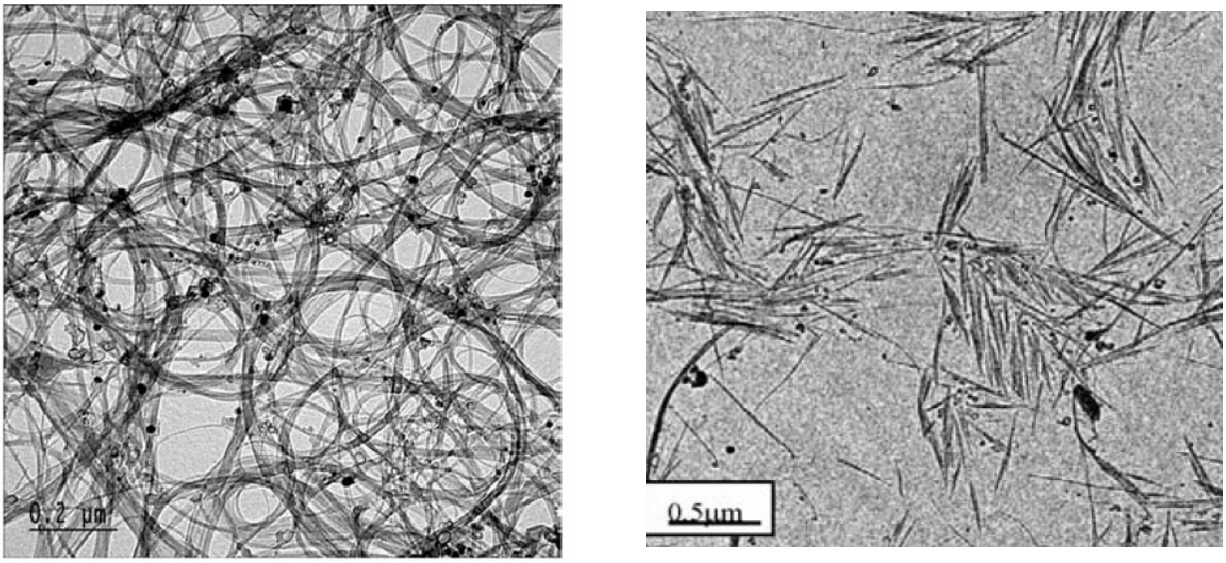

(a) (b)

Figure 4.2: (a): TEM image of purified SWNT bundles. (b): Low resolution TEM image of acid treated SWNT bundles. (Geng et al., 2004)

The system was leak-tested rigorously. No increase of NMR proton signal was detected after several days with sample under vacuum but without dynamic pumping. All ^{1}H NMR measurements were carried out at room temperature (RT) in either a superconducting magnet of 4.7 Tesla or an iron magnet of 0.8 Tesla. All samples were first annealed at 400°C for 1 hour at 5×10^{-6} torr in the quartz NMR sample tube before NMR measurements.

4.3 Results and discussions

The results and discussion will include four parts: adsorption isotherm, spin-spin and spin-lattice relaxation, endohedral adsorption and effects of exposure to oxygen.

4.3.1 Adsorption Isotherms

Figure 4.3 shows RT ^{1}H spectra of cut SWNTs exposed to methane and ethane, respectively, at a pressure of 0.045 MPa. Both spectra have a sharp peak and a broad peak. The sharp peak is attributed to gas molecules in the region of the NMR sample tube unoccupied by SWNTs, about 80% of the sample tube volume within the NMR coil.

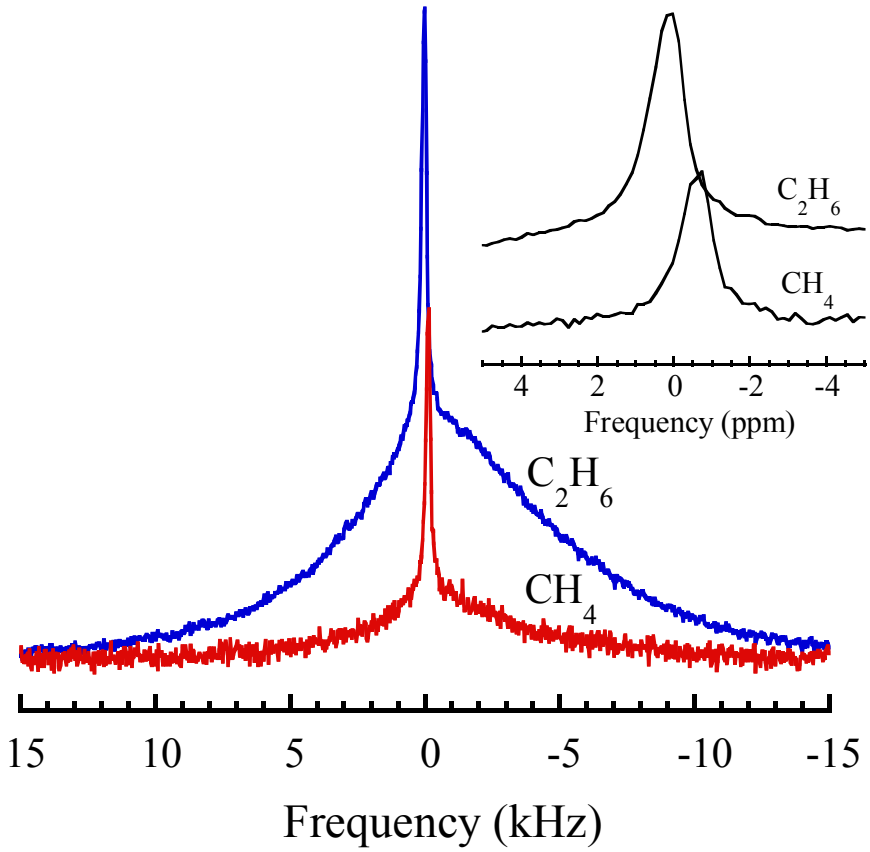

Figure 4.3: RT ^{1}H spectra of cut SWNTs exposed to 0.045 MPa CH_4 and C_2H_6 measured at 4.7 Tesla. The central narrow peaks (see inset) represent gas molecules in the free space between SWNT bundles in the NMR tube. The observed chemical shift difference of 0.75 ppm is characteristic of the two gases. The broad peaks represent gas molecules adsorbed on SWNTs. Both the broad and narrow peaks can be fit with Lorentzian lines.

Fig 4.4 shows the intensities of these two peaks versus pressure for both methane and

ethane. The intensity of the sharp peak is proportional to the pressure, consistent with the ideal gas behavior. The chemical shift difference of 0.75 ppm between the sharp peaks in the ethane and methane proton spectra, as shown in the inset of Fig. 4.3, is in perfect agreement with the expected chemical shift difference between free ethane and methane gas molecules.

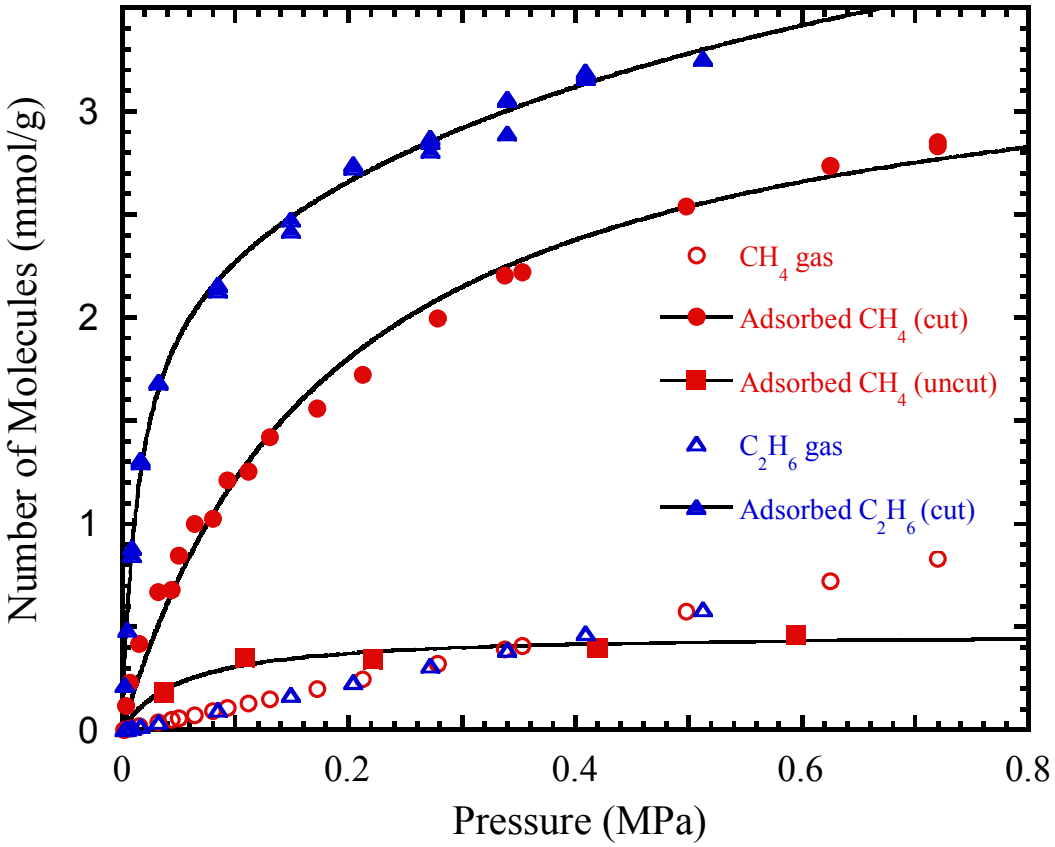

Figure. 4.4: Pressure dependence of the intensities of the narrow (free gas) and broad (adsorbed) peaks of the ^{1}H spectra (see Fig. 4.3) of cut SWNTs exposed to CH_4 and C_2H_6 at RT.

For comparison, CH_4 adsorption in uncut SWNTs at RT is also shown. Both the cut and uncut SWNT samples were produced under the same conditions. The solid lines are Langmuir-type adsorption curve fits discussed in the text. No significant hysteresis effect was observed for the adsorption curves. The unit of adsorption is mmol per gram, namely, the number of mmol adsorbent molecules per gram of SWNTs. A multiplication factor of 1.33 g/cm^3, the density of maximum-packed SWNT sample, converts the unit to $mmol/cm^3$. For the gas peak, the intensity

is the number of mmol of free gas molecules in our NMR sample tube divided by 0.015 g of SWNTs. A factor of 15×10^{-3} $g/4.1\times10^{-2}$ cm^3 converts the gas peak intensity to a gas density in unit of $mmol/cm^3$.

To further confirm the negligible contribution of adsorption to this sharp peak we compared this sharp peak intensity for CH_4, C_2H_6, and H_2. In all three cases, the measured intensity of the sharp peak corresponds to the same number of molecules at the same pressure. Since the adsorption energy of H_2 on SWNTs is expected to be much smaller than that of C_2H_6 and CH_4,(Stan & Cole, 1998; Zhao et al., 2002) this proves that the contribution of adsorbed molecules to this sharp peak is negligible. The absolute number of molecules associated with this sharp peak can be calculated by assuming an ideal gas occupying a volume of 4.1×10^{-2} cm^3 (80% of the NMR sample space volume).

In contrast to the sharp peak, the broad peak in Fig. 4.3 shows characteristic

behaviors of adsorption. Its intensity increases nonlinearly with pressure as shown in Fig. 2. An analytical description of such adsorption isotherm, although an oversimplified one, is Langmuir adsorption described by(Boer, 1968)

$$n(P,T) = n_\infty \frac{bP}{1+bP} \tag{5.1}$$

where $n(P,T)$ is the number of adsorbed molecules as a function of pressure P and temperature T, n_∞ is the number of adsorption sites, and b is given by(Boer, 1968)

$$b = \frac{\sigma}{\nu_0 \sqrt{2\pi m k_B T}} \exp(E_d / k_B T) \tag{5.2}$$

where σ is the effective area covered by an adsorbed molecule with mass m and k_B is the Boltzmann constant. ν_0 is the prefactor of the desorption rate constant $k = \nu_0 \exp(-E_d / k_B T)$ with a typical value of $\nu_0 = 1 \times 10^{13}$ s^{-1}, E_d is the activation energy of desorption. The adsorption isotherm of methane can be fit by Eq. (1) with $E_d = 235 \pm 2$ meV (22.7 kJ/mol) and $n_\infty = 3.5 \mp 0.2$ mmol/g as shown in Fig. 2. For this fitting $\sigma = 1.6 \times 10^{-19}$ m^2 was used based on the bulk liquid density of methane. Measurement of endohedral adsorption of supercritical methane in SWNTs has not been reported previously. Calculations based on nonlocal density functional theory (DFT) and grand canonical Monte Carlo (GCMC) simulation showed that endohedral adsorption of supercritical methane in SWNT of diameter 1.4 nm deviates strongly from linear pressure dependence at 1 MPa where the level of saturation is nearly achieved (Skoulidas et al., 2002; Tanaka et al., 2002). In contrast to the calculated endohedral adsorption, the

calculated adsorption on the outside of SWNT shows linear pressure dependence up to 1 MPa with no effect of saturation(Tanaka et al., 2002). Thus, the strongly nonlinear pressure dependence of the broad peak intensity is inconsistent with adsorption on the outside of bundles and is consistent with endohedral adsorption based on DFT and GCMC simulations. The observed number of adsorbed CH_4 molecules shown in Fig. 4.4 is also consistent with what was expected from filling the inside of SWNTs as evidenced by the good agreement with GCMC simulations for endohedral adsorption of (10,10) SWNT (Skoulidas et al., 2002) and SWNTs with diameter of 1.4 nm(Tanaka et al., 2002). It is interesting to note that the activation energy $E_d = 235$ meV is comparable to the observed adsorption energy of 222 meV associated with the groove sites of SWNT bundles.(Talapatra & Migone, 2002; Weber et al., 2000) The concave curvature of endohedral adsorption sites could lead to the increased adsorption energy as compared to that on graphite. Similarly, the effective concave curvature of the grooves on SWNT bundles could also lead to such enhancement. The adsorption energy of groove sites is the largest among all other adsorption sites on the external surface of SWNT bundles. However, the number of groove sites is much smaller than that of endohedral adsorption sites in our sample. The derived activation energy E_d should only be considered as a crude estimate of the adsorption energy of endohedral sites because of the oversimplified nature of the Langmuir adsorption isotherm. There are other uncertainties such as the prefactor ν_0 which could deviate somewhat from 1×10^{13} s^{-1} as assumed in the fitting

(Fichthorn & Miron, 2002).

Since an ethane molecule contains more atoms than methane, the adsorption energy of ethane is expected to be larger than that of methane on the same surface. The reported adsorption energy of methane on graphite surface is 126 meV whereas that of ethane is 170-190 meV.(Vidali et al., 1991) The adsorption isotherm of the broad peak for ethane shows that this is indeed the case. Figure 2 shows that significant adsorption of ethane occurs at much lower pressure compared to methane. The fitting of the adsorption isotherm, however, requires two components with different activation energies. The component with higher activation energy is well constrained by the data with $E_d = 303 \pm 15$ meV (29.2 kJ/mol) and $n_\infty = 2.2 \mp 0.2$ mmol/g. Here, $\sigma = 2.0 \times 10^{-19}$ m^2 was used in the fitting based on the bulk liquid density of ethane. Because of the lack of data at higher pressure, the component with lower adsorption energy around 200 meV is not well constrained and has a very large degree of freedom in the fitting parameters of E_d and n_∞. Obviously, the fitting procedure here does not necessarily imply the existence of two adsorption sites for ethane. The functional form of the adsorption isotherm for the current case needs to be calculated using DFT and GCMC simulations. Langmuir adsorption is an oversimplified description for endohedral adsorption in SWNTs where molecular interactions are expected to be dependent on the degree of loading inside the tubes. Nevertheless, the Langmuir fitting analysis provides some useful information for comparing the adsorption data of methane and ethane. The adsorption of

methane in the pressure range of current experiments corresponds to the portion of ethane adsorption described by the component with $E_d = 303$ meV. The ratio of 303 meV and 235 meV is comparable to the ratio of the adsorption energies of ethane and methane on graphite surface. The component with smaller adsorption energy for ethane does not have a corresponding component in the observed methane adsorption isotherm. This is fully expected since the corresponding component for methane would have much lower adsorption energy and will not contribute significantly to the adsorption isotherm in the pressure range of current experiments. It is worth to point out that adsorption on residual Ni/Co particles cannot contribute to the observed adsorption by NMR since the magnetic effect on such magnetic particle surfaces will wipe out the NMR signals. Also, under the current experimental conditions, no evidence of molecular hydrogen adsorption was observed by NMR method.

4.3.2 Spin-Spin and Spin-Lattice Relaxations

The spin-spin relaxation time was measured with the Hahn-echo pulse sequence 90°-τ-180°-τ-echo (Slichter, 1989). Figure 4.5 shows the decay of the Hahn-echo height S_{echo} as a function of the dephasing time 2τ for ethane at 0.093 MPa measured at 4.7 Tesla.

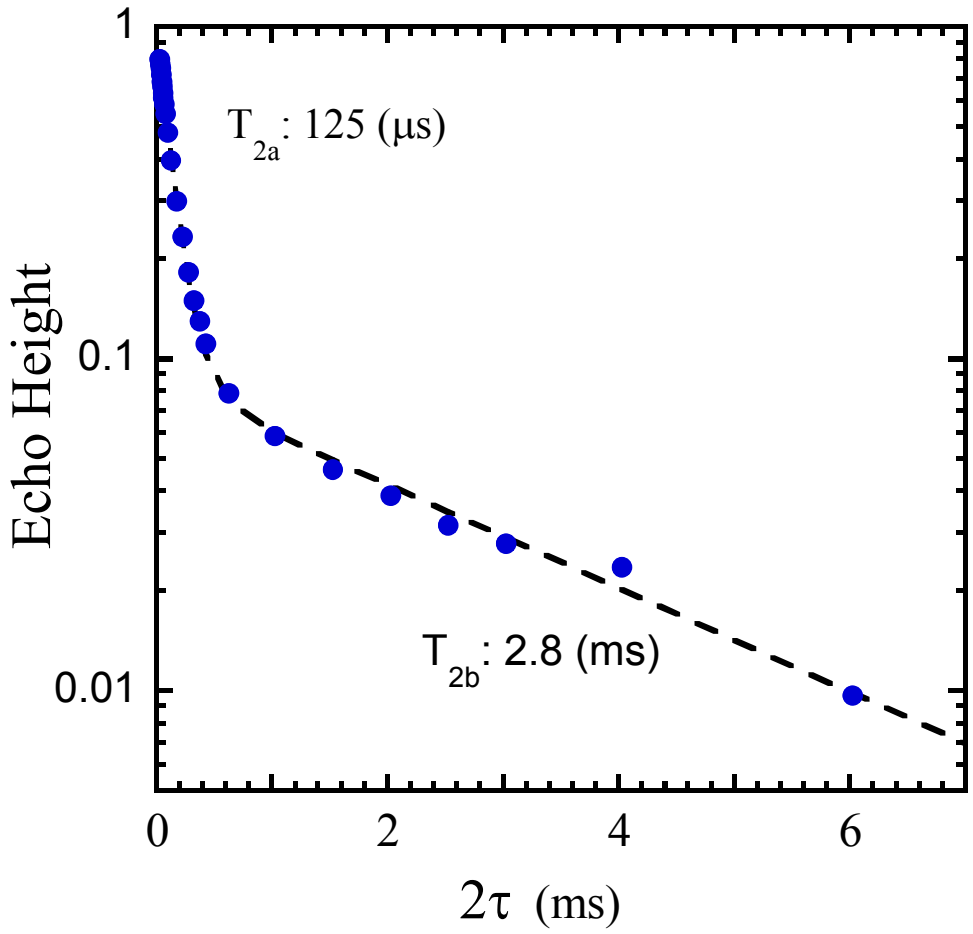

Figure 4.5: Decay of the 1H Hahn echo intensity at RT as a function of dephasing time 2τ measured for C_2H_6 gas at 0.093 MPa in contact with cut SWNTs (4.7 T). The plot clearly indicates two components in the echo decay. The dashed line is a fit using double exponential decays. The component with T_{2a} = 0.125ms is associated with molecules adsorbed inside SWNTs whereas the much longer T_{2b} = 2.8 ms corresponds to free gas molecules.

It clearly shows that there exist two components of exponential decays described by $S_{echo} = a\exp(-2\tau / T_{2a}) + b\exp(-2\tau / T_{2b})$ where a and b are the intensities and T_{2a} and T_{2b} are the spin-spin relaxation times of the two components. Fitting shows that $T_{2a} = 125 \pm 3\,\mu s$ and $T_{2b} = 2.8 \pm 0.1$ ms. Analysis of the spectrum corresponding to each

2τ value shows that the $T_{2a} = 125\,\mu s$ component corresponds to the broad peak and the $T_{2b} = 2.8$ ms component corresponds to the sharp peak. The ratio *a*/*b* is exactly the same as the intensity ratio of the broad and sharp peaks of the spectrum. Within experimental error, T_{2a} does not depend on the pressure or the magnetic field. For methane the observed $T_{2a} = 160 \pm 10$ μs is also independent of the pressure and the magnetic field. T_2 in porous media could originate from diffusion-induced local field variation due to magnetic susceptibility effect.(Callaghan, 1991) In general, carrying out measurements at low magnetic field where the magnetic susceptibility effect is reduced can reduce such fluctuations. The reason that such field dependence did not occur for T_{2a} can be understood by analyzing the origin of the line broadening for the broad peak. Small amount of Co/Ni magnetic particles exist in SWNT samples even after purification and cutting. Such magnetic particles produce a distribution of local fields throughout the sample. For gas molecules moving rapidly throughout the sample space, such local field distribution is averaged out over the NMR timescale leading to the sharp resonance peak. For adsorbed molecules confined in space over the NMR timescale, molecules experience different local fields depending on their locations. This local field distribution causes line broadening. As long as the external magnetic field is larger than the coercive field of the magnetic particles, the local field distribution caused by such magnetic particles is independent of the external magnetic field. The lineshape of the broad peak can be fit very well by a Lorentzian line. The full-width-at-half-height (FWHH) linewidth are

7.5 ± 0.5 kHz and 7.0 ± 0.5 kHz for the spectra taken at 4.7 and 0.8 Tesla, respectively. The effect of T_2=125 μs contributes to a Lorentzian line broadening of FWHH=2.5 kHz. Clearly, the local field is dominated by the contribution of magnetic particles. This explains the observed independence of the broad peak T_2 on the external magnetic field. The small difference of the broad peak T_2 for methane and ethane are most likely due to the different diffusion rate of methane and ethane inside SWNTs (Mao & Sinnott, 2000).

Spin-lattice relaxation was also measured for both the sharp and broad peaks. Spin-lattice relaxation time T_1 was determined by measuring the recovery rate of the nuclear magnetization (M) after saturation. Here, M was measured as a function of recovery time t after saturation and T_1 is the time constant of the curve $M^*(t)=1-M(t)/M(\infty)$.

Figure 4.6 shows the T_1 values of both the sharp and broad peaks of ethane as a function of pressure measured at 4.7 Tesla. As expected from the well-known NMR properties of gases in the fast motion limit(Abragam, 1985), T_1 of the gas phase peak increases linearly with pressure due to the increased rate of molecular collision. However, the straight line of T_1 versus P does not go through the origin (0,0) when extrapolated to zero pressure.

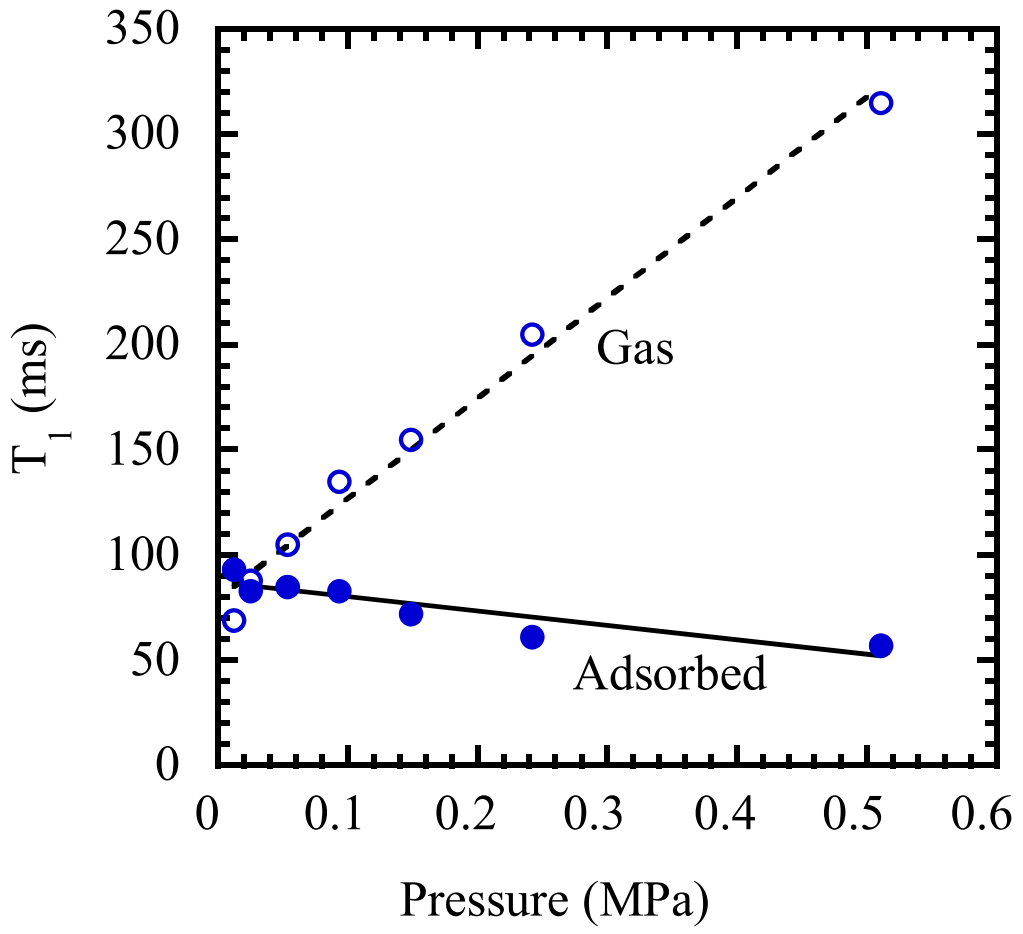

Figure 4.6: Pressure Dependence of the spin lattice relaxation time T_1 for C_2H_6 gas in contact with cut SWNTs (4.7 T). The T_1 of the free gas in the NMR tube (narrow peak) shows a linear increase with pressure characteristic of gas systems. The broad peak representing the adsorbed molecules displays a slight decrease with pressure in T_1.

This is most likely due to molecular collisions with walls of SWNT bundles in the porous sample space. Here, T_1 is determined by $T_1 = \alpha_{gas} P + R_{wall}$ where the first term is proportional to the pressure-dependent collision rate of a gas molecule with other gas molecules and the second term is proportional to the collision rate of a gas molecule with

walls of SWNT bundles. The last term is independent of pressure. Unlike the sharp peak, T_1 of the broad peak decreases slightly with increasing pressure. The much weaker pressure dependence of T_1 is consistent with adsorption although the relaxation mechanism remains to be determined. It is interesting, however, that the T_1 values of the broad and sharp peaks merge toward a common value at low pressure. This seems to indicate that molecules in the gas phase and the adsorbed phase undergo sufficient exchanges at low pressure on the T_1 timescale of about 80 ms. Two-dimensional exchange spectroscopy needs to be carried out for further investigation.

4.3.3 Endohedral adsorption

As discussed earlier, the adsorption isotherms are consistent with endohedral adsorption. The properties of the spin systems also support this assignment. When the adsorbed phase and the gas phase are in equilibrium, adsorbed molecules and gas molecules undergo rapid exchanges due to adsorption and desorption. The residence time t_s of a molecule adsorbed on the surface before desorbing into the gas phase can be estimated by(Boer, 1968):

$$t_s = 10^{-13} s \exp(E_d / k_B T). \qquad (5.3)$$

For $E_d = 235$ meV and T=300 K, $t_s = 9 \times 10^{-10}$ s. The average time t_g a molecule spends in the gas phase can be estimated by $N_g / t_g = N_s / t_s$ where N_g and N_s are the number of gas and adsorbed molecules involved in the exchange, respectively. The

exchange rate between the gas and adsorbed molecules is given by $R_{exch} = 1/(t_g + t_s)$. If the broad peak (Fig. 4.3) were due to adsorption on a surface, which is in direct contact with the gas phase, such as the surface of SWNT bundles, N_g and N_s would be on the same order of magnitude (Fig. 4.3) and t_g would be comparable to t_s. Therefore, $1/R_{exch}$ would be much shorter than the free-induction decay timescale of hundred microseconds and only one resonance peak would be observed by NMR due to rapid exchange. This is clearly not the case as shown in Fig. 4.3. It is worth to mention that despite the uncertainty with regard to the value of E_d, the residence time is undoubtedly much shorter than the NMR timescale. For instance, even with $E_d = 400$ meV, the estimated residence time of $t_s = 5 \times 10^{-7}$ s would still be much shorter than the free-induction decay timescale.

The two distinguished T_2 values for the adsorbed and gas peaks indicate also that the timescale of exchange is longer than hundred microseconds. In fact, the two distinguished T_1 values at higher loading (Fig. 4.6) indicate that the exchange time could be comparable to 80 ms. This is inconsistent with adsorption on a surface which is in direct contact with the gas phase. The long exchange time is consistent with endohedral adsorption. There, adsorbed molecules could not be desorbed directly into the gas phase without exiting the ends of SWNTs. Thus, the effective number of N_s involved in the exchange is extremely small (on the order of the number of tube ends). This makes t_g extremely long according to $t_g = t_s N_g / N_s$. This supports again the assignment of the observed

adsorption to endohedral adsorption. Further support for the assignment of endohedral adsorption comes from the NMR adsorption measurement of methane in an uncut SWNT sample produced under the same conditions as the cut SWNT sample. The result is shown in Fig. 2. Here, the adsorption isotherm has a very similar functional form and apparent adsorption energy as that in the cut SWNT sample. However, the level of adsorption is about 10 times smaller. This is consistent with the understanding that the ends of most SWNTs are capped without cutting. A small fraction of SWNTs are accessible for endohedral adsorption due to defective walls or ends.

4.3.4 Effects of exposure to oxygen and other gases

In order to evaluate the influence of oxygen on adsorption of methane and ethane in SWNTs, competitive adsorption between O_2 and methane and between O_2 and ethane were studied. Figure 4.7 shows a proton spectrum under exposure of 0.055MPa pure methane. Also shown is a proton spectrum obtained by first exposing SWNTs to 0.079 MPa O_2 and then adding methane with a partial pressure of 0.055 MPa. The two spectra are virtually identical. Similar experiments were done also with ethane and no effect of O_2 on ethane adsorption was observed.

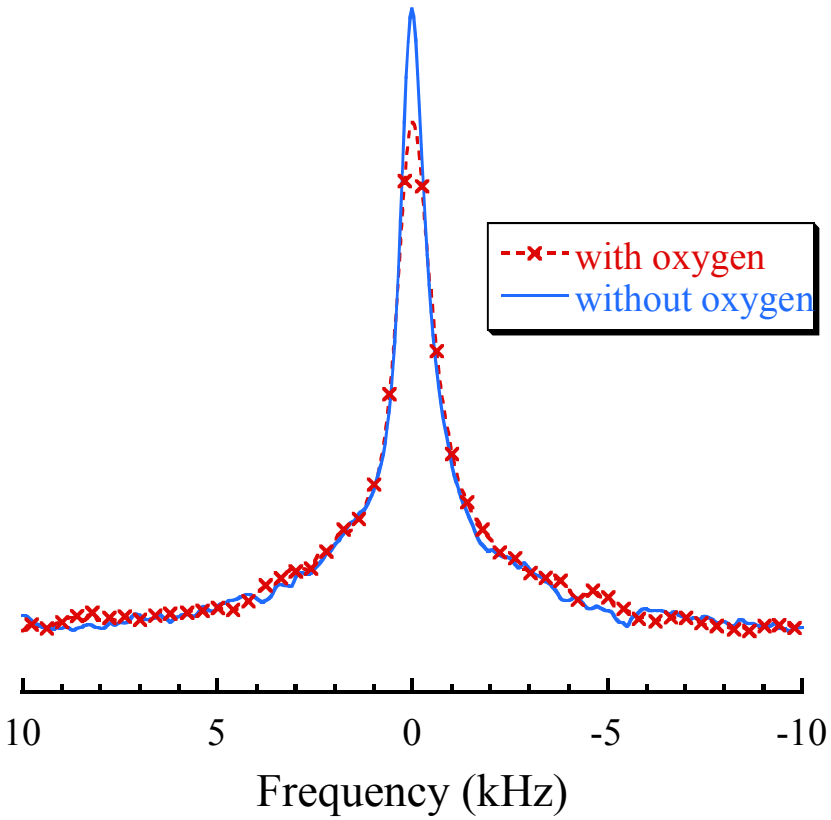

Figure 4.7: ^{1}H spectrum of cut SWNTs exposed to 0.055 MPa CH_4 measured at 0.8 Tesla and RT. Also shown is a ^{1}H spectrum measured at 0.8 Tesla and RT obtained by first exposing cut SWNTs to 0.079 MPa O_2 and then adding CH_4 which has a partial pressure of 0.055 MPa. The two spectra are virtually identical. The small difference in the gas peak height is due to a slightly larger line broadening of the spectrum with oxygen due to magnetic field drift of the iron magnet. This drift is also responsible for the broader appearance of the gas peaks compared to that in Figure 4.2.

This experiment demonstrates that endohedral adsorptions of methane and ethane are stronger than endohedral adsorption of O_2 in SWNTs. This is consistent with recent measurements and calculations showing that adsorption energy of O_2 in SWNTs is small (Ricca & Drocco, 2002; Ulbricht, Moos & Hertel, 2002).

There is another novel feature associated with gas adsorption in SWNTs. That is, if gas molecules could access the interstitial sites of the bundles, they can access all carbon atoms areas. As a result, ^{13}C NMR could be affected upon exposure to gas molecules. Figure 6 shows the changes of the ^{13}C saturation recovery curve upon exposure to different gases in an uncut SWNT sample made with 2.4 at% (each) Rh/Pd as catalyst.

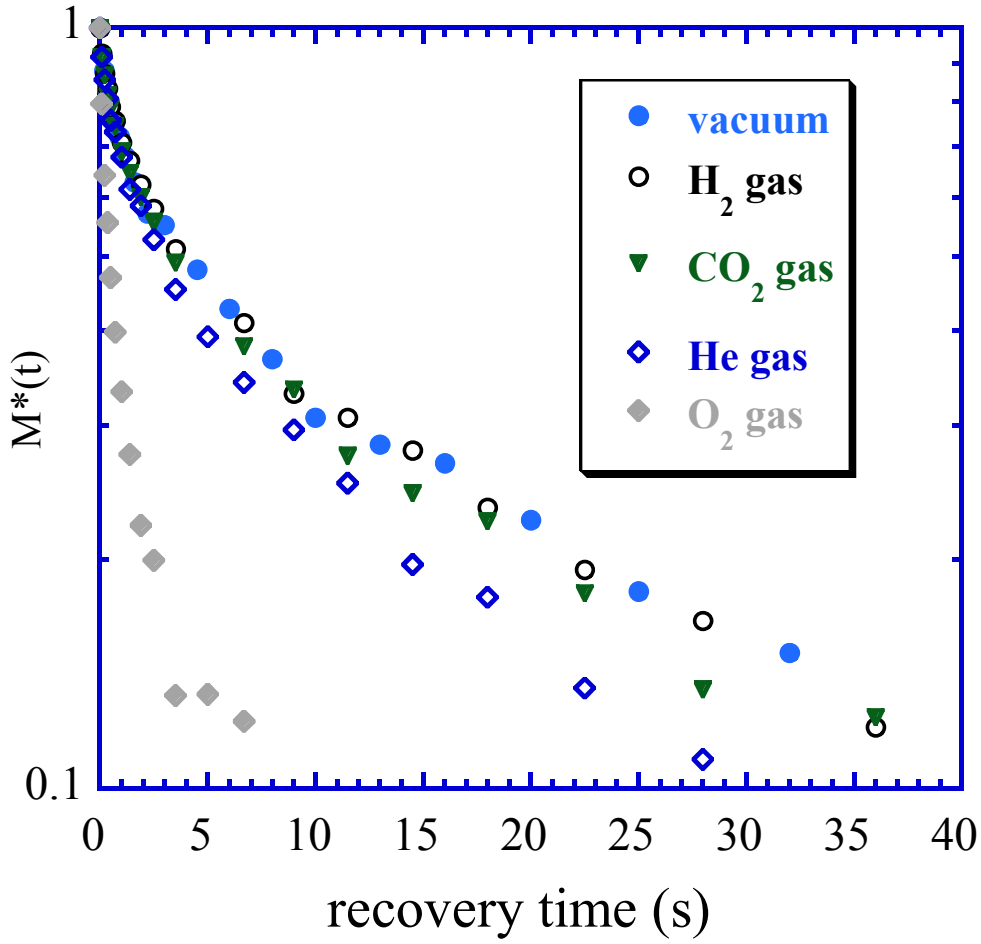

Figure 4.8: ^{13}C saturation recovery curve measured for SWNTs (10 % enriched in ^{13}C, uncut, Pd/Rh catalysts) at 9.4 Tesla. ^{13}C nuclei on SWNTs in vacuum, exposed to H_2, CO_2, and N_2 (not shown for clarity) gases at 0.17 MPa show the same relaxation behavior.

It is clear that oxygen has a dramatic effect on the relaxation behavior. We believe that this effect is due to the fact that oxygen molecules are paramagnetic. Magnetic field fluctuations caused by O_2 create an additional channel for energy relaxation of ^{13}C nuclear spins. Since ^{13}C relaxation time is very long, the effect of O_2 is quite significant. In contrast, exposures of SWNTs to 0.17 MPa CO_2, H_2, and N_2 have no effect on ^{13}C spin-lattice relaxation. It is interesting to note that exposure to 0.1 MPa helium does have a noticeable effect on ^{13}C spin-lattice relaxation. This means that He could access the majority of carbon atoms in uncut SWNTs. The perturbation of the electron cloud around carbon due to collisions with He atoms could contribute to spin-lattice relaxation. This shows that He atoms can access the interstitial sites of the bundles whereas CO_2, H_2, and N_2 cannot. The effect of helium is consistent with previous studies (Sumanasekera et al., 2000).

4.4 Conclusions

The reported study shows that NMR is an effective tool for studying gas adsorption in SWNTs. Proton NMR shows that the interior of SWNTs becomes available for methane and ethane adsorption after cutting of SWNTs. Such endohedral adsorption dominates methane and ethane adsorption in SWNTs below 1 MPa. The observation agrees with calculations of endohedral adsorption using DFT and GCMC simulations. It was found that exposure to oxygen has no effect on methane and ethane endohedral adsorption in

SWNTs. This suggests that the adsorption energy of oxygen molecules inside SWNTs is smaller than that of methane. No evidence of adsorbed molecular hydrogen was found by NMR method under the current experimental conditions. ^{13}C NMR indicates that helium could access the interstitial sites of SWNT bundles whereas H_2, CO_2, and N_2 molecules cannot do that under atmospheric pressure. (Sumanasekera et al., 2000; Teizer et al., 1999; Teizer et al., 2000)

CHAPTER 5

NMR Study of Water Adsorption in SWNTs

5.1 Introduction.

The behavior of water in hydrophobic nanochannels is of great interest for its biological importance. This has inspired intensive research of water in SWNTs including both theory such as molecular dynamics simulation and experiments, which includes X-Ray diffraction, neutron diffraction, and NMR. In this chapter, we study the adsorption isotherm of water in SWNTs at room temperature using NMR. The effect of primary adsorption sites is proved to be significant in our SWNT sample.

5.2 Research Background

The relatively large endohedral volume of SWNTs makes them possible candidates for adsorption for a variety of energy gases as well as water (Dillon et al., 1997; Eswaramoorthy, Sen & Rao, 1999; Kleinhammes et al., 2003; Stan & Cole, 1998; Stan et al., 1999; Strobel et al., 1999; Tanaka et al., 2002; Zhao et al., 2002). The

quasi-one-dimensional character of SWNTs has attracted more and more research attention on the adsorption of water in it, partly due to the fact that it may make SWNTs be used as a model system for understanding water transport in biological cells and possibly for drug delivery applications (Allen, Hansen & Melchionna, 2003; Dellago & Hummer, 2006; Dellago et al., 2003; Hummer et al., 2001; Kalra, Garde & Hummer, 2003; Kotsalis, Walther & Koumoutsakos, 2004; Liu & Wang, 2005; Liu et al., 2005; Truskett, 2003; Xue & Chen, 2006; Zheng et al., 2005). Dujardin studied the capillarity and wetting of carbon nanotube, and predicted that water can wet the nanotube (Dujardin et al., 1994). It is believed that when confined in such small cylinder pore of SWNT, water will have much different dynamic and phase properties than bulk state, which has stimulated a variety of researches (Gordillo & Marti, 2000; Koga et al., 2001; Maniwa et al., 2002; Mart & Gordillo, 2001). So far, most of the researches are based on molecular dynamics simulation(Gogotsi, Naguib & Libera, 2002; Gordillo & Marti, 2000; Koga et al., 2001; Kolesnikov et al., 2006; Mann & Halls, 2003; Maranon Di Leo & Maranon, 2003; Walther et al., 2001), experimental research with X-ray diffraction (XRD), neutron diffraction, and NMR are also reported(Alexander et al., 2004; Ghosh, Ramanathan & Sood, 2004; Maniwa et al., 2002; Mao et al., 2006; Matsuda et al., 2006; Sekhaneh et al., 2006). With controversial reporting, the key question, whether water can be adsorbed inside SWNTs at room temperature are yet to be clarified. In this chapter, we will discuss our NMR results on this topic.

5.2.1 Current Reports Based on Compute Simulation

Hummer et al. reported the first influential simulation result of water in SWNT in 2001(Hummer et al., 2001). They predicted water chains of 5 to 7 molecular flipping in and out SWNT in nanoseconds, which was one of the earliest reports of water in SWNT, by changing the potential of water molecules in nanotube,.

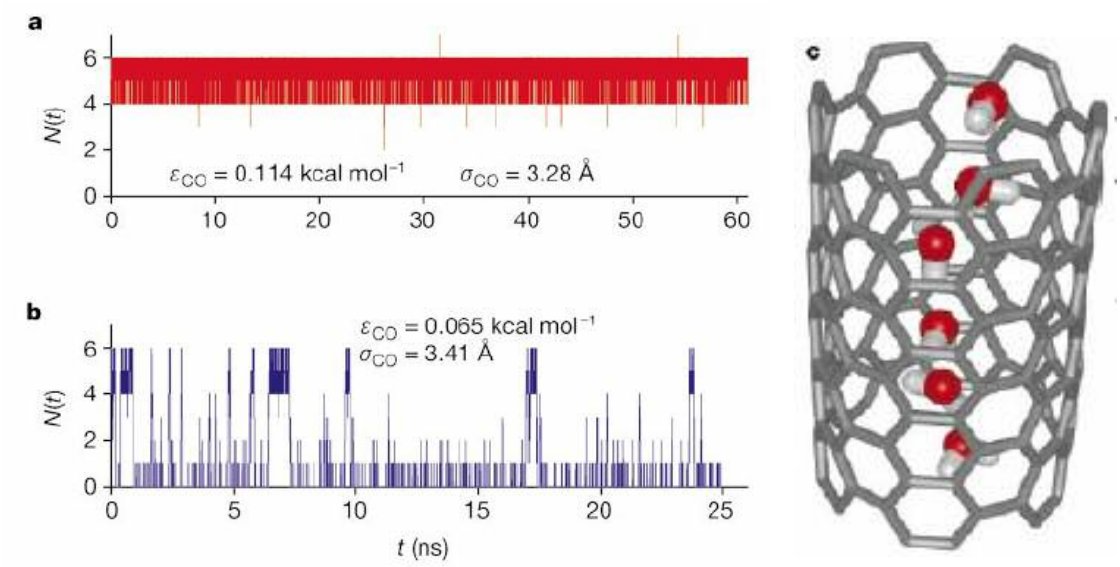

Figure 5.1: Water chains flipping in SWNT predicted by simulation. Number of water molecules inside the nanotube as a function of time for sp^2 carbon parameters (a) and reduced carbon water attractions (b), structure of the hydrogen-bonded water chain inside the nanotube (c). Nanotubes fills in several picoseconds and remain filled for 66 ns (G. Hummer et al. Nature 414, 188(2001).

At high pressure (50MPa) and low temperature (230K), water inside cylindrical pores of SWNT of diameter of 1.42 nm is expected to form ice of orderly stacked 6-to 7-moclular water rings (Alexander et al., 2004; Koga et al., 2001; Koga et al., 2002; Koga, Tanaka &

Zeng, 2000; Koga, Zeng & Tanaka, 1997; Maniwa et al., 2002).

Another characteristics of water confined in SWNT is the change of hydrogen bond. Compare to bulk water, the average number of hydrogen bond in SWNT will be decreased and the density of hydrogen bonds always redistribute.

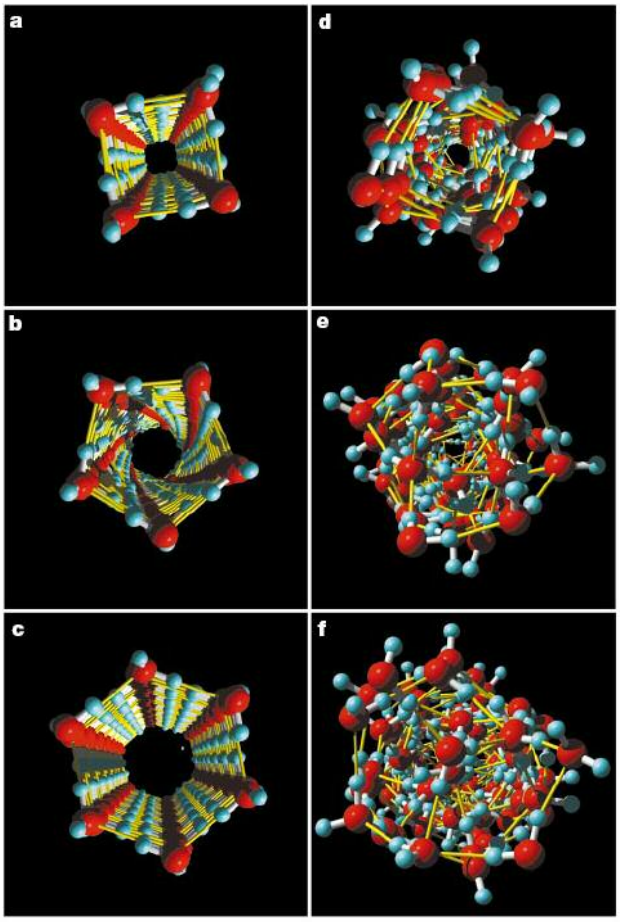

Figure 5.2: Snapshots of ice formed in SWCNs with different molecular coordinates. a, Square; b, pentagonal; c, hexagonal ice nanotubes in (14,14), (15,15) and (16,16) SWCNs; d to f, the corresponding liquid phases. The ice nanotubes were formed on cooling under an axial pressure of 50 MPa in molecular dynamics simulations. The nearest-neighbor distances in both ice nanotube and encapsulated liquid water are fairly constant, about 2.7 to 2.8 Å, and this is in part responsible for the novel phase behavior (Koga. et al, Nature Vol. 412, 802(2001).

The average number of hydrogen bonds for water inside the tube has a maximum between the center and walls of nanotube (Gordillo & Marti, 2000; Gordillo & Marti, 2001; Marti & Gordillo, 2002; Marti & Gordillo, 2003). Zhao et al predicted that water should be at a distance of 0.27 nm from the surface of the nanotubes (Zhao et al., 2002).Dellago et al. predicted that the proton transport through water-filled carbon nanotubes, the proton mobility along 1D water chains exceeds that in bulk water by a factor of 40 and reduced with orientational defects(Dellago et al., 2003). Walther studied the structure properties of water surrounding a carbon nanotube and found that the average number of hydrogen bonds decreases from a value of 3.73 in the bulk phase to a value of 2.89 at the carbon-water interface(Walther et al., 2001). Striolo used Grand canonical Monte Carlo simulations and found that at room temperature and low pressure, the adsorption of water in SWNT is negligible and then followed by sudden and complete filling after passing the threshold pressure, the layered structures are observed when the internal diameter of the nanotubes is commensurate to the establishment of a hydrogen-bonded network. The structure of water in (8:8) and (10:10) SWNTs is ordered when the temperature is 298 and 248 K, respectively. The hysteresis critical temperature vitiates with temperature. (Striolo et al., 2006; Striolo et al., 2005a; Striolo et al., 2005b; Striolo et al., 2005c). Similar molecular dynamic simulation results are also reported (Banerjee et al., 2007; Byl et al., 2006; Dellago & Naor, 2005; Desbiens et al., 2005; Gordillo & Marti, 2003; Gordillo, Nagy & Marti, 2005; Hanasaki & Nakatani, 2006;

Huang et al., 2006; Ju & Chang, 2004; Kolesnikov et al., 2006; Kolesnikov et al., 2004; Mamontov et al., 2006a; Mann & Halls, 2003; Maranon Di Leo & Maranon, 2003; Sriraman, Kevrekidis & Hummer, 2005; Striolo et al., 2005c; Walther et al., 2004; Wang et al., 2003; Werder et al., 2003).

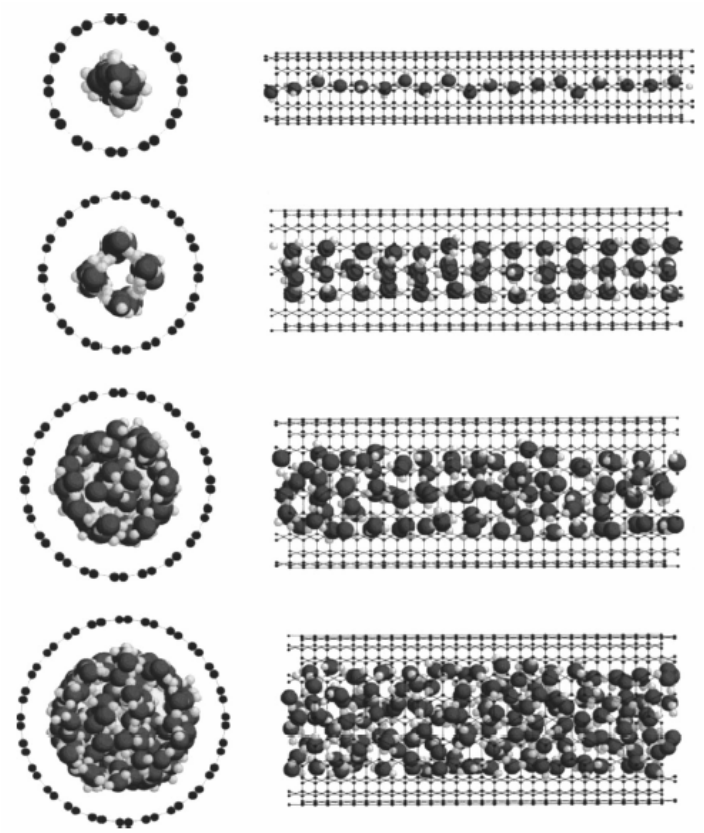

Figure 5.3: Simulation of water in SWNT. Front and lateral views of simulation snapshots for water adsorbed in SWCNs at 298K. From top to bottom figures are water confined in (6:6), (8:8), (10:10) and (12:12) SWCNs (A. Striolo et al., J. Chem. Phys. 122, 234712 (2005)).

Noon et al performed molecular dynamics simulations in the physiological condition (300 K and 1 atm), on nanotube segments of various diameters submerged in water. The

results show that water molecules can exist inside the nanotube segments, and, most importantly, the water molecules inside the tubes tend to organize themselves into a highly hydrogen-bonded network, i.e., solid-like wrapped-around ice sheets. The disorder-to-order transition of these ice-sheets can be achieved purely by tuning the size of the tubes (Noon et al., 2002).

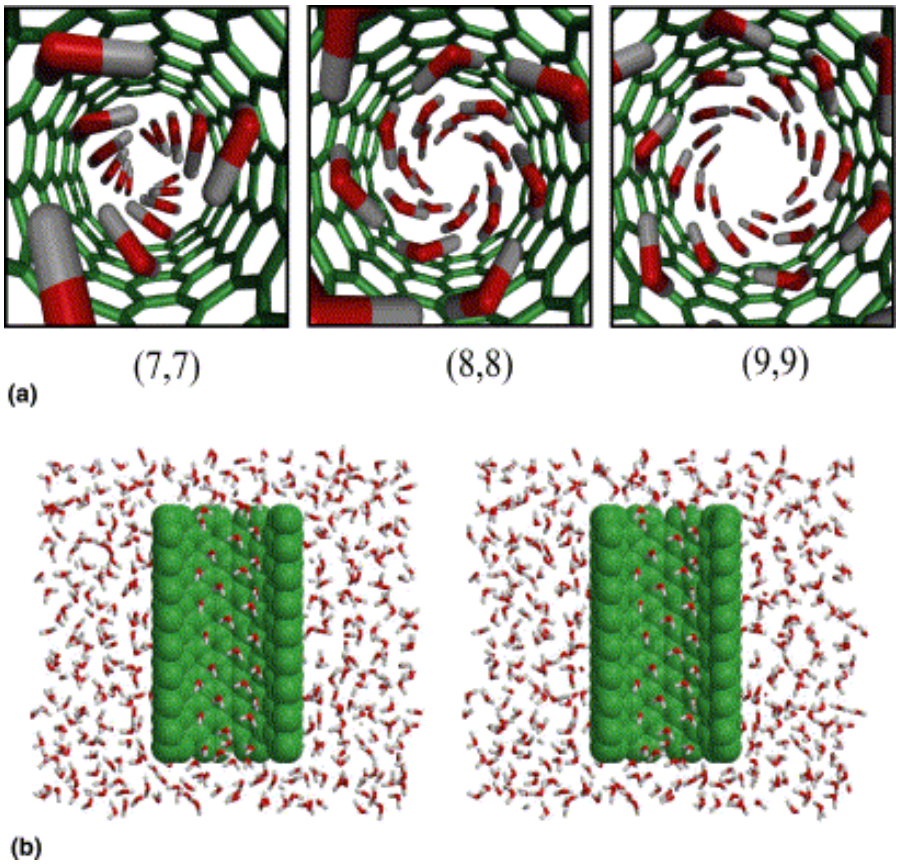

Figure 5.4: Cross-sections of the water configurations inside various tube segments. (a) A top view. The ordered water columns are clearly visible. There are three water columns in the (7,7) tube, four water columns in the (8,8) tube, six water columns in the (9,9) tube. The disorder-to-order transition is evident (Noon et al. Chem. Phys. Lett. 355(2002) 445).

In general, most of the simulation results indicated that water could fill in SWNT and form structures at different temperature, and the structures are also decided by the diameters of carbon nanotube. The discussion on dynamic process of water filling is limited and results are also controversial (Banerjee et al., 2007; Byl et al., 2006; de Souza et al., 2006; Dellago et al., 2003; Gordillo & Marti, 2003; Mamontov et al., 2006b; Maniwa et al., 2005; Striolo, 2006; Zheng et al., 2005; Zhou, Li & Iwamoto, 2004).

5.2.2 Experimental Side of Background

Compared with computer simulation, experimental research on water adsorption in SWNTs has been limited by the difficulty of obtaining high purity and high quality samples. Because usually the amount of sample available for water adsorption experiment is very little, conventional ways such as mass measurement are not applicable to this study. Experimental tools employed are XRD, neutron diffraction and NMR(Alexander et al., 2004; Ghosh et al., 2004; Maniwa et al., 2002; Mao et al., 2006; Matsuda et al., 2006; Sekhaneh et al., 2006).

In-situ nanofluidic experiment, which is done in the vacuum of transmission electron microscope, showed that the inner walls of multi-wall closed cap nanotubes are accessible to liquid water. But the diameters of the tubes are ranged from 10 nm to 50 nm, which means that by IUPAC, they are macrospores, thus water condensation can occurs in them.(Gogotsi et al., 2001). X-Ray diffraction study indicated that substantial amount

of water is absorbed inside SWNTs at room temperature, while the desorption-adsorption of water molecule occurred reversibly at room temperature, liquid-like water is transformed into an ice form at 235 K, the crossover from bulk to atomic scale phenomenon with decreasing SWNT diameter (Maniwa et al., 2002; Maniwa et al., 2005).

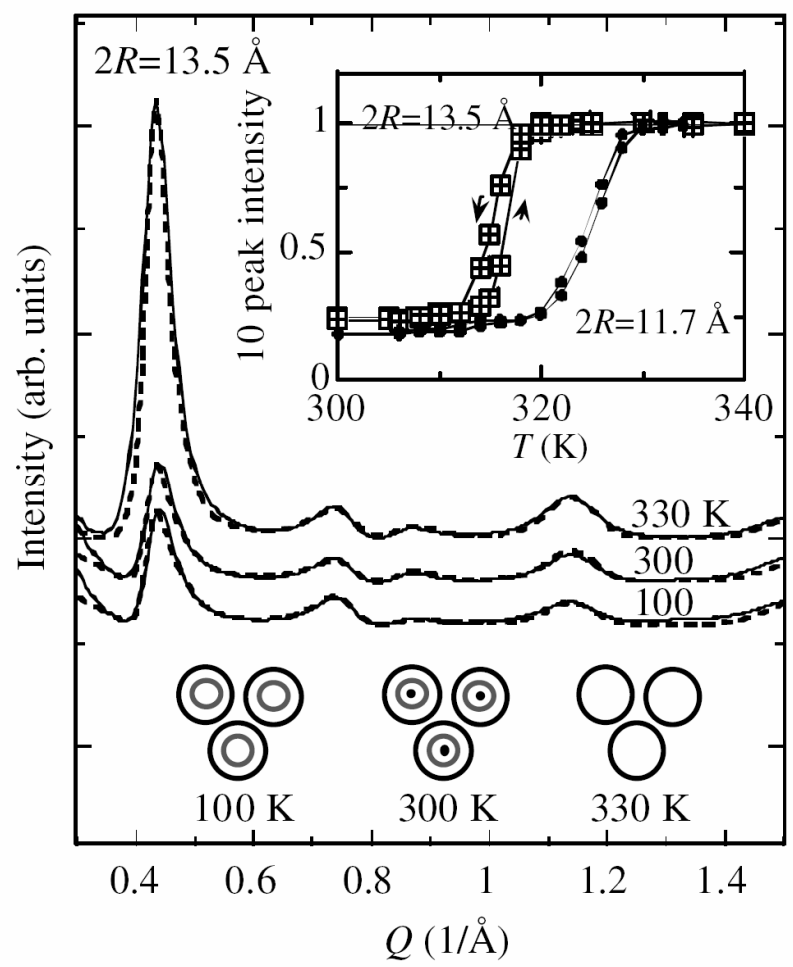

Figure 5.5: Observed XRD profiles of water-exposed SWNT bundles at 330, 300 and 100 K. Dotted lines represent calculated XRD profiles. The water density profile inside the SWNTs at each temperature is schematically illustrated in the figure. The inset is the *T*-dependence of the 10 peak intensity, the intensity is normalized by that of the empty SWNTs (Maniwa et al Chem. Phys. Lett. 401 (2005) 534).

So far, both the experimental and theoretical reports of water adsorption assume that water can access the endohedral part of nanotube, under certain temperature and certain pressure, but some basic questions such as whether water fill the inside of cut-SWNTs completely or what is the dynamic processes of water adsorption still remains unclear. Controversial results are reported depending on the structure and purity of nanotubes.

5.3 NMR Study of Water in SWNTs

5.3.1 Experiment Description

The adsorption and desorption of water is studied in a magnetic field of 0.8 T, related to the hydrogen resonance frequency of 34.1MHz. The sample SWNTs were highly purified with diameter of 13.6 A, with both ends opened by the process described in previous chapter. The variation of length is about several hundred nanometers. Sample was annealed in vacuum at 700 K for 12 hours for degassing. Room temperature is kept at 289 K, the saturated water vapor pressure at this temperature is 13.6 mmHg.

SWNTs were synthesized by laser ablation using 0.6 at% (each) Ni/Co as catalyst. The raw SWNTs were purified following a procedure described in detail elsewhere (Tang et al., 2000). The purified SWNTs were cut to shorter tubes by sanitation in 3:1 ratio of H_2SO_4 and HNO_3 solution for 24 hours(H. Shimoda & O. Zhou, 2002). The cut SWNTs have an average length of about 0.5 μm and are in the form of bundles with average diameters of about 12 nm based on transmission electron microscopy. The SWNT sample

is over 90% pure. The average diameter of the nanotubes estimated by Raman measurements is 1.4 nm. The section of the quartz NMR sample tube within the NMR coil has a volume of 7.5×10^{-2} cm^3 and is filled with 15 mg of SWNTs. For SWNTs with a diameter of 1.4 nm and an average bundle size of 12 nm (about 37 SWNTs per bundle), the estimated specific density of such a close-packed SWNT bundle is 1.33 g/cm^3. Therefore, SWNTs of 15 mg would occupy an estimated volume of only 1.2×10^{-2} cm^3, 16% of 7.5×10^{-2} cm^3 NMR sample tube volume within the NMR coil. Thus, although the SWNTs spread out over the entire volume of the sample space, there is plenty of empty space for free gas molecules. For in-situ loading of water, the NMR sample tube was attached to a quartz manifold connected to various attachments including distilled water source, pressurized gas sources, pressure gauges, and vacuum pumps. The system was leak-tested rigorously. No change of NMR proton signal was detected after several days with sample under vacuum but without dynamic pumping.

Experimental setup

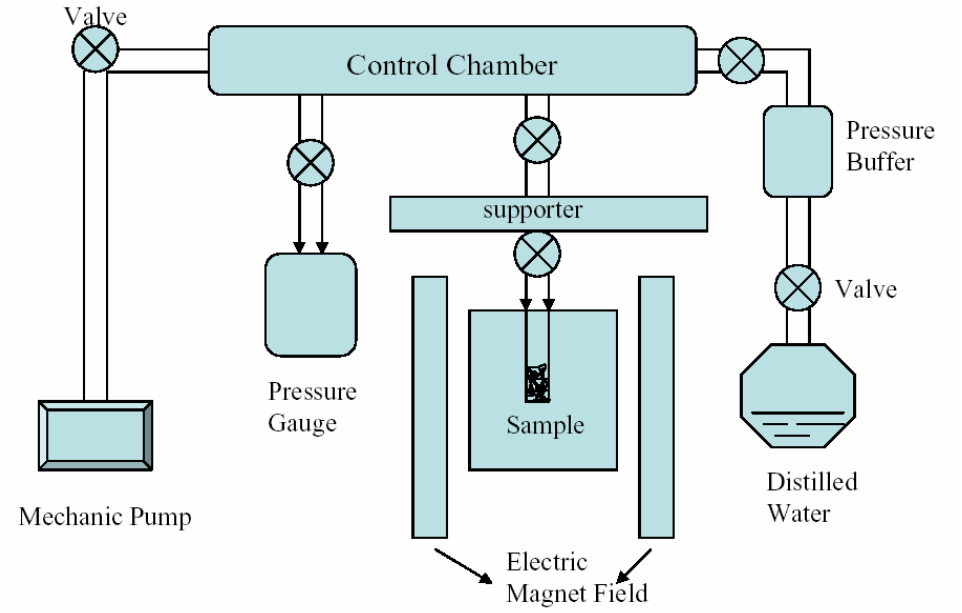

Figure 5.6: Experimental setting of study for water adsoprtion in SWNTs.

The mechanic pump has limit of 10^{-2} torr. The water vapor from the soruce bottle is diffused to the main chamber through a pressure buffer with certain volume so that we can adjust the water vapor pressure. Since the volume of the control chamber is about 7 times larger than that of the quartz tube holding the sample, we can adjust the pressure without opening the valve close to the sample, which will be more accurate to control the vapor pressure in SWNT smaple area.

During the experiment, water pressure was manually conctrolled. Experiment temperature was kept at 289 K, so that the saturated pressure of water vapor is constant with value of 13.6 torr.We measure the NMR spectrum intensity of hydrogen spins in

water molecules with the dependence of relative pressure, which is the ratio of real pressure to the saturated vapor pressure. At each pressure point, we wait for about 1 hour to let the system reaching equilibrium.

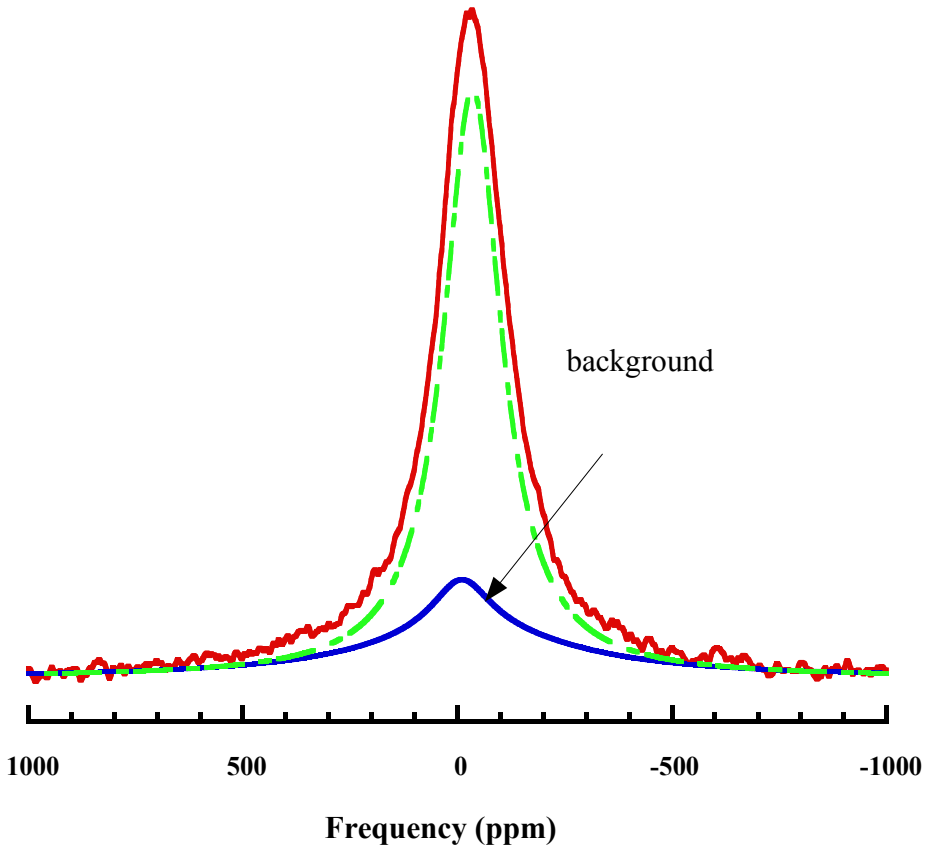

Figure 5.7: ^{1}H NMR spectrum of cut-SWNTs under saturated H_2O vapor at room temperature along with the ^{1}H spectrum of cut-SWNTs under vaccum, referred to there as background. The dashed line is the difference between these two spectra.

The background subtracted NMR spectrum of water in SWNT consists of a broad peak with linewidth of about 5000 Hz. The supporting experiment proved that this peak is due

to the adsorption of water in nanotube, because the NMR spectrum intensity at the same pressure of water without SWNT is almost equal to zero. It is believed that the spectrum width of water in SWNT is mainly due to dipole-dipole interactions between hydrogen spins(Matsuda et al., 2006).

5.3.2 Hysteresis Loop of Water Adsorption in SWNTs

We study the water adsorption isotherm by changing the vapor pressure. The adsorption and desorption curve of water in SWNT shows a clear hysteresis loop, which usually accompanies the process of capillary condensation. This leads us to guess that there might be at least partially liquid-like state of water inside. This conclusion is further confirmed by NMR relaxation time study.

In the filling process, at low relative pressure, there is not much adsorption. The adsorption curve takes off at relative pressure of P/P_0=0.55. After that, the adsorption increases almost linearly with pressure till saturation. In desorption process, the hysteresis effect started from saturated pressure and ended at P/P_0=0.45. The amount of water adsorbed in SWNT at saturated pressure is about 3mmol/g, which is obtained by calibration of hydrogen as described in subsequent part of this chapter.

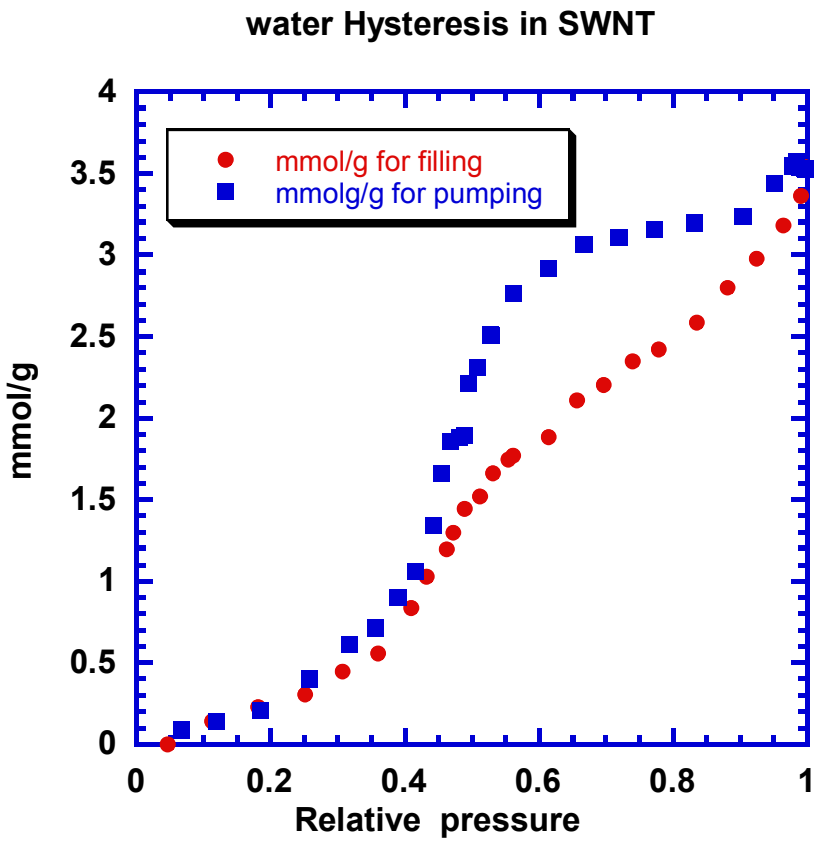

Figure 5.8: Water hysteresis plot in SWNT. The filling process is related to adsorption and the pumping process is related to desorption.

Hysteresis loop is generally discovered for capillary condensation, which usually occurs when liquid adsorption in macropores or mesopores(Birkett & Do, 2006; Brovchenko, Geiger & Oleinikova, 2001; Gusev, 1997; Inoue et al., 1998; Kaneko et al., 1999; Kierlik et al., 2001; Monson, 2005; Ravikovitch et al., 1995; Tompsett et al., 2005). Basically two ideas are accepted, the first is the cluster-mediated effect. The second is the effect of primary adsorption sites.

In a series of reports, Striolo and Gubbins performed grand canonical Monta Carlo simulation and studied the adsorption of water in single-walled carbon nanotube with various diameters (Striolo et al., 2006; Striolo et al., 2005a; Striolo et al., 2004; Striolo et al., 2005c). The amount of water in adsorption in this model agreed with our experimental result at low pressure, but difference happened at the take off pressure (P/P_0=0.55). The increase of water amount is not a sudden jump and reaching the saturation as the model predicted, but at a slower rate at the take off point and even smaller rate after that till saturation. Kierlik et al used mean-field density functional theory of disordered lattice gas model and studied the hysteresis and condensation of fluids in mesoporous systems. They found that the combination of disorder and interconnectivity of the pore network change the picture of capillary condensation theory built on independent-pore model. Hysteresis is no longer related to a equilibrium phase transition, thermodynamics consistency is not satisfied along the hysteresis loop (Kierlik et al., 2001).

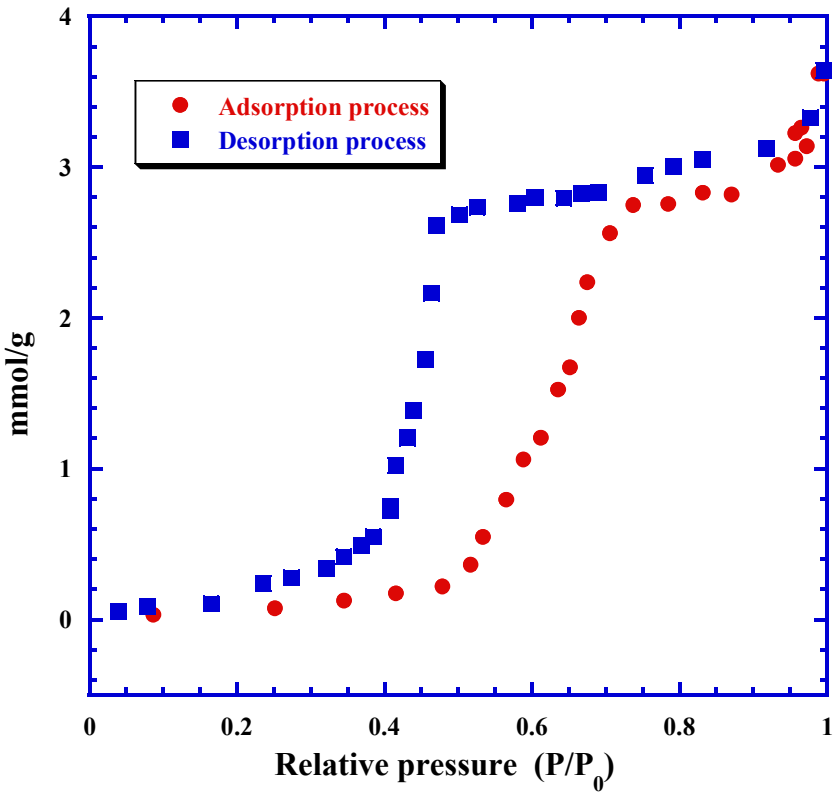

Figure 5.9: The adsorption and desorption of water in activated carbon.

It is helpful to compare the isotherm of water adsorption in SWNT and that in activated carbon with similar pore size. For water in activated carbon, theoretically, if the sample is pure, there is little adsorption below relative pressure of 0.5. But after that, the adsorption curve has steep take off and become saturated at relative pressure of 0.75, which clearly indicates the capillary condensation effect. But for water in SWNT, the adsorption curve did not show such effect. A reasonable explanation is that the one-dimension structure of SWNT prevents the capillary condensation, which requires formation of water clusters. While in activated carbon, the pores are interlinked; cluster formation is much easier than that in SWNT. Also, the functional group will play important roles.

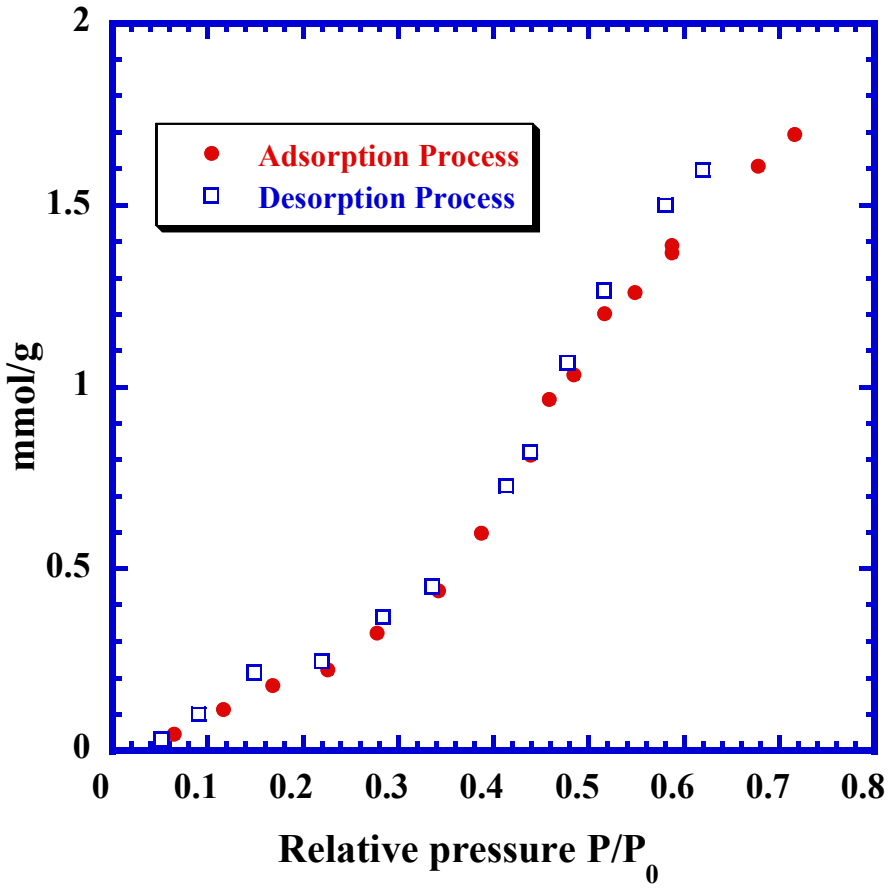

Figure 5.10: Study of water adsorption and desorption in SWNT before saturation.

The above plot clearly indicates that there is no clear hysteresis effect if desorption starts at point before saturation filling. Based on this result, we can see that at saturation filling, water does form some liquid like structure in SWNT, which will lead to the hysteresis loop. Whether this structure is similar to bulk liquid or just some water clusters at some primary adsorption sites can be further checked by T_2 analysis and the calculation of density of water.

5.3.3 Effect of Functional Groups

In most simulation and current researches on water adsorption in SWNT it was assumed that the sample is ideally pure and only the carbon-water and water-water molecular interactions are considered. However, in real systems, the existence of primary adsorption sites (PAS) affects the interactions and thus the adsorption curves greatly. The PAS are functional groups such as hydroxyl, carboxyl and -COOH groups produced during sample preparation (H. Shimoda & O. Zhou, 2002; Kleinhammes et al., 2003). Since most chemically cut SWNTs contain such functional groups, their effect on the adsorption and desorption of water deserves to be addressed. So far, no results have been reported regarding water adsorption in SWNTs. Similar studies on single wall nanohorn (SWNHs) (Bekyarova et al., 2002; Bekyarova et al., 2003) and activated carbon (Muller, Hung & Gubbins, 2000; Muller et al., 1996) have addressed the effect of functional groups to the adsorption and desperation of water in these carbon materials. Vartapetyan studied the experimental adsorption isotherms of water vapor and nitrogen on nonporous carbon adsorbents with various specific surfaces and concentrations of primary adsorption centers (PACs). The adsorption of water molecules could form either individual isolated cluster in equilibrium with saturated vapor or a continuous adsorption film depending on the concentration of the PACs. The threshold adsorption value of water vapor is proportional to the concentration of PACs and corresponds to the formation of fractions of a dense monomolecular layer on the adsorbent surface.

(Vartapetian & Voloshchuk, 1995; Vartapetyan et al., 2005; Vartapetyan et al., 1995)

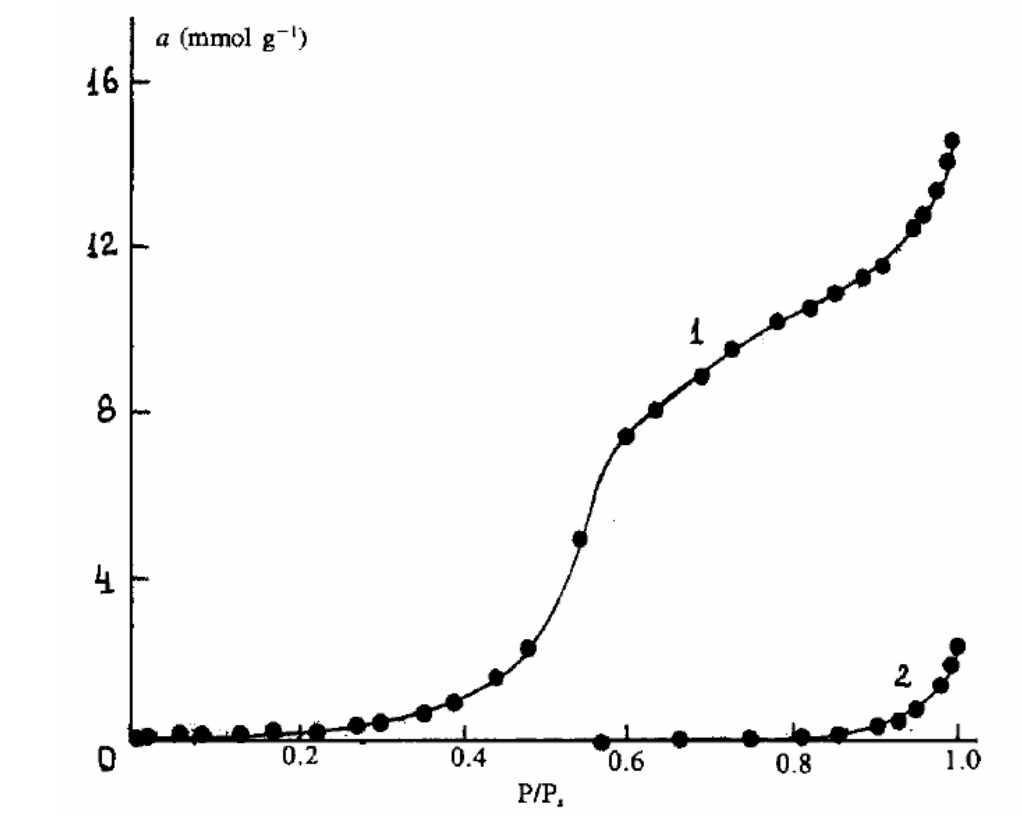

Figure 5.11: Water vapor adsorption at 20 ^{0}C on FAZS type active carbon (curve 1) and on gas channel carbon black (curve 2) (R. Sh. Vartapetyan et al., Colloids Surfaces A: Physicochem. Eng. Aspects 101 (1995) 22~232).

It is believed that primary active sites (PAS), which consist of some functional groups, play an important role for the water adsorption in SWNT (Maniwa et al., 2005; Mashl et al., 2003). In this study, we can get the number of primary adsorption sites by fitting the low-pressure part of the hysteresis loops. At low pressure, the adsorption amount of water in SWNT and activated carbon is closely related to the PAS, which can be fitted with the Dubinin-Sperpinskii equation given as:

$$P / P_0 = a /[c(a_0 + a)(1 - ka)] \tag{5.1}$$

In which P is the pressure of water we observed, P_0 is the saturated water pressure at the experimental temperature. The parameter a stands for the amount of adsorption at pressure P, a_0 is density of primary adsorption sites, c is a kinetic constant, and k is the reduction rate of in available adsorption sites at current condition which is usually with value from 0 to 0.1 mmol/g.

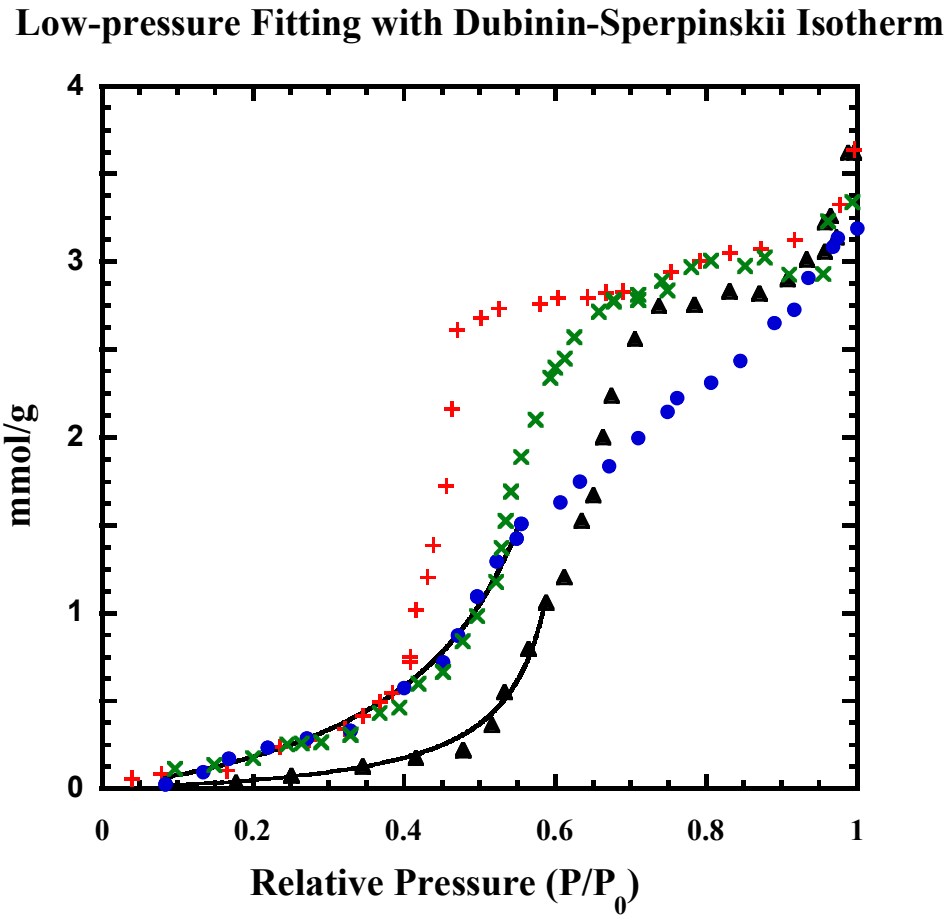

Figure 5.12: Curve fit of water adsorption in SWNTs and activated carbon at relative pressure below 0.55 with Dubinin-Sperpinskii Isotherm.

From Dubinin-Sperpinskii equation, the number of PAS estimated for the cut SWNT

sample is 0.45mmol/g and the related density of water in SWNT is 3mmol/g. Molecular dynamic simulation of water in SWNTs predict ice structure with related water density of 16 mmol/g. Based on our result, it suggested that only about 20% of the interior space of SWNT is filled with water. The result we obtained is similar to that of water in activated carbon (Kolesnikov et al., 2004), but the mechanism of adsorption is much different: for water in SWNT, condensed water molecules mostly accumulate near the opening and defects while in activated carbon, water can fill inside and form capillary condensation.

5.3.4 NMR Relaxation Analysis of Water in SWNTs

The NMR relaxation techniques are excellent tools for studying the liquid dynamics and motional behavior of liquid confined in porous media such as porous silica glasses, oil rock. NMR T_2 analysis is used as a reliable tool to study the pore size for porous material, which is based on the fact that T_2 value will change when confined in small region. Previous reports indicated that the NMR spin-lattice relaxation time T_1 of liquids confined in porous materials is considerably shorter than T_1 in bulk liquid. Bounded water and free water will have different spin-relaxation time.

Specific property of water in FAS-3 active carbon is studied by **Gogelashvili u**sing NMR relaxation method **(Gogelashvili et al., 2002; Gogelashvili et al., 2004)**. The ratio of water adsorption is closely related to the volume and pore size of the sample. The dependences of the times of spin–lattice (T_1) and spin–spin (T_2) NMR relaxation of

adsorbed water molecules on the amount of adsorption are established. The character of the dependences of T_1 and T_2 on the number of adsorbed water molecules per primary adsorption site reflects the specific features of the volume filling of micropores and the formation of a continuous adsorption layer on the mesoporous surface due to cluster coalescence on the one wall of a pore. The results obtained are compared with the data for typical macroporous active carbons, as well as with the data obtained by the adsorption method. The adsorption of water in SWNT can be use to compare to this result.

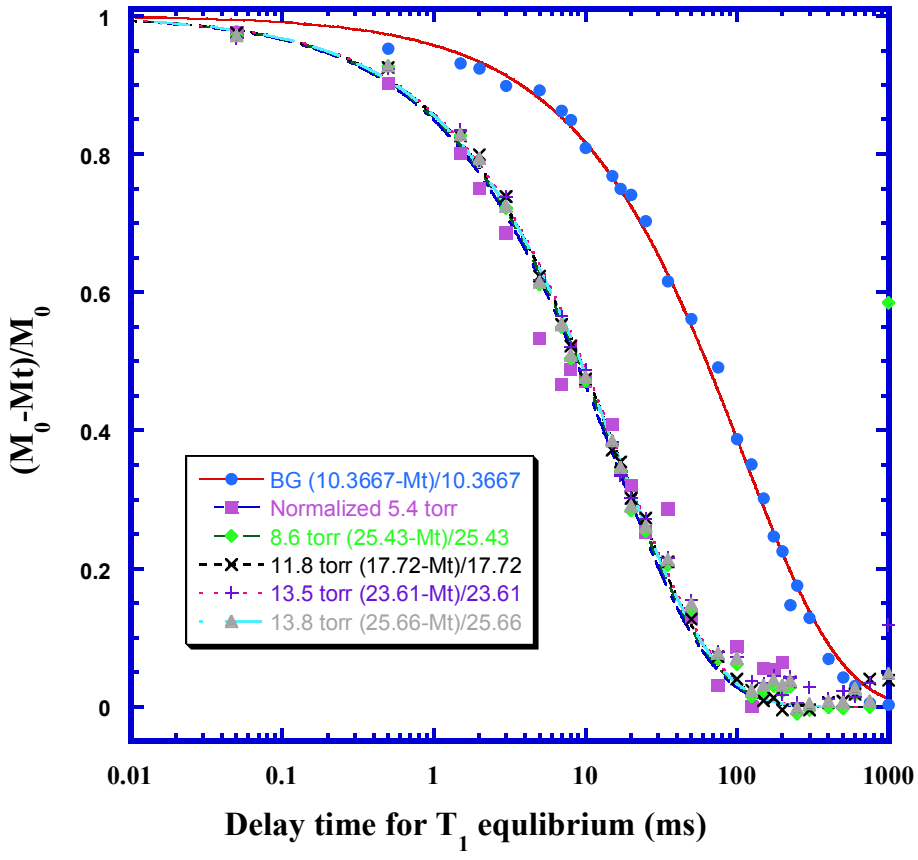

Figure 5.13: T_1 curve of water in SWNT at different pressures. Only the background signal (no water) shows different T_1 value, while the other five pressure of water curve show exactly same T_1 value.

The plot shows that except the background has T_1 value of 106 ms, the water signal in SWNT has the same T_1 value of 15 ms in the pressure range from 5.4 to saturation (13.8 mmHg), which is drastically different from T_1 value of bulk liquid of several seconds. So clearly the phase of water in SWNT is quite different from that of bulk liquid.

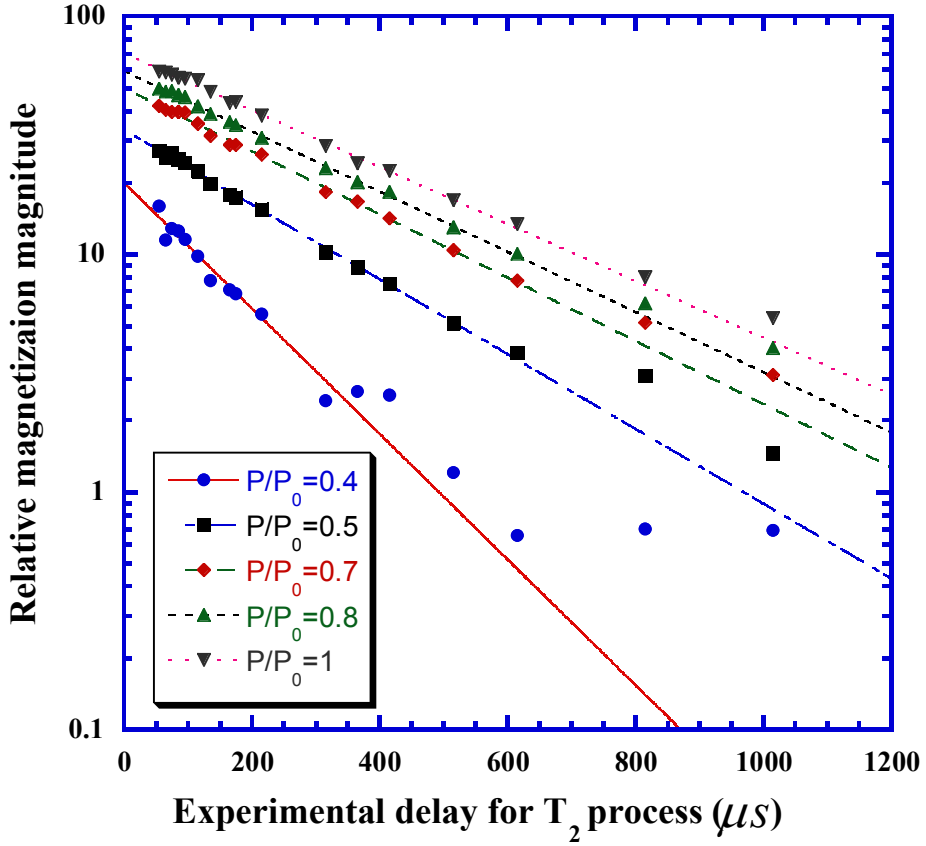

Figure 5.14. T_2 relaxation curves of water in SWNT at different relative pressures

The spin-spin relaxation curves are shown for several relative pressure values. For P/P_0 from 0.4 to 1, the five measured T_2 values are: 164 μs, 276 μs, 326 μs, 343 μs and 363 μs.

The T_2 of water at lower than P/P_0=0.5 is significantly different from that above

P/P_0=0.5, suggesting that after the take off, water form some kind of liquid-like structure. The T_2 for P/P_0=0.7, 0.8 and 1 are virtually the same, indicating that there is no significant difference between the states of water among them.

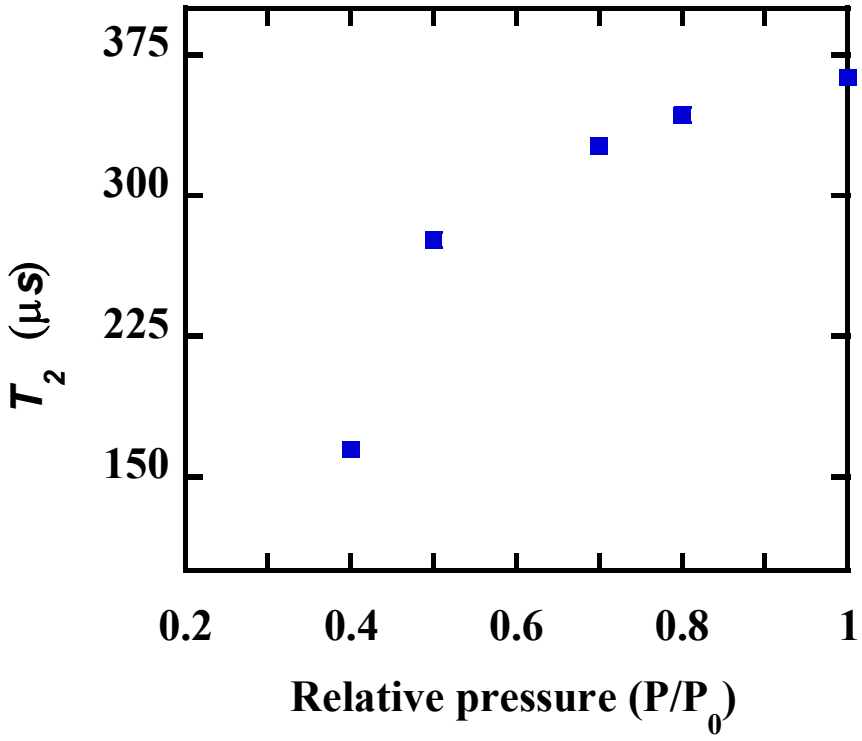

Figure 5.15: Spin-spin relaxation time of water at different pressures.

Comparing these T_2 values with the T_2 in bulk water, which is of several seconds, the spin-spin relaxation time in our sample is much different from that of bulk water. Further study by NMR calibration brings up the result that water density in SWNT is only about 20% of that in bulk liquid, thus the liquid or ice state of water inside SWNT is not the same as that in bulk liquid.

5.4 Estimation of the Amount of Water Adsorption in SWNTs

The amount of water adsorption in SWNT can be obtained with the calibration of C_2H_6, based on two assumptions. First, we assume that the experimental condition for water and C_2H_6 can be kept exactly the same throughout the measurement, the stability of NMR spectrum is usually well acknowledged, so with same 90 degree pulse width, same amplification value, the relation of NMR signal intensity with number of hydrogen spins derived from C_2H_6 can be extracted to water in SWNT. Secondly, we assume that the Fourier transformation spectrum of C_2H_6 can be decomposed to two peaks: the narrow peak with linewidth of ~500Hz is related to free gas peak, the broad peak with linewidth of 8 kHz is due to C_2H_6 adsorbed inside SWNT. The validity of this fitting is shown in our paper on gas adsorption (Kleinhammes et al., 2003; Mao et al., 2006).

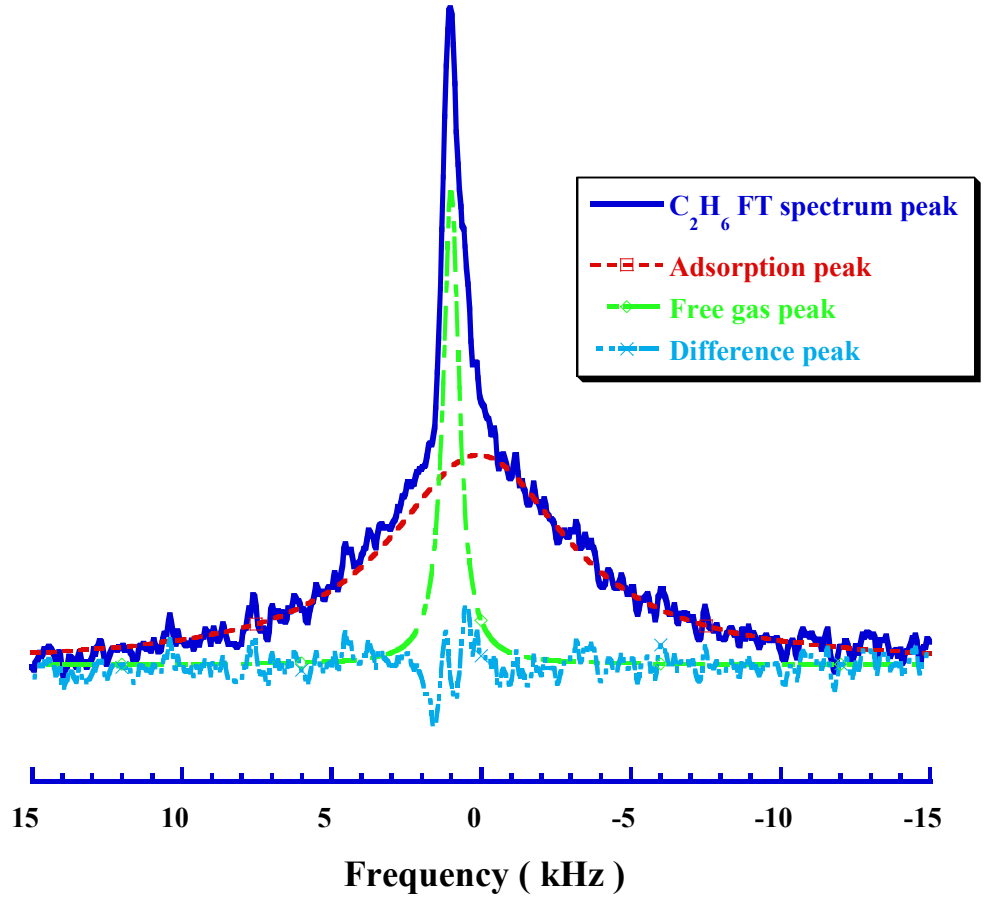

Figure. 5.16: Calibration of adsorption amount by C_2H_6.

As discussed in chapter 4, the Fourier transformation (FT) spectrum of C_2H_6 clearly consists of two peaks: the broader adsorption peak and narrower gas peak. Their relative ratio can be obtained from peak fitting. Assume gas component follows ideal gas law, given the available volume of sample holder for free gas, the total number of hydrogen spins in free gas component can be calculated. The amount of adsorption is derived proportionally by the ratio of adsorption peak area to the free gas peak area.

The pulse sequence used is: pre-π/2-tau- π-delay-acquisition at center of echoes.

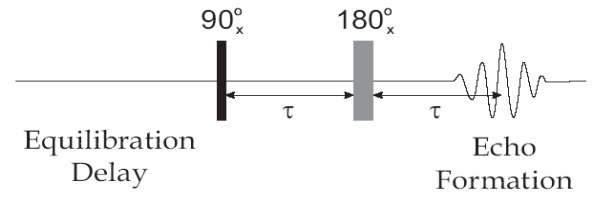

Figure 5.17: Spin-echo pulse sequence for signal calibration

The 90-degree pulse used is 2.26 μs . The time interval from center of the π/2 pulse to the point we record FID (highest point of echo) is 42.67 μs . T_2 for free C_2H_6 is 250 μs , which is similar to that of saturated water in SWNT (350-400 μs). In the following calculation, we use 375 μs .

The size of quartz tube holding sample is $5.3*10^{-2}$ cm^3. The amount of SWNT sample is 15 mg, which occupies volume of $1*10^{-2}cm^3$. The volume available for free gas C_2H_6 is $4.3*10^{-2}cm^3$. The ethane pressure is 205 mmHg, with 4096 scans. For accuracy, we checked the background signal effect. For background spectrum, FID at observation point is $1.4*10^5$ unit the integration of FT spectrum area $5*10^6$, while for the C_2H_6 at 205 mmHg, the background subtracted FID of is $7*10^4$ unit, which includes free gas peak and adsorbed gas peak. Their ratios can be obtained by FT spectrum peak fitting as 5 to 1. At 290 K, mole number of 205 mmHg of gas C_2H_6 is:

N= PV/RT=$205*133*4.3*10^{-8}/(8.31*290)=4.86*10^{-7}$ mol. The Mole number of H spin is

$6*4.86*10^{-7}$ mol=$2.92*10^{-6}$mol. This amount of hydrogen spin contributed to $1.3*10^4$ unit of FID at observation point.

For saturated water in SWNTs, the FID intensity is $2.5*10^5$ unit. In order to get the correct amount of H_2O, we need to extrapolate the intensity to zero tau value, which is 42.67 μs before our observation point. The signal intensity of pure C_2H_6 extrapolated is $(1/6)*7*10^4/\exp(-42.67/250) = (7/6)*10^4*\exp(42.67/250)$ unit. Similarly, H_2O intensity extrapolated is $2.5*10^5*\exp(42.67/375)$. Further adjustment will give us the value of 3 mmol/g.

5.5 Effect of Water to Adsorption of Gases in SWNTs

It is interesting to study the effect of water adsorption on the adsorption of other gases such as ethane and methane. Due to the larger adsorption energy and strong hydrogen-hydrogen bond, the water clusters in SWNT can block the further adsorption of gases as methane and ethane. The result is proved by the ^1H NMR spectrum on adsorption of ethane with pre-saturated deuterium-oxide (D_2O) in SWNT. The plot below indicates that with pre-saturated D_2O, the spectrum of ethane in SWNT (peak b) is much different from the spectrum of ethane in SWNT (peak a). Further analysis of this two spectrum suggest that with pre-saturated D_2O, the spectrum is very similar to the free gas component of ethane in SWNT without water (peak c), while the adsorption peak is almost vanished, thus saturated water (or D_2O) significantly block the adsorption of other

gases. Similar results can be found on the study of water in porous media such as activated carbon (Muller et al., 2000).

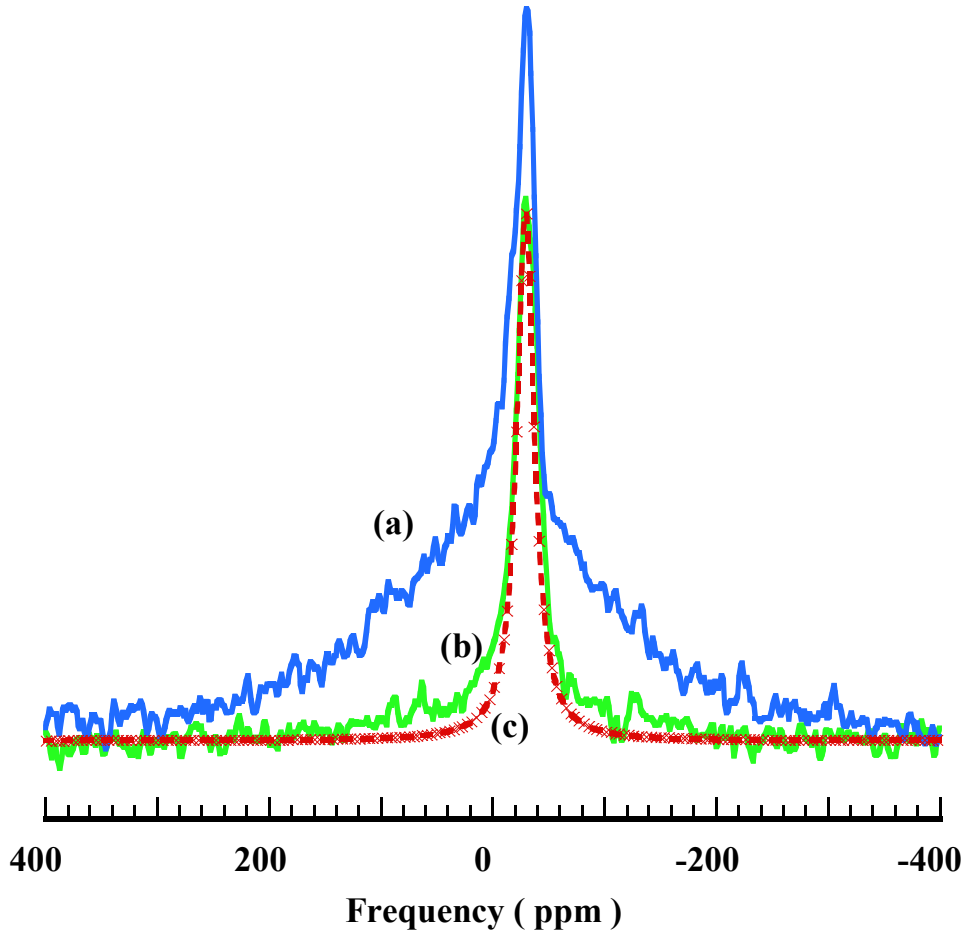

Figure 5.18: Effect of D_2O to adsorption of other gases. (a): Experimental peak of C_2H_6 400 torr in SWNTs. (b): Fitted free gas peak in SWNTs. (c): Experimental peak of C_2H_6 400 torr with saturated D_2O vapor. With pre-saturated D_2O in SWNTs, the adsorption of C_2H_6 is decreased significantly.

5.6 Comparison of Water Adsorption Amount

From Dubinin-Sperpinskii equation, the number of PAS estimated for the cut SWNT

sample is 0.45mmol/g and the related density of water in SWNT is 3 mmol/g. While molecular dynamics simulation of water in SWNTs predict ice structure and related water density of 16 mmol/g. Based on our result, it suggested that only about 20% of the interior space of SWNT is accessible to water. The result we obtained is similar to that of water in activated carbon (Kolesnikov et al., 2004), but the mechanism of adsorption is much different: for water in SWNT, condensed water molecules mostly accumulate near the opening and defects while in activated carbon, water can fill inside and form capillary condensation.

5.7 Conclusions

The NMR study indicated that water adsorption in SWNTs shows strong hysteresis loop, comprehensive studies support the ideal that the hysteresis of water in SWNTs is likely due to the adsorption at functional groups and multiple layer effect. During the process of adsorption, the first layer of water molecules tend to be adsorbed at the functional groups first and subsequent adsorption leads to formation of water clusters. The amount of water in SWNTs at saturated pressure is only about 3 mmol/g, which indicated that water does not fill the SWNTs as liquid state. In our study, the effect of primary adsorption sites is very important and the lower pressure part of adsorption isotherm from NMR can be fitted with Dubinin-Sperpinskii Isotherm. Further research on water adsorption in pure and perfect SWNT sample and at low temperature is continuing in our lab.

CHAPTER 6

Hydrogen Storage in Carbon Based Materials

In this chapter, we will concentrate on the adsorption of hydrogen in carbon-based materials at room temperature, which could be developed for future hydrogen storage application. The materials studied are carbon nanotubes, boron-doped nanotubes, and boron-doped graphite. Adsorption energy is derived from adsorption isotherm obtained by NMR technique. It is proved that substitutional doping with boron can increase the adsorption energy of hydrogen by considerable amount.

6.1: Introduction

Shortly after its discovery, carbon nanotubes have attracted tremendous attention as potential adsorbent material, due to their high surface/volume ratio and hollow endohedral structures. Among all the adsorbate gases that were usually studied, hydrogen has gained special attention because of the possible application as energy gas in fuel cell electric vehicles, which requires efficient storage and transportation method.

Early research on hydrogen storage is usually based on gravimetric and volumetric techniques (Dillon et al., 1997; Liu et al., 1999; Ye et al., 1999). Reported storage capacity ranges from 0.6wt% to 14wt% at various temperatures and pressures (Cheng et al., 2001; Darkrim, Malbrunot & Tartaglia, 2002; Deshpande et al., 2006; Dillon et al., 1997; Hirscher et al., 2002b; Hou et al., 2003; Jorda-Beneyto et al., 2007; Lee et al., 2000; Liu et al., 1999; Luxembourg et al., 2004; Panella, Hirscher & Roth, 2005; Pietra & Shen, 2006; Schlapbach & Zuttel, 2001; Strobel et al., 1999; Ye et al., 1999; Zhu et al., 2001; Zuttel et al., 2002).

In this research, we study hydrogen adsorption at moderate pressure up to 10Mpa by ^{1}H NMR spectrum. Previous reports on hydrogen adsorption in multi-walled carbon nanotubes by NMR indicate that the resonance frequency is shifted inversely proportion to temperature due to the super-paramagnetic Fe catalysts that remained in the nanotubes (Yu, Lee & Lee, 2003). The signal from hydrogen adsorbed on carbon nanotubes is also differentiated from that of gas phase hydrogen by the difference in relaxation times (Yu et al., 2003). In another study, single-walled carbon nanotubes (CNTs) are exposed to hydrogen pressure up to 14.3 MPa. The results suggest when pressure is lower than 1.5 MPa, hydrogen adsorption is fast and reversible and can be described by physisorption. However, exposure to pressure above 14.3 MPa, longer exposure causes greater hydrogen uptake. The data suggest that adsorption in interstitial sites and the tube interior could take place (Pietra & Shen, 2006).

Although in some specific reports, under certain conditions, which are usually low temperature (77K) and pressure of up to 10Mpa, the amount of hydrogen can be higher than 7wt% (Jorda-Beneyto et al., 2007; Lee et al., 2000; Ye et al., 1999), their commercial application is limited because most of the commercial applications occur around room temperature. Motivated by finding some materials, which can obtain the goal of 7wt% adsorption at room temperature and moderate pressure, people have tried variety of modified carbon-based materials. Due to the weak van der Waals interaction of about 4 kJ/mol between H_2 and carbon surface, so far, most studies on the nanotube materials only reach the adsorption rate of 0.6 wt% to 3 wt% (Kojima et al., 2006; Strobel et al., 1999; Xu et al., ; Zuttel et al., 2002). Recently, Zhang et al predicted adsorption at substitution ally doped boron sites with adsorption energy above 20 kJ/mol per H_2, such materials as boron doped graphite and boron doped nanotubes may lead to a new way on hydrogen adsorption (Kim et al., 2006; Lim et al., 2007; Liu et al., ; Rakov, 2001; Sankaran & Viswanathan, 2006; Zhao et al., 2005).

The adsorption energy analysis for hydrogen in boron-doped fulleren indicates that by substitutionally doping, there is no significant barrier for adsorption and no additional desorption barrier beyond the adsorption energy. The adsorption overcomes the binding between H_2 and B atom in the fulleren, which makes storage reversible. The integrity of hydrogen molecule is maintained (Kim et al., 2006).

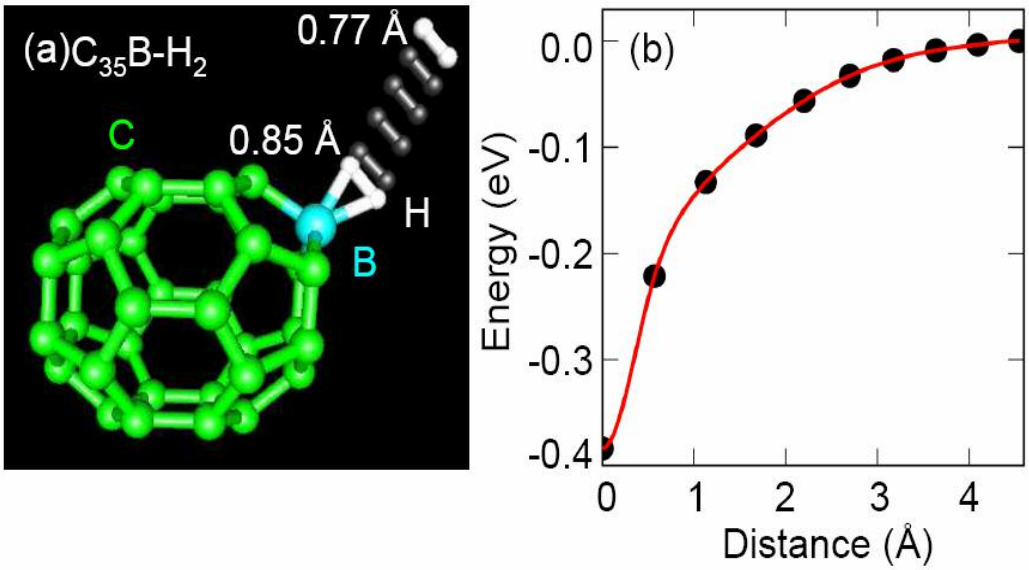

Figure 6.1: Adsorption energy of H_2 in boron substitutionally doped fullerene (Y.H. Kim et al, 2006). H_2 binds to substitutional B or Be with significantly larger local density approximation binding energies, which are 0.39 and 0.65 eV/H_2, respectively. Left: The binding process of H2 to substitutional B in $C_{35}B$. Right: Total energy curve as a function of geometric center of H_2 from its minimum-energy position.

The goal of our research here is to find whether boron doping is effective to increase the adsorption energy(Ulbricht, Moos & Hertel, 2003; Xu et al.). If it is effective, efforts can then be aimed at increasing the number of such sites to increase the weight percent of adsorption, which may lead to a new method of improving hydrogen storage.

6.2 Sample Descriptions and Experimental Setup

The boron-doped graphite we used is from Prof. Chung's lab in Penn State and the Boron doped SWNT sample is from Dr. Heben's lab of NREL. The details of sample preparation are described elsewhere (Seung-Hoon & Young-Kyun, 2004; Zhao et al., 2005).

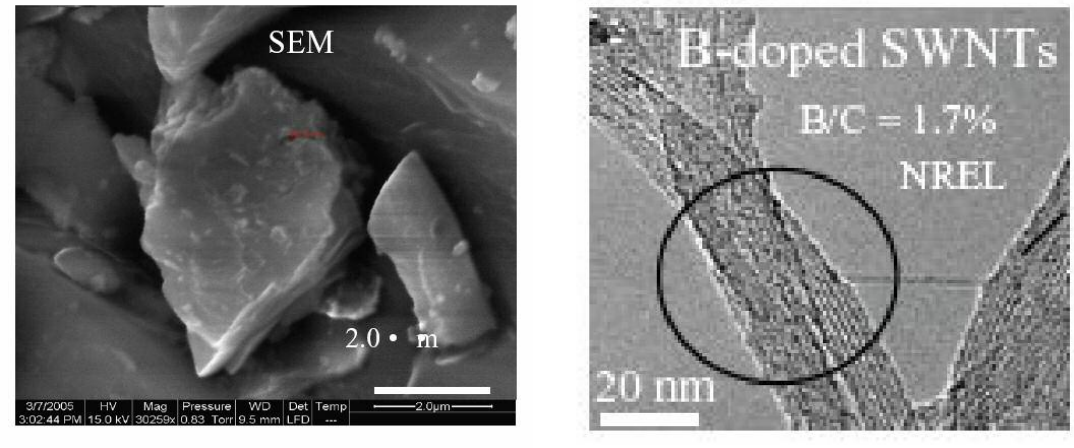

(a): B-doped graphite (b): B-doped SWNT.

Figure 6.2: (a): SEM spectrum of Boron doped graphite (From Prof. Chung's lab).
(b): SEM spectrum of Boron doped SWNTs (From Dr. Heben's lab).

The experimental system can hold hydrogen with pressure above 100 atm. The sample tube is made of sapphire so that it can endure the high pressure. We can control the pressure of hydrogen by the valves.

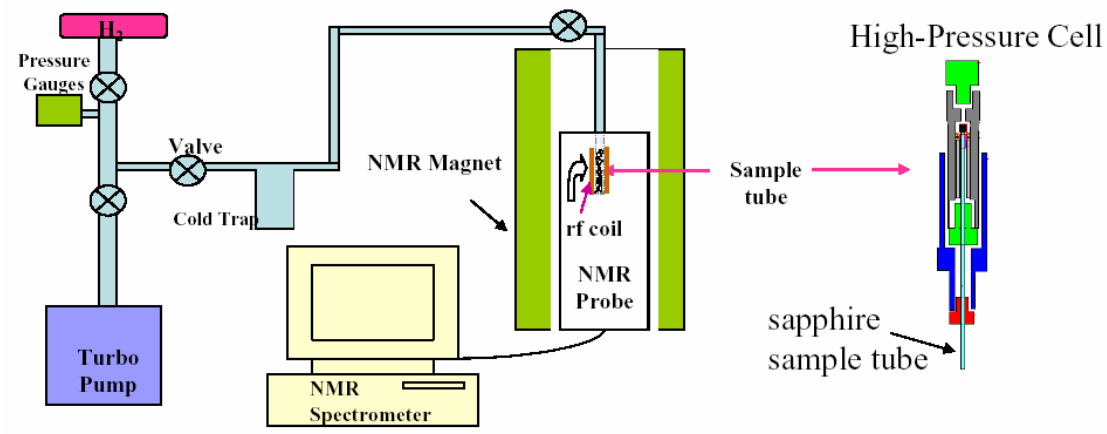

Figure 6.3: Experimental setting for high-pressure hydrogen study. The sapphire sample tube is specifically designed to hold pressure above 100 atm.

The experiments were performed at room temperature. Hydrogen pressure was changed

with roughly constant steps from zero to 100 atm. At each point, we take ^{1}H NMR spectrum and compare the linewidth, area and lineshape with previous ones. The spin-spin relaxation time and spin-lattice relaxation time were also measured. The sample mass is 136 mg for B-doped graphite and 45.2 mg for B-doped nanotubes.

6.3 Results and Discussions

6.3.1 Hydrogen storage in B-Doped graphite

A capillary is inserted to the sample tube as an internal standard of intensity and shift using free H_2 gas in the capillary, which allows accurate determination of adsorption isotherms by NMR. Since NMR characteristics of hydrogen spins at different locations are distinct, this method provides an unambiguous way for peak allocation.

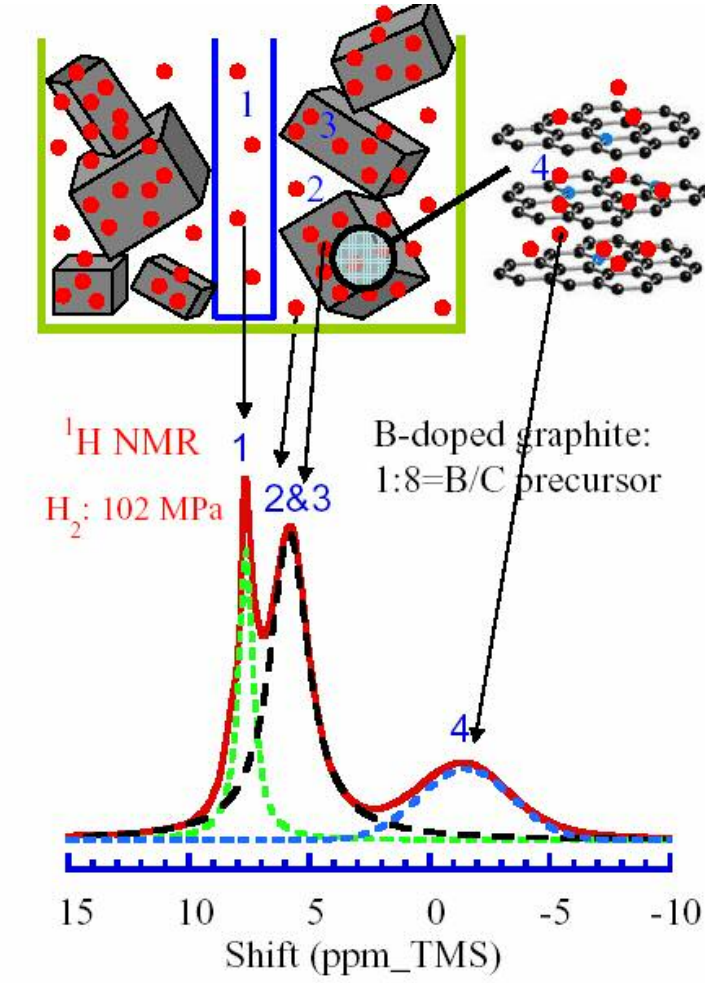

Fig.6.4: Peak assignments of the ^{1}H NMR spectrum. The four peaks are related to hydrogen gases at different locations of the sample. Peak 1 in ^{1}H NMR spectrum is the reference free gas peak in small capillary, peak 2 is free gas in the unfilled space of the sample region, peak 3 is related to adsorbed H_2 on outer surfaces of grains, peak 4 is due to adsorbed H_2 on confined surfaces such as in-between somewhat exfoliated layers, nano-slit pores, and nanovoids.

When H_2 molecules at two different environments exchange rapidly on the timescale of the NMR experiment (about 1 ms for free induction decay), both of them will contribute to a single peak that reflects the average properties of the two environments. If adsorption occurs on an exposed surface, such as the surface of a crystal grain or the outer surface of

a carbon nanotube bundle, the adsorbed H_2 can exchange rapidly with desorbed free H_2. The exchange rate can be estimated by the residence time of adsorption given by:

$$\tau = 10^{-13} * \exp(E / k_B T) \quad \text{(s)} \qquad (6.1)$$

For an adsorption energy E_{ads} of 0.1 eV (9.6 kJ/mol), τ is 5 ps at room temperature and 0.35 μ s at 77 K. Thus, both free gas hydrogen and adsorped hydrogen will contribute to the same peak, nevertheless, the intensity and shift of this peak still contains adsorption contributions from both environments. In case of hydrogen in confined surfaces, spatial restriction could limit the exchange with free H_2 and a separate peak could be preserved reflecting the confined nature of the corresponding local environment.

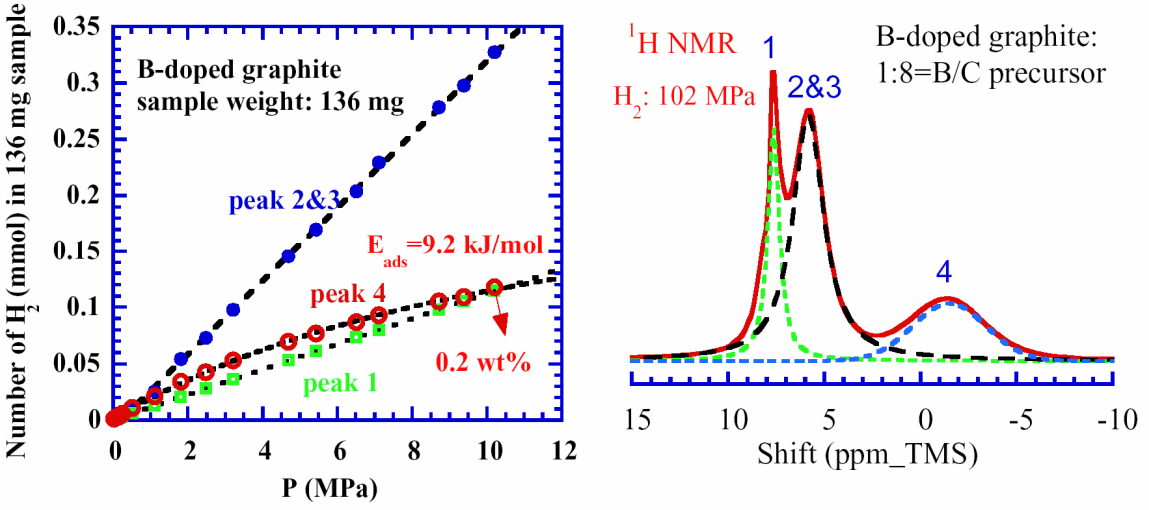

Figure 6.5: (a): Peak intensities of the ^{1}H NMR spectrum as functions of pressure for a 136 mg B-doped graphite sample (b): Peaks fitted

Peak 1, 2 and peak 3 depend linearly on pressure even up to 10 MPa as expected for free

H_2 gas and adsorption with adsorption energy E_{ads} comparable to kT. In contrast, peak 4 clearly shows nonlinear pressure dependence. This could be interpreted as an indication of increased E_{ads}. Based on the Langmuir equation defined below:

$$n(P,T) = n_\infty \frac{bp}{1+bp}$$
$$b = \frac{\sigma}{\upsilon_0 \sqrt{2\pi m k_B T}} \exp(E_{ads} / k_B T) \tag{6.2}$$

an estimate of E_{ads} =9.2 kJ/mol is obtained. The enhanced banding energy demonstrates the existence of adsorption sites in B-doped graphite that are better suited for hydrogen storage at ambient conditions. So far, the intensity of the peak 4 is rather weak, which is 0.2 wt% at 100 atm. However, given the fact that the system is nonporous, there is a possibility that such adsorption sites can be increased substantially. Also we need to establish the correlations between storage capacity and morphology and defects.

6.3.2 Hydrogen storage study in B-doped SWNTs

The NMR study of hydrogen storage in boron doped SWNTs was carried out with the same procedure as above. The locations of hydrogen in B-doped nanotube with related to NMR spectrum peaks are shown as following:

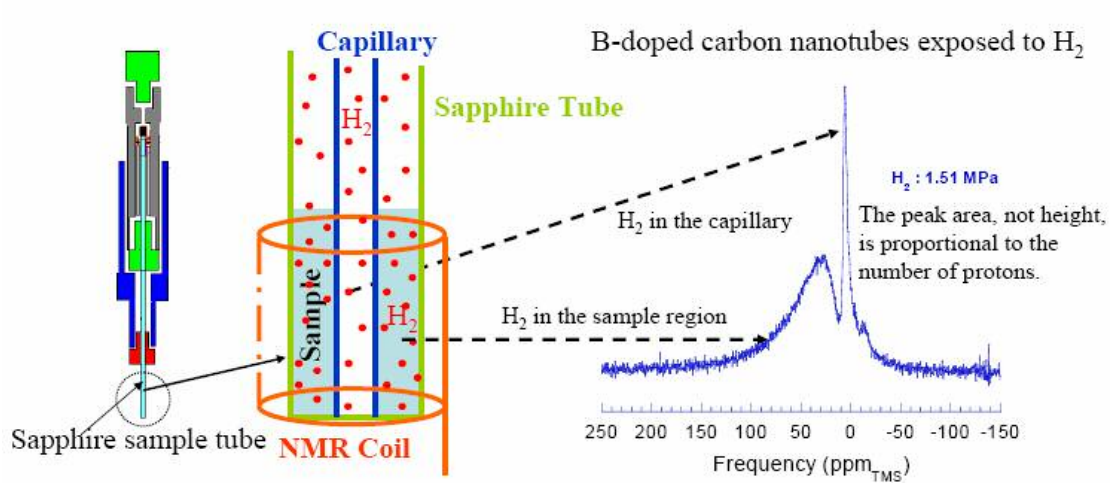

Figure 6.6: NMR spectrum of hydrogen adsorption in B-doped SWNTs

In this spectra, we see only two peaks. The sharp peak corresponds to free H_2 in the capillary. The broad peak is associated with H_2 in the sample region. This peak contains contributions both from free H_2 in the unfilled space in the sample region and from adsorbed H_2 (peak 2, 3 and 4). Unlike in B-doped graphite, we cannot distinguish peak 2&3 and peak 4 (even if molecular exchange between them is slow) due to the significant line broadening caused by the residual magnetic catalytic particles in the sample. Such particles also give rise to the large 30 ppm shift due to the effect of demagnetization (packing and sample shape dependence). For comparison, ^{1}H NMR of ethane is also shown. The lineshape of the broad peak is very similar to that of H_2 gas.

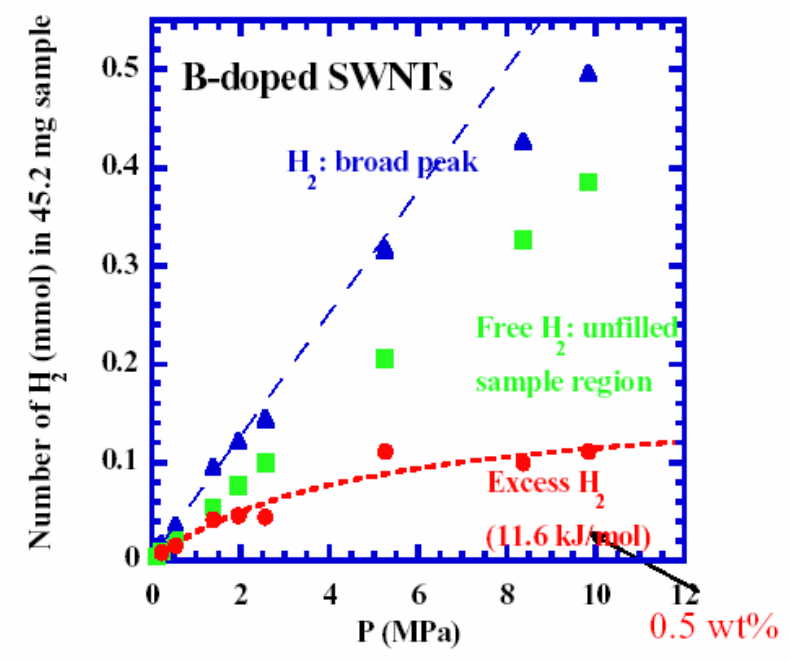

Figure 6.7: Adsorption isotherms. The broad peak intensity of the ^{1}H NMR spectrum is shown as a function of H_2 pressure for a 45.2mg B-doped SWNTs sample.

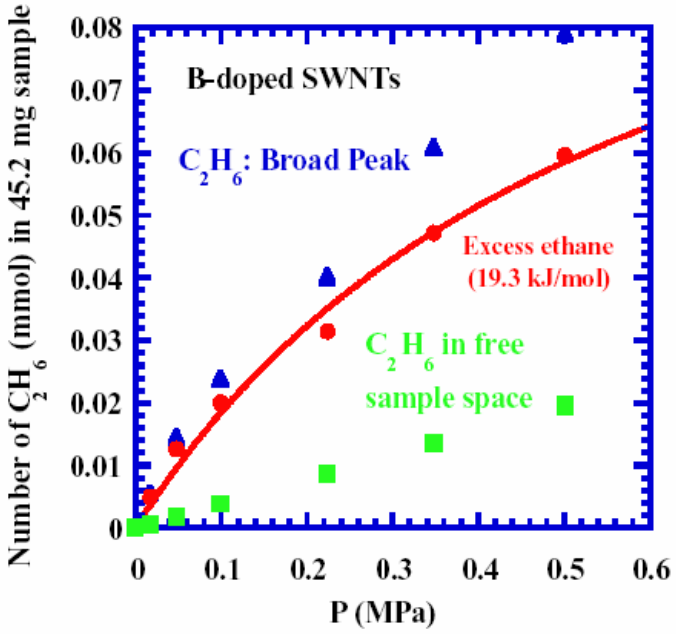

Figure 6.8: Isotherm of C_2H_6 in B-doped SWNT by NMR

The broad peak intensity of the ^{1}H NMR spectrum is shown as a function of H_2 pressure for a 45.2 mg B-doped SWNTs sample. For comparison, the isotherm for ethane measured by NMR is shown on the right. Based on an estimate of skeletal density using 1.3 g/cm3 for SWNTs and the peak intensity of H_2 gas in the capillary, we can estimate the contribution to the broad line from free H_2 in the unfilled space of the sample region. This led to the estimation of excess H_2 shown above. Using the Langmuir equation, adsorption energy of 11.6 kJ/mol is obtained for H_2. Again, the amount is quite small, 0.5 wt%, and again, the role of boron remains to be investigated.

6.4 Summary and conclusion

The study indicates that with substitutional doping, the adsorption energy of hydrogen in graphite and SWNTs can be increased considerably, from 4 KJ/mol to 9.2 KJ/mol and 11.6 KJ/mol. Thus this type of doping may lead to a new mechanism for improving hydrogen storage. Although at room temperature, the adsorption of hydrogen in boron doped graphite and boron doped carbon nanotube is still less than 1 Wt%, considering the low porosity of these samples, the adsorption amount can be increased when sample porosity increase. The boron-doped carbon materials show some promising characters in hydrogen storage.

BIBLIOGRAPHY

ABRAGAM, A. (1985). *Principles of Nuclear Magnetism* Oxford University New York.

ALEXANDER, I. K., JEAN-MARC, Z., CHUN-KEUNG, L., PAPPANNAN, T., ALEXANDER, P. M., RAOUF, O. L. & CHRISTIAN, J. B. (2004). Anomalously Soft Dynamics of Water in a Nanotube: A Revelation of Nanoscale Confinement. *Physical Review Letters* **93,** 035503.

ALLEN, R., HANSEN, J. P. & MELCHIONNA, S. (2003). Molecular dynamics investigation of water permeation through nanopores. *Journal of Chemical Physics* **119,** 3905-3919.

BANERJEE, S., MURAD, S. & PURI, I. K. (2007). Preferential ion and water intake using charged carbon nanotubes. *Chemical Physics Letters* **434,** 292-296.

BEKYAROVA, E., HANZAWA, Y., KANEKO, K., SILVESTRE-ALBERO, J., SEPULVEDA-ESCRIBANO, A., RODRIGUEZ-REINOSO, F., KASUYA, D., YUDASAKA, M. & IIJIMA, S. (2002). Cluster-mediated filling of water vapor in intratube and interstitial nanospaces of single-wall carbon nanohorns. *Chemical Physics Letters* **366,** 463-468.

BEKYAROVA, E., KANEKO, K., YUDASAKA, M., KASUYA, D., IIJIMA, S., HUIDOBRO, A. & RODRIGUEZ-REINOSO, F. (2003). Controlled opening of single-wall carbon nanohorns by heat treatment in carbon dioxide. *Journal of Physical Chemistry B* **107,** 4479-4484.

BIGGIN, M. S. P. S. P. C. (2001). Biophysics: Water at the nanoscale. *Nature* **414**.

BIRKETT, G. R. & DO, D. D. (2006). The adsorption of water in finite carbon pores. *Molecular Physics* **104,** 623-637.

BOER, J. H. D. (1968). *Dynamical Character of Adsorption* Oxford University Press, London.

BROVCHENKO, I., GEIGER, A. & OLEINIKOVA, A. (2001). Phase equilibria of water in cylindrical nanopores. *Physical Chemistry Chemical Physics* **3,** 1567-1569.

BROWNSTEIN, K. R. & TARR, C. E. (1979). Importance of classical diffusion in NMR

studies of water in biological cells. *Physical Review A* **19,** 2446.

BYL, O., LIU, J. C., WANG, Y., YIM, W. L., JOHNSON, J. K. & YATES, J. T. (2006). Unusual hydrogen bonding in water-filled carbon nanotubes. *Journal of the American Chemical Society* **128,** 12090-12097.

CALBI, M. M., COLE, M. W., GATICA, S. M., BOJAN, M. J. & STAN, G. (2001). Colloquium: Condensed phases of gases inside nanotube bundles. *Reviews of Modern Physics* **73,** 857-865.

CALLAGHAN, P. T. (1991). *Principles of Nuclear Magnetic Resonance Microscopy* Oxford, Clarendon.

CHANG, J.-Y., GHULE, A., CHANG, J.-J., TZING, S.-H. & LING, Y.-C. (2002). Opening and thinning of multiwall carbon nanotubes in supercritical water. *Chemical Physics Letters* **363,** 583-590.

CHENG, H.-M., YANG, Q.-H. & LIU, C. (2001). Hydrogen storage in carbon nanotubes. *Carbon* **39,** 1447-1454.

COLLINS, P. G., BRADLEY, K., ISHIGAMI, M. & ZETTL, A. (2000). Extreme Oxygen Sensitivity of Electronic Properties of Carbon Nanotubes. *Science* **287,** 1801-1804.

DARKRIM, F. L., MALBRUNOT, P. & TARTAGLIA, G. P. (2002). Review of hydrogen storage by adsorption in carbon nanotubes. *International Journal of Hydrogen Energy* **27,** 193-202.

DE SOUZA, N. R., KOLESNIKOV, A. I., BURNHAM, C. J. & LOONG, C. K. (2006). Structure and dynamics of water confined in single-wall carbon nanotubes. *Journal of Physics-Condensed Matter* **18,** S2321-S2334.

DELLAGO, C. & HUMMER, G. (2006). Kinetics and mechanism of proton transport across membrane nanopores. *Physical Review Letters* **97**.

DELLAGO, C. & NAOR, M. M. (2005). Dipole moment of water molecules in narrow pores. *Computer Physics Communications* **169,** 36-39.

DELLAGO, C., NAOR, M. M. & HUMMER, G. (2003). Proton Transport through Water-Filled Carbon Nanotubes. *Physical Review Letters* **90,** 105902.

DEMONTIS, P., STARA, G. & SUFFRITTI, G. B. (2003). Behavior of water in the hydrophobic zeolite silicalite at different temperatures. A Molecular Dynamics Study. *Journal of Physical Chemistry B* **107,** 4426-4436.

DESBIENS, N., DEMACHY, I., FUCHS, A. H., KIRSCH-RODESCHINI, H., SOULARD, M. & PATARIN, J. (2005). Water condensation in hydrophobic nanopores. *Angewandte Chemie-International Edition* **44,** 5310-5313.

DESHPANDE, R., DILLON, A. C., MAHAN, A. H., ALLEMAN, J. & MITRA, S. (2006). Hydrogen adsorption in single-walled and multi-walled carbon nanotubes grown in a hot-wire CVD (Cat-CVD) reactor. *Thin Solid Films* **501,** 224-226.

DI LEO, J. M. & MARANON, J. (2004). Confined ions and water in nanotube. *Journal of Molecular Structure: THEOCHEM* **709,** 163-166.

DILLON, A. C., JONES, K. M., BEKKEDAHL, T. A., KIANG, C. H., BETHUNE, D. S. & HEBEN, M. J. (1997). Storage of hydrogen in single-walled carbon nanotubes. *Nature* **386,** 377-379.

DONOHUE, M. D. & ARANOVICH, G. L. (1998a). Adsorption Hysteresis in Porous Solids. *Journal of Colloid and Interface Science* **205,** 121-130.

DONOHUE, M. D. & ARANOVICH, G. L. (1998b). Classification of Gibbs adsorption isotherms. *Advances in Colloid and Interface Science* **77,** 137-152.

DONOHUE, M. D. & ARANOVICH, G. L. (1999). A new classification of isotherms for Gibbs adsorption of gases on solids. *Fluid Phase Equilibria* **158-160,** 557-563.

DUJARDIN, E., EBBESEN, T. W., HIURA, H. & TANIGAKI, K. (1994). Capillarity and Wetting of Carbon Nanotubes. *Science* **265,** 1850-1852.

ESWARAMOORTHY, M., SEN, R. & RAO, C. N. R. (1999). A study of micropores in single-walled carbon nanotubes by the adsorption of gases and vapors. *Chemical Physics Letters* **304,** 207-210.

FICHTHORN, K. A. & MIRON, R. A. (2002). Thermal Desorption of Large Molecules from Solid Surfaces. *Physical Review Letters* **89,** 196103.

FUJIWARA, A., ISHII, K., SUEMATSU, H., KATAURA, H., MANIWA, Y., SUZUKI, S. & ACHIBA,

Y. (2001). Gas adsorption in the inside and outside of single-walled carbon nanotubes. *Chemical Physics Letters* **336,** 205-211.

GENG, H. Z., ZHANG, X. B., MAO, S. H., KLEINHAMMES, A., SHIMODA, H., WU, Y. & ZHOU, O. (2004). Opening and closing of single-wall carbon nanotubes. *Chemical Physics Letters* **399,** 109-113.

GHOSH, S., RAMANATHAN, K. V. & SOOD, A. K. (2004). Water at nanoscale confined in single-walled carbon nanotubes studied by NMR. *Europhysics Letters* **65,** 678-684.

GOGELASHVILI, G. S., LADYCHUK, D. V., GRUNIN, Y. B. & VARTAPETIAN, R. S. (2002). Amount of Primary Sites of water Adsorption n Carbon Adsorbents as Measured by Pulsed NMR. *Russian Journal of Physical Chemistry* **76,** 1906.

GOGELASHVILI, G. S., VARTAPETYAN, R. S., LADYCHUK, D. V., GRUNIN, Y. B. & KHOZINA, E. V. (2004). Specific features of the adsorption and nuclear magnetic relaxation of the water molecules in active carbons: 2. The state of water in active carbon with relatively large pores according to the NMR relaxation data. *Colloid Journal* **66,** 271-276.

GOGOTSI, Y., LIBERA, J. A., GUVENC-YAZICIOGLU, A. & MEGARIDIS, C. M. (2001). In situ multiphase fluid experiments in hydrothermal carbon nanotubes. *Applied Physics Letters* **79,** 1021-1023.

GOGOTSI, Y., NAGUIB, N. & LIBERA, J. A. (2002). In situ chemical experiments in carbon nanotubes. *Chemical Physics Letters* **365,** 354-360.

GORDILLO, M. C. & MARTI, J. (2000). Hydrogen bond structure of liquid water confined in nanotubes. *Chemical Physics Letters* **329,** 341-345.

GORDILLO, M. C. & MARTI, J. (2001). Hydrogen bonding in supercritical water confined in carbon nanotubes. *Chemical Physics Letters* **341,** 250-254.

GORDILLO, M. C. & MARTI, J. (2003). Water on the outside of carbon nanotube bundles. *Physical Review B* **67**.

GORDILLO, M. C., NAGY, G. & MARTI, J. (2005). Structure of water nanoconfined between hydrophobic surfaces. *Journal of Chemical Physics* **123**.

GUSEV, V. Y. (1997). Hysteresis thermodynamics of capillary condensation in mesopores. *Journal of Colloid and Interface Science* **194,** 256-259.

H. SHIMODA & O. ZHOU. (2002). *Physical Review Letters* **88,** 015502.

HANASAKI, I. & NAKATANI, A. (2006). Microscopic structure of water flow through carbon nanotubes. In *Advanced Structural and Functional Materials Design, Proceedings*, vol. 512. *Materials Science Forum*, pp. 399-404.

HASLEY, G. D. (1948). *J.Chem.Phys.* **16,** 931.

HATA, K., TAKAKURA, A. & SAITO, Y. (2001). Field emission microscopy of adsorption and desorption of residual gas molecules on a carbon nanotube tip. *Surface Science* **490,** 296-300.

HIRSCHER, M., BECHER, M., HALUSKA, M., QUINTEL, A., SKAKALOVA, V., CHOI, Y. M., DETTLAFF-WEGLIKOWSKA, U., ROTH, S., STEPANEK, I., BERNIER, P., LEONHARDT, A. & FINK, J. (2002a). **- 330-332,** - 658.

HIRSCHER, M., BECHER, M., HALUSKA, M., QUINTEL, A., SKAKALOVA, V., CHOI, Y. M., DETTLAFF-WEGLIKOWSKA, U., ROTH, S., STEPANEK, I., BERNIER, P., LEONHARDT, A. & FINK, J. (2002b). Hydrogen storage in carbon nanostructures. *Journal of Alloys and Compounds* **330-332,** 654-658.

HOU, P.-X., XU, S.-T., YING, Z., YANG, Q.-H., LIU, C. & CHENG, H.-M. (2003). Hydrogen adsorption/desorption behavior of multi-walled carbon nanotubes with different diameters. *Carbon* **41,** 2471-2476.

HUANG, L. L., ZHANG, L. Z., SHAO, Q., WANG, J., LU, L. H., LU, X. H., JIANG, S. Y. & SHEN, W. F. (2006). Molecular dynamics simulation study of the structural characteristics of water molecules confined in functionalized carbon nanotubes. *Journal of Physical Chemistry B* **110,** 25761-25768.

HUMMER, G., RASAIAH, J. C. & NOWORYTA, J. P. (2001). Water conduction through the hydrophobic channel of a carbon nanotube. *Nature* **414,** 188-190.

IIJIMA, S. (1991). Helical microtubules of graphitic carbon. *Nature* **354,** 56-58.

INOUE, S., ICHIKUNI, N., SUZUKI, T., UEMATSU, T. & KANEKO, K. (1998). Capillary Condensation of N2 on Multiwall Carbon Nanotubes. *J. Phys. Chem. B* **102,**

4689-4692.

IUPAC. (1972). *J. Colloid Interface Chem; Pure Appl. Chem.* **31**.

JOHNSON, C. S. & WAUGH, J. S. (1962). Nuclear Relaxation in Adulterated Hydrogen. *Journal of Chemical Physics* **36,** 2266-&.

JORDA-BENEYTO, M., SUAREZ-GARCIA, F., LOZANO-CASTELLO, D., CAZORLA-AMOROS, D. & LINARES-SOLANO, A. (2007). Hydrogen storage on chemically activated carbons and carbon nanomaterials at high pressures. *Carbon* **45,** 293-303.

JU, S. P. & CHANG, J. G. (2004). A molecular dynamics simulation investigation into the behavior of water molecules inside Au nanotubes of various sizes. *Microporous and Mesoporous Materials* **75,** 81-87.

KALRA, A., GARDE, S. & HUMMER, G. (2003). Osmotic water transport through carbon nanotube membranes. *Proceedings of the National Academy of Sciences of the United States of America* **100,** 10175-10180.

KANEKO, K., HANZAWA, Y., IIYAMA, T., KANDA, T. & SUZUKI, T. (1999). Cluster-mediated water adsorption on carbon nanopores. *Adsorption-Journal of the International Adsorption Society* **5,** 7-13.

KIERLIK, E., MONSON, P. A., ROSINBERG, M. L., SARKISOV, L. & TARJUS, G. (2001). Capillary Condensation in Disordered Porous Materials: Hysteresis versus Equilibrium Behavior. *Physical Review Letters* **87,** 055701.

KIM, Y.-H., ZHAO, Y., WILLIAMSON, A., HEBEN, M. J. & ZHANG, S. B. (2006). Nondissociative Adsorption of H2 Molecules in Light-Element-Doped Fullerenes *Phys. Rev. Lett* **96,** 016102.

KISELEV, A. V. (1968). *J. Colloid Interface Sci.* **24,** 430.

KLEINHAMMES, A., MAO, S. H., YANG, X. J., TANG, X. P., SHIMODA, H., LU, J. P., ZHOU, O. & WU, Y. (2003). Gas adsorption in single-walled carbon nanotubes studied by NMR. *Physical Review B* **68,** 075418.

KOGA, K., GAO, G. T., TANAKA, H. & ZENG, X. C. (2001). Formation of ordered ice nanotubes inside carbon nanotubes. *Nature* **412,** 802-805.

KOGA, K., GAO, G. T., TANAKA, H. & ZENG, X. C. (2002). How does water freeze inside carbon nanotubes? *Physica A: Statistical Mechanics and its Applications* **314,** 462-469.

KOGA, K., TANAKA, H. & ZENG, X. C. (2000). First-order transition in confined water between high-density liquid and low-density amorphous phases. *Nature* **408,** 564-567.

KOGA, K., ZENG, X. C. & TANAKA, H. (1997). Freezing of confined water: A bilayer ice phase in hydrophobic nanopores. *Physical Review Letters* **79,** 5262-5265.

KOJIMA, Y., KAWAI, Y., KOIWAI, A., SUZUKI, N., HAGA, T., HIOKI, T. & TANGE, K. (2006). Hydrogen adsorption and desorption by carbon materials. *Journal of Alloys and Compounds* **421,** 204-208.

KOLESNIKOV, A. I., LOONG, C. K., DE SOUZA, N. R., BURNHAM, C. J. & MORAVSKY, A. P. (2006). Anomalously soft dynamics of water in carbon nanotubes. *Physica B-Condensed Matter* **385,** 272-274.

KOLESNIKOV, A. I., ZANOTTI, J. M., LOONG, C. K., THIYAGARAJAN, P., MORAVSKY, A. P., LOUTFY, R. O. & BURNHAM, C. J. (2004). Anomalously soft dynamics of water in a nanotube: A revelation of nanoscale confinement. *Physical Review Letters* **93**.

KONG, J., FRANKLIN, N. R., ZHOU, C., CHAPLINE, M. G., PENG, S., CHO, K. & DAI, H. (2000). Nanotube Molecular Wires as Chemical Sensors. *Science* **287,** 622-625.

KOTSALIS, E. M., WALTHER, J. H. & KOUMOUTSAKOS, P. (2004). Multiphase water flow inside carbon nanotubes. *International Journal of Multiphase Flow* **30,** 995-1010.

KRATSCHMER, W., RATHOUSKY, J. & ZUKAL, A. (1999). *Carbon* **37**.

LEE, S. M., PARK, K. S., CHOI, Y. C., PARK, Y. S., BOK, J. M., BAE, D. J., NAHM, K. S., CHOI, Y. G., YU, S. C., KIM, N.-G., FRAUENHEIM, T. & LEE, Y. H. (2000). Hydrogen adsorption and storage in carbon nanotubes. *Synthetic Metals* **113,** 209-216.

LIM, S. H., LUO, J., JI, W. & LIN, J. (2007). Synthesis of boron nitride nanotubes and its hydrogen uptake. *Catalysis Today* **120,** 346-350.

LIU, C., FAN, Y. Y., LIU, M., CONG, H. T., CHENG, H. M. & DRESSELHAUS, M. S. (1999). Hydrogen Storage in Single-Walled Carbon Nanotubes at Room Temperature.

Science **286,** 1127-1129.

LIU, Y., BROWN, C. M., BLACKBURN, J. L., NEUMANN, D. A., GENNETT, T., SIMPSON, L., PARILLA, P., DILLON, A. C. & HEBEN, M. J. Inelastic Neutron Scattering of H2 Adsorbed on Boron Substituted Single Walled Carbon Nanotubes. *Journal of Alloys and Compounds* **In Press, Accepted Manuscript**.

LIU, Y. C. & WANG, Q. (2005). Transport behavior of water confined in carbon nanotubes. *Physical Review B* **72**.

LIU, Y. C., WANG, Q., WU, T. & ZHANG, L. (2005). Fluid structure and transport properties of water inside carbon nanotubes. *Journal of Chemical Physics* **123**.

LUXEMBOURG, D., FLAMANT, G., GUILLOT, A. & LAPLAZE, D. (2004). Hydrogen storage in solar produced single-walled carbon nanotubes. *Materials Science and Engineering B* **108,** 114-119.

MAMONTOV, E., BURNHAM, C. J., CHEN, S. H., MORAVSKY, A. P., LOONG, C. K., DE SOUZA, N. R. & KOLESNIKOV, A. I. (2006a). Dynamics of water confined in single- and double-wall carbon nanotubes. *Journal of Chemical Physics* **124**.

MAMONTOV, E., BURNHAM, C. J., CHEN, S. H., MORAVSKY, A. P., LOONG, C. K., SOUZA, N. R. D. & KOLESNIKOV, A. I. (2006b). Dynamics of water confined in single- and double-wall carbon nanotubes. *The Journal of Chemical Physics* **124,** 194703.

MANIWA, Y., KATAURA, H., ABE, M., SUZUKI, S., ACHIBA, Y., KIRA, H. & MATSUDA, K. (2002). Phase transition in confined water inside carbon nanotubes. *Journal of the Physical Society of Japan* **71,** 2863-2866.

MANIWA, Y., KATAURA, H., ABE, M., UDAKA, A., SUZUKI, S., ACHIBA, Y., KIRA, H., MATSUDA, K., KADOWAKI, H. & OKABE, Y. (2005). Ordered water inside carbon nanotubes: formation of pentagonal to octagonal ice-nanotubes. *Chemical Physics Letters* **401,** 534-538.

MANN, D. J. & HALLS, M. D. (2003). Water Alignment and Proton Conduction inside Carbon Nanotubes. *Physical Review Letters* **90,** 195503.

MAO, S., KLEINHAMMES, A. & WU, Y. (2006). NMR study of water adsorption in single-walled carbon nanotubes. *Chemical Physics Letters* **421,** 513-517.

MAO, Z. & SINNOTT, S. B. (2000). A Computational Study of Molecular Diffusion and Dynamic Flow through Carbon Nanotubes. *J. Phys. Chem. B* **104,** 4618-4624.

MARANON DI LEO, J. & MARANON, J. (2003). Confined water in nanotube. *Journal of Molecular Structure: THEOCHEM* **623,** 159-166.

MART, J. & GORDILLO, M. C. (2001). Effects of confinement on the vibrational spectra of liquid water adsorbed in carbon nanotubes. *Physical Review B* **63,** 165430.

MARTI, J. & GORDILLO, M. C. (2002). Microscopic dynamics of confined supercritical water. *Chemical Physics Letters* **354,** 227-232.

MARTI, J. & GORDILLO, M. C. (2003). Structure and dynamics of liquid water adsorbed on the external walls of carbon nanotubes. *Journal of Chemical Physics* **119,** 12540-12546.

MASHL, R. J., JOSEPH, S., ALURU, N. R. & JAKOBSSON, E. (2003). Anomalously Immobilized Water: A New Water Phase Induced by Confinement in Nanotubes. *Nano Lett.* **3,** 589-592.

MATSUDA, K., HIBI, T., KADOWAKI, H., KATAURA, H. & MANIWA, Y. (2006). Water dynamics inside single-wall carbon nanotubes: NMR observations. *Physical Review B* **74**.

MONSON, P. A. (2005). Recent progress in molecular modeling of adsorption and hysteresis in mesoporous materials. *Adsorption-Journal of the International Adsorption Society* **11,** 29-35.

MULLER, E. A., HUNG, F. R. & GUBBINS, K. E. (2000). Adsorption of Water Vapor-Methane Mixtures on Activated Carbons. *Langmuir* **16,** 5418-5424.

MULLER, E. A., RULL, L. F., VEGA, L. F. & GUBBINS, K. E. (1996). Adsorption of Water on Activated Carbons: A Molecular Simulation Study. *J. Phys. Chem.* **100,** 1189-1196.

MURATA, K., YUDASAKA, M., IIJIMA, S., EL-MERRAOUI, M. & KANEKO, K. (2002). Classification of supercritical gas adsorption isotherms based on fluid-fluid interaction. *Journal of Applied Physics* **91,** 10227-10229.

NOON, W. H., AUSMAN, K. D., SMALLEY, R. E. & MA, J. P. (2002). Helical ice-sheets

inside carbon nanotubes in the physiological condition. *Chemical Physics Letters* **355,** 445-448.

NUTZENADEL, C., ZUTTEL, A., CHARTOUNI, D. & LOUIS, S. (1999). Electrochemical Storage of Hydrogen in Nanotube Materials. *Electrochemical and Solid-State Letters* **2,** 30-32.

PANELLA, B., HIRSCHER, M. & ROTH, S. (2005). Hydrogen adsorption in different carbon nanostructures. *Carbon* **43,** 2209-2214.

PIETRA, T. & SHEN, K. (2006). NMR spectroscopy of hydrogen adsorption on single-walled carbon nanotubes after exposure to high pressure. *Solid State Nuclear Magnetic Resonance* **29,** 125-131.

RAKOV, E. G. (2001). The chemistry and application of carbons nanotubes. *Uspekhi Khimii* **70,** 934-973.

RAVIKOVITCH, P. I., ODOMHNAILL, S. C., NEIMARK, A. V., SCHUTH, F. & UNGER, K. K. (1995). Capillary hysteresis in nanopores: Theoretical and experimental studies of nitrogen adsorption on MCM-41. *Langmuir* **11,** 4765-4772.

RICCA, A. & DROCCO, J. A. (2002). Interaction of O2 with a (9,0) carbon nanotube. *Chemical Physics Letters* **362,** 217-223.

SAITO, R., DRESSELHAUS, G. & DRESSELAHUS, M. S. (1999). *Physical Properties of Carbon Nanotubes*. Imperial College Press, London.

SAITO, Y., HATA, K., TAKAKURA, A., YOTANI, J. & UEMURA, S. (2002). Field emission of carbon nanotubes and its application as electron sources of ultra-high luminance light-source devices. *Physica B: Condensed Matter* **323,** 30-37.

SANKARAN, M. & VISWANATHAN, B. (2006). The role of heteroatoms in carbon nanotubes for hydrogen storage. *Carbon* **44,** 2816-2821.

SCHLAPBACH, L. & ZUTTEL, A. (2001). Hydrogen-storage materials for mobile applications. *Nature* **414,** 353-358.

SEKHANEH, W., KOTECHA, M., DETTLAFF-WEGLIKOWSKA, U. & VEEMAN, W. S. (2006). High resolution NMR of water absorbed in single-wall carbon nanotubes. *Chemical Physics Letters* **428,** 143-147.

SEUNG-HOON, J. & YOUNG-KYUN, K. (2004). Hydrogen adsorption on boron nitride nanotubes: A path to room-temperature hydrogen storage. *Physical Review B (Condensed Matter and Materials Physics)* **69,** 245407.

SHIM, M., KAM, N. W. S., CHEN, R. J., LI, Y. M. & DAI, H. J. (2002). *Nano Letters* **2,** 285.

SKOULIDAS, A. I., ACKERMAN, D. M., JOHNSON, J. K. & SHOLL, D. S. (2002). Rapid transport of gases in carbon nanotubes. *Physical Review Letters* **89**.

SLICHTER, C. P. (1989). *Principles of Magnetic Resonance* Springer-Verlag, Berlin.

SRIRAMAN, S., KEVREKIDIS, I. G. & HUMMER, G. (2005). Coarse nonlinear dynamics and metastability of filling-emptying transitions: Water in carbon nanotubes. *Physical Review Letters* **95**.

STAN, G. & COLE, M. W. (1998). Low coverage adsorption in cylindrical pores. *Surface Science* **395,** 280-291.

STAN, G., GATICA, S. M., BONINSEGNI, M., CURTAROLO, S. & COLE, M. W. (1999). Atoms in nanotubes: Small dimensions and variable dimensionality. *American Journal of Physics* **67,** 1170-1176.

STRIOLO, A. (2006). The mechanism of water diffusion in narrow carbon nanotubes. *Nano Letters* **6,** 633-639.

STRIOLO, A., CHIALVO, A. A., CUMMINGS, P. T. & GUBBINS, K. E. (2006). Simulated water adsorption in chemically heterogeneous carbon nanotubes. *Journal of Chemical Physics* **124**.

STRIOLO, A., CHIALVO, A. A., GUBBINS, K. E. & CUMMINGS, P. T. (2005a). Water in carbon nanotubes: Adsorption isotherms and thermodynamic properties from molecular simulation. *Journal of Chemical Physics* **122**.

STRIOLO, A., GUBBINS, K. E., CHIALVO, A. A. & CUMMINGS, P. T. (2004). Simulated water adsorption isotherms in carbon nanopores. *Molecular Physics* **102,** 243-251.

STRIOLO, A., GUBBINS, K. E., CHIALVO, A. A. & CUMMINGS, P. T. (2005b). The effect of pore connectivity on water adsorption isotherms in non-activated graphitic nanopores. *Adsorption-Journal of the International Adsorption Society* **11,**

337-341.

STRIOLO, A., NAICKER, P. K., CHIALVO, A. A., CUMMINGS, P. T. & GUBBINS, K. E. (2005c). Simulated water adsorption isotherms in hydrophilic and hydrophobic cylindrical nanopores. *Adsorption-Journal of the International Adsorption Society* **11,** 397-401.

STROBEL, R., JORISSEN, L., SCHLIERMANN, T., TRAPP, V., SCHUTZ, W., BOHMHAMMEL, K., WOLF, G. & GARCHE, J. (1999). Hydrogen adsorption on carbon materials. *Journal of Power Sources* **84,** 221-224.

SUMANASEKERA, G. U., ADU, C. K. W., FANG, S. & EKLUND, P. C. (2000). Effects of Gas Adsorption and Collisions on Electrical Transport in Single-Walled Carbon Nanotubes. *Physical Review Letters* **85,** 1096.

TALAPATRA, S. & MIGONE, A. D. (2002). Adsorption of methane on bundles of closed-ended single-wall carbon nanotubes. *Physical Review B* **65,** 045416.

TANAKA, H., EL-MERRAOUI, M., STEELE, W. A. & KANEKO, K. (2002). Methane adsorption on single-walled carbon nanotube: a density functional theory model. *Chemical Physics Letters* **352,** 334-341.

TANG, X. P., KLEINHAMMES, A., SHIMODA, H., FLEMING, L., BENNOUNE, K. Y., SINHA, S., BOWER, C., ZHOU, O. & WU, Y. (2000). Electronic Structures of Single-Walled Carbon Nanotubes Determined by NMR. *Science* **288,** 492-494.

TEIZER, W., HALLOCK, R. B., DUJARDIN, E. & EBBESEN, T. W. (1999). ^{4}He Desorption from Single Wall Carbon Nanotube Bundles: A One-Dimensional Adsorbate. *Physical Review Letters* **82,** 5305.

TEIZER, W., HALLOCK, R. B., DUJARDIN, E. & EBBESEN, T. W. (2000). Erratum:^{4}He Desorption from Single Wall Carbon Nanotube Bundles: A One-Dimensional Adsorbate [Phys. Rev. Lett. 82, 5305 (1999)]. *Physical Review Letters* **84,** 1844.

TOMPSETT, G. A., KROGH, L., GRIFFIN, D. W. & CONNER, W. C. (2005). Hysteresis and scanning behavior of mesoporous molecular sieves. *Langmuir* **21,** 8214-8225.

TRUSKETT, T. M. (2003). The Subtleties of Water in Small Spaces. *Proceedings of the National Academy of Sciences of the United States of America* **100,** 10139-10140.

ULBRICHT, H., MOOS, G. & HERTEL, T. (2002). Physisorption of molecular oxygen on single-wall carbon nanotube bundles and graphite. *Physical Review B* **66,** 075404.

ULBRICHT, H., MOOS, G. & HERTEL, T. (2003). Interaction of molecular oxygen with single-wall carbon nanotube bundles and graphite. *Surface Science* **532-535,** 852-856.

VARTAPETIAN, R. S. & VOLOSHCHUK, A. M. (1995). The Mechanism of adsorption of water molecules on carbon adsorbents. *Uspekhi Khimii* **64,** 1055-1072.

VARTAPETYAN, R. S., VOLOSHCHUK, A. M., BURYAK, A. K., ARTAMONOVA, C. D., BELFORD, R. L., CEROKE, P. J., KHOLINE, D. V., CLARKSON, R. B. & ODINTSOV, B. M. (2005). Water vapor adsorption on chars and active carbons-oxygen sensors prepared from a tropical tree wood. *Carbon* **43,** 2152-2159.

VARTAPETYAN, R. S., VOLOSHCHUK, A. M., ISIRIKYAN, A. A., POLYAKOV, N. S. & TARASEVICH, Y. I. (1995). Chemistry of carbon surface and mechanism of water molecule adsorption. *Colloids and Surfaces A: Physicochemical and Engineering Aspects* **101,** 227-232.

VIDALI, G., IHM, G., KIM, H.-Y. & COLE, M. W. (1991). Potentials of physical adsorption. *Surface Science Reports* **12,** 135-181.

WALLQVIST, A., GALLICCHIO, E. & LEVY, R. M. (2001). A Model for Studying Drying at Hydrophobic Interfaces: Structural and Thermodynamic Properties. *J. Phys. Chem. B* **105,** 6745-6753.

WALTHER, J. H., JAFFE, R., HALICIOGLU, T. & KOUMOUTSAKOS, P. (2001). Carbon nanotubes in water: Structural characteristics and energetics. *Journal of Physical Chemistry B* **105,** 9980-9987.

WALTHER, J. H., WERDER, T., JAFFE, R. L. & KOUMOUTSAKOS, P. (2004). Hydrodynamic properties of carbon nanotubes. *Physical Review E* **69**.

WANG, J., ZHU, Y., ZHOU, J. & LU, X. H. (2003). Molecular dynamics study of water molecules confined in carbon nanotubes with different helicity. *Acta Chimica Sinica* **61,** 1891-1896.

WANG, J., ZHU, Y., ZHOU, J. & LU, X. H. (2004). Diameter and helicity effects on static properties of water molecules confined in carbon nanotubes. *Physical Chemistry*

Chemical Physics **6,** 829-835.

WEBER, S. E., TALAPATRA, S., JOURNET, C., ZAMBANO, Z. & MIGONE, A. D. (2000). Determination of the binding energy of methane on single-walled carbon nanotube bundles. *Physical Review B* **61,** 13150-13154.

WERDER, T., WALTHER, J. H., JAFFE, R. L., HALICIOGLU, T. & KOUMOUTSAKOS, P. (2003). On the water-carbon interaction for use in molecular dynamics simulations of graphite and carbon nanotubes. *Journal of Physical Chemistry B* **107,** 1345-1352.

XU, W. C., TAKAHASHI, K., MATSUO, Y., HATTORI, Y., KUMAGAI, M., ISHIYAMA, S., KANEKO, K. & IIJIMA, S. Investigation of hydrogen storage capacity of various carbon materials. *International Journal of Hydrogen Energy* **In Press, Corrected Proof**.

XUE, Y. Q. & CHEN, M. D. (2006). Dynamics of molecules translocating through carbon nanotubes as nanofluidic channels. *Nanotechnology* **17,** 5216-5223.

YE, Y., AHN, C. C., WITHAM, C., FULTZ, B., LIU, J., RINZLER, A. G., COLBERT, D., SMITH, K. A. & SMALLEY, R. E. (1999). Hydrogen adsorption and cohesive energy of single-walled carbon nanotubes. *Applied Physics Letters* **74,** 2307-2309.

YU, I., LEE, J. & LEE, S. (2003). NMR of hydrogen adsorbed on carbon nanotubes. *Physica B: Condensed Matter* **329-333,** 421-422.

ZHAO, J., BULDUM, A., HAN, J. & LU, J. P. (2002). Gas molecule adsorption in carbon nanotubes and nanotube bundles. *Nanotechnology* **13,** 195-200.

ZHAO, Y., KIM, Y.-H., DILLON, A. C., HEBEN, M. J. & ZHANG, S. B. (2005). Hydrogen Storage in Novel Organometallic Buckyballs. *Physical Review Letters* **94,** 155504.

ZHENG, J., LENNON, E. M., TSAO, H. K., SHENG, Y. J. & JIANG, S. Y. (2005). Transport of a liquid water and methanol mixture through carbon nanotubes under a chemical potential gradient. *Journal of Chemical Physics* **122**.

ZHOU, X., LI, C. Q. & IWAMOTO, M. (2004). Equilibrium and kinetics: Water confined in carbon nanotubes as one-dimensional lattice gas. *Journal of Chemical Physics* **121,** 7996-8002.

ZHU, H., CAO, A., LI, X., XU, C., MAO, Z., RUAN, D., LIANG, J. & WU, D. (2001). Hydrogen adsorption in bundles of well-aligned carbon nanotubes at room temperature. *Applied Surface Science* **178,** 50-55.

ZUTTEL, A., NUTZENADEL, C., SUDAN, P., MAURON, P., EMMENEGGER, C., RENTSCH, S., SCHLAPBACH, L., WEIDENKAFF, A. & KIYOBAYASHI, T. (2002). Hydrogen sorption by carbon nanotubes and other carbon nanostructures. *Journal of Alloys and Compounds* **330-332,** 676-682.